ELECTRON PARAMAGNETIC RESONANCE STUDIES OF $3d^3$ IONS IN MAGNESIUM OXIDE

by

A.J.B. Codling, M.Sc.

Being a thesis
submitted to the University of Keele
for the Degree of Doctor of Philosophy

Department of Physics,
University of Keele,
Keele,
Staffordshire.

December, 1969.

SYNOPSIS

This thesis reports some electron spin resonance spectra of V^{2+} and Cr^{3+} ions in magnesium oxide.

Chapters I and II describe the basic features of electron paramagnetic resonance and its application to transition metal ions in insulating crystalline environments. A review of previous work on $3d^3$ ions in magnesium oxide is given in Chapter III, together with the theory underlying the resonances observed.

In Chapter V this theory is adapted to a previously unreported spectrum of V^{2+} in orthorhombic sites in magnesium oxide, an unusual and unexpected situation in this cubic oxide. With the help of a digital computer we find the following Hamiltonian parameters for the observed resonances at X-band and Q-band:- $g_x = g_y = g_z = 1.991$, $|D| = 0.182cm^{-1}$, $|E| = 0.042cm^{-1}$, $|A| = 0.0072cm^{-1}$. The orthorhombic distortion is attributed to a nearest neighbour cation vacancy.

A "forbidden" hyperfine pattern is also observed, which becomes allowed off-axis due to the mixing of zero field splitting and hyperfine terms. The observed and computed intensities of these lines were comparable.

Chapter VI deals with the resonances observed from the S=2 state of next nearest neighbour pairs of super-exchange-coupled V^{2+} ions. The spectra may be fitted to the following spin Hamiltonian:

$= \beta g.H.S + D(S_z^2 - \frac{1}{3}S(S+1)) + A.I.S$, with the following parameters:

$g_x = g_y = g_z = 1.980$, $D = -0.072cm^{-1}$, $|A| = 0.004cm^{-1}$. From the temperature variation of line intensity the exchange energy J is determined to be $\sim 60cm^{-1}$. A temperature dependent linewidth of the pair spectra was explained as due to spin-lattice relaxation processes via phonons of energy comparable to the level splittings.

Finally, we describe measurements on Cr^{3+} ions in orthorhombic sites at a frequency higher than those previously used. In contra-distinction to measurements at X- and K-bands by other authors, all possible transitions were observed and their orientation dependence determined. The Hamiltonian parameters obtained were found to be consistent with those of other workers.

ACKNOWLEDGMENTS

The author would like to express his sincere gratitude to the following:

Professor D.J.E. Ingram, for providing facilities for research in his department.

Dr. B. Henderson for his guidance, help and supervision of the work.

Miss K.B. Davies for her care and patience in the typing and duplicating of this thesis.

Miss M.S. Highfield for her help in the preparation of readable manuscripts.

Dr. R.D. Dowsing for his help with computing and the loan of programmes; also for many helpful discussions.

Miss P.A. Highfield for running the computer programmes and her instruction in my use of the machine.

Mr. M. Cheney for carrying out the photographic work.

The Technical Staff of the Physics Department for their advice and assistance.

Mr. P. Weightman and other members of the Department for their co-operation, assistance and helpful discussions.

The Science Research Council and The University of Keele for providing maintenance grants.

CONTENTS

Chapter 6 (continued)

CHAPTER I

BASIC E.P.R. THEORY

1.1 Introduction

The phenomenon of electron paramagnetic resonance (hereafter E.P.R.) finds application in many areas of scientific research, not the least of which is Solid State Physics. The present thesis is concerned with investigations of paramagnetic point defects in crystals of the alkaline earth oxides, especially the spectra observed when transition metal ions replace cations in the lattice. Such spectra give detailed structural information at the atomic level since impurity atoms disrupt the regular rank and file of the host crystal. The resonance spectrum will depend not only on the foreign ion but also on its surroundings. In the cubic alkaline earth oxides substitutional cation impurities experience a crystalline electric field of octahedral symmetry which results from the distribution of neighbouring ions. There are six nearest neighbour anions and twelve nearest neighbour cations. Other defects in near neighbour sites to the paramagnetic centre lower its symmetry so changing the observed E.P.R. spectrum. Such neighbouring defects may be charge compensating vacancies, or other impurity ions which may be the same as, or different from, the initial imperfection. An interesting situation arises when there are two or more neighbouring paramagnetic ions, for then quantum mechanical exchange effects become apparent. For example MgO, heavily doped with V^{2+} ions was a material

playing a major role in this research work. The high concentration of impurity ions led to close association of V^{2+} ions, and spectra attributable to exchange coupled pairs of ions were observed. This is discussed in detail later.

1.2 Theoretical Considerations

The basic requirement, for the observation of E.P.R., is that the electrons on the atoms under investigation have a resultant electronic angular momentum. Whether this angular momentum arises from a pure electron spin or from an admixture of spin and orbital momentum depends on the system in question. Free radicals give resonances typical of free electrons and the observed spectra can be interpreted on the assumption that the orbital angular momentum is zero. On the other hand paramagnetic ions in crystals undergo various interactions characteristic of the solid state and the orbital contribution to the total angular momentum must be considered. The extent to which orbital momentum is involved depends on both the degree of quenching by the crystalline environment and the magnitude of the spin-orbit coupling. The quenching and spin-orbit coupling are in mutual competition.

For many 3d transition metal ions the spin-orbit coupling is to first order relatively unimportant in its effect on the angular momentum, and spectra can be attributed to resonance of fairly free electrons. But for ions such as Fe^{2+}, Co^{2+}, Ni^{3+} and rare earth ions, the reverse is the case and the g-value departs greatly from 2.

Whatever the contributions to the electronic angular momentum, it remains clear that the unpaired electron acts as a small magnetic dipole and is influenced by an external magnetic field. If the magnetic moment of the electron is $\underline{\mu}$ and the applied field $\underline{H}$, the interaction between them can be represented by the Hamiltonian

$$\mathcal{H} = -\underline{\mu}.\underline{H}_o \qquad (1.1)$$

The magnetic moment is proportional to the total angular momentum $\underline{J}\hbar$ according to:

$$\underline{\mu} = -\gamma \underline{J}\hbar \qquad (1.2)$$

where γ is the gyromagnetic ratio. Since the vector $\underline{J}$ has (2J+1) values corresponding to the different projections of this vector in the direction of the applied field there are (2J+1) energy levels available to a paramagnetic ion situated in a magnetic field. Paramagnetic resonance may be observed when electronic transitions take place between these levels. It is important to understand that owing to the quantisation of $\underline{J}$ its maximum resolved component along the field direction is $\underline{J}\hbar$ while the length of the vector is $\sqrt{J(J+1)}.\hbar$. This means that the vector is never aligned exactly parallel or anti-parallel to the field. Instead it executes a precession about the field axis, the angle it makes with the field remaining constant. This motion is described in greater detail in the next section.

1.2.1 Classical approach to the resonance phenomenon

Since we are dealing with quantum effects in matter, paramagnetic resonance is correctly described in terms of quantum mechanics. However, a classical approach can be very instructive provided that the limitations are borne in mind. We assume a classical dipole can be associated with the unpaired electron, and given this, the effect of the external magnetic field is readily understood in terms of precessing vectors.

The magnetic moment $\underline{\mu}$ experiences a torque according to

$$\underline{T} = \underline{\mu} \times \underline{H}_o \qquad (1.3)$$

when situated in an external magnetic field $\underline{H}_o$ which we shall assume is along the z direction. Since the torque is the rate of change of angular momentum $\underline{T} = \frac{\hbar d\underline{J}}{dt}$.

Substituting from equations (1.2) and (1.3) gives

$$\frac{\hbar d\underline{J}}{dt} = -\gamma\hbar\underline{J} \times \underline{H}_o$$

Multiplying by $-\gamma$ gives

$$\frac{d\underline{\mu}}{dt} = \gamma\underline{\mu} \times \underline{H}_o \qquad (1.4)$$

Equation (1.4) describes the precessional motion of a vector $\underline{\mu}$ about the direction of the field $\underline{H}_o$, at an angular frequency $\omega_o = \gamma H_o$. The magnitude of ω_o is independent of the orientation of $\underline{\mu}$ with respect to H_o.

If now a second field $\underline{H}_1$ say a microwave field is applied, $\underline{\mu}$ will be affected by this also. The high frequency field can either be circularly polarised or a plane wave. The latter can be considered as two counter-rotating circularly polarised waves. $\underline{H}_1$ is generally represented by a rotating magnetic vector which is in a plane perpendicular to the direction of the steady field $\underline{H}_o$.

The oscillating field can be expressed as $\underline{H}_x = 2\underline{H}_1 \cos \omega_1 t$, or in the imaginary form

$$H_1 = \underline{i}\, H_1 \cos \omega_1 t + \underline{j}\, H_1 \sin \omega_1 t$$
$$H_1 = \underline{i}\, H_1 \cos \omega_1 t - \underline{j}\, H_1 \sin \omega_1 t$$

which are the two counter rotating components. Only that component rotating in the same sense as $\underline{\mu}$ will change the motion of the dipole. Considering the component rotating with $\underline{\mu}$ it is clear that if the angular velocity of the $\underline{H}_1$ vector is different from that of $\underline{\mu}$, only a momentary force would be exerted on $\underline{\mu}$, this reversing in sign when $\underline{\mu}$ and $\underline{H}_1$ were closest in their orbits. The average torque due to $\underline{H}_1$ is zero in this case. When the angular velocities of both $\underline{\mu}$ and $\underline{H}_1$ are equal, the resonance condition is satisfied and there is a constant force on $\underline{\mu}$. It precesses about the microwave field in addition to its precession about $\underline{H}_o$. This precession about $\underline{H}_1$ has an angular frequency $\underline{\omega}_1 = \gamma \underline{H}_1$ The resulting motion of the $\underline{\mu}$ vector is helical.

A simplification is affected if we view the resonance behaviour from a set of coordinates rotating with an angular frequency ω_1 about $\underline{H}_o$.

The transformation can be performed using

$$\frac{d\underline{\mu}}{dt} = \left(\frac{d\underline{\mu}}{dt}\right)_R + \underline{\omega}_1 \times \underline{\mu} ,$$

the left hand side being the time rate of change $\underline{\mu}$ in the laboratory frame of reference, $\left(\frac{d\underline{\mu}}{dt}\right)_R$ the change of $\underline{\mu}$ in the rotating frame and $(\underline{\omega} \times \underline{\mu})$ the change in $\underline{\mu}$ due to the rotation.

From (1.4)

$$\gamma\underline{\mu} \times \underline{H}_o = \left(\frac{d\underline{\mu}}{dt}\right)_R + \underline{\omega}_1 \times \underline{\mu}$$

or

$$\left(\frac{d\underline{\mu}}{dt}\right)_R = \gamma\underline{\mu} \times (\underline{H}_o + \underline{\omega}_1/\gamma) \qquad (1.5)$$

Comparing this with (1.4) we see that $(\underline{H}_o + \underline{\omega}_1/\gamma)$ represents the apparent fixed magnetic field, as seen from the rotating frame. For electron spins, γ is negative, so $\underline{\omega}_1/\gamma$ is a field opposed to $\underline{H}_o$. The effective field seen by the rotating observer can be obtained by a vector summation of $(\underline{H}_o + \underline{\omega}/\gamma)$ and $\underline{H}_1$, and is of magnitude

$$H_{eff} = \left[(H_o - \omega_1/\gamma)^2 + H_1^2\right]^{\frac{1}{2}} \qquad (1.6)$$

The angle θ between $\underline{H}_o$ and $\underline{H}_{eff}$ is

$$\theta = \tan^{-1}\left[\frac{H_1}{H_o - \omega_1/\gamma}\right] \qquad (1.7)$$

At resonance $\omega_1 = \omega_o$, hence $\theta = 90^o$ and $\underline{H}_{eff} = \underline{H}_1$. In this case, the motion of $\underline{\mu}$ as seen by the rotating observer is simply a precession about $\underline{H}_1$, angular frequency $\underline{\omega}_1 = \underline{H}_1$. Off resonance, $\underline{\mu}$ precesses about $\underline{H}_{eff}$.

In a macroscopic system, the resonance is not restricted to just one magnetic dipole since all the spins, which point with or against the applied field, give rise to a net magnetisation vector $\underline{M}$. It is this vector that precesses in the magnetic field. Since the antiparallel orientation of $\underline{M}$ with respect to $\underline{H}_o$ is a higher energy configuration than the parallel orientation, energy is absorbed from the microwave field as the $\underline{M}$ vector spirals down and given up as the reverse motion proceeds.

At this point it becomes difficult to reconcile the classical and quantum descriptions of the resonance phenomenon. Experimentally resonance is accompanied by the absorption of microwave power, and not by the repetitive absorption and emission implied in the simple model. Before abandoning the classical description in favour of the quantum view of resonance it is useful to mention briefly the relaxation processes.

If the microwave field is turned off, with $\underline{M}$ in some arbitrary orientation, a re-establishment of the vector in an equilibrium direction along the field will take place, with a characteristic time T_1. This process requires that energy be given up by the dipole to the lattice and is known as spin lattice relaxation. A second process involving interactions between the individual magnetic dipoles making up $\underline{M}$, and known as spin-spin relaxation causes a reduction in the net magnetisation in the xy plane. This is due to the fact that each dipole sees a local varying field due to its neighbours, the effect of which is to dephase it with respect to all the others, since each precesses in a slightly different field. This randomisation of the coherence of the individual components making up M can be seen as a fanning out of the $\underline{M}$ vector in

the xy plane. The characteristic time for the net magnetisation in the xy plane to be reduced to zero is the spin-spin relaxation time, T_2.

1.2.2 Quantum theoretical description of resonance

The energy of an isolated ion in a magnetic field is given by the Hamiltonian in Equation (1.1), i.e.

$$\mathcal{H} = \gamma\hbar \underline{J}.\underline{H}_o$$

In the simplest system, $J=\frac{1}{2}$, and the resolved components M_J of the vector along $\underline{H}_o$ have values $\pm\frac{1}{2}$. Thus the ion has energy levels $E_M = \pm\frac{1}{2}\gamma\hbar H_o$. This may be rewritten as $E_M = \pm\frac{1}{2}g\beta H_o$, where $\beta = e\hbar/2mc$ is the Bohr magneton and g the spectroscopic splitting factor. Consequently the magnetic field splits the free ion energy levels by an amount $g\beta H_o$. A time dependent perturbation containing terms in $J^{\pm}$ will connect the two levels, enabling electronic transitions to occur between them. The familiar resonance condition is accordingly $h\nu = g\beta H_o$, $h\nu$ being the microwave quantum required for the transition. The upward transition corresponds to an absorption of energy while the reverse process is manifest as stimulated emission in the presence of the radiation field.

Clearly if the populations of paramagnets in the two levels are equal there is no net absorption of energy. However normally, on account of the levels being different in energy, the ratio of the populations will differ from unity and is given by the Maxwell-Boltzmann equation,

$$\frac{N^+}{N^-} = \exp(-\frac{h\nu}{kT}) \qquad (1.8)$$

where $N^{\pm}$ are the populations of the upper and lower levels respectively.

The excess of paramagnets parallel to the applied magnetic field over those antiparallel is enhanced at lower temperature and working at high magnetic fields and therefore high resonant frequencies. Defining $N = N^+ + N^-$ and $n = N^- - N^+$, one can write the rate equation for the change in population of the lower state in the presence of a resonant microwave field as

$$\frac{dN^-}{dt} = N^+P^+ - N^-P^- \qquad (1.9)$$

where $P^\pm$ are the transition probabilities from the upper and lower states respectively. Under the action of the microwave radiation alone, these probabilities are equal. Since $N^- = \frac{1}{2}(N + n)$, (1.9) becomes

$$\frac{dN^-}{dt} = \frac{1}{2}\frac{dn}{dt} = -Pn \, . \qquad (1.10)$$

The solution to this equation takes the form $n = n_o e^{-2P^\pm}$, which represents an exponential decay of the population difference under the influence of the resonant microwave field. The final result is an equality of population in the levels and no net absorption of radio-frequency power. If resonant absorption is to continue indefinitely then some mechanism must exist to return paramagnets from the upper level and so maintain a population excess in the lower. Relaxation processes provide such a mechanism.

1.3 Relaxation Processes

Consider the paramagnetic sample to be in zero magnetic field, then since the two energy levels + and - coincide, $N^+ = N^-$. On the

application of a field a rearrangement of paramagnets is required to bring about the inequality in populations of the levels. This process is known as spin lattice relaxation. In this case the "spin" refers to the individual paramagnets that contribute to the total magnetisation vector, and the "lattice" to all the other nuclei and electrons in the sample. The mechanism of spin lattice relaxation involves an exchange of a quantum of energy with the lattice thermal vibrations by a paramagnet while it undergoes a transition between levels. Since the lattice is at thermal equilibrium then the transition probabilities in the downward and upward directions, $W^{\pm}$ can not be equal.

The rate equation for the lower level is by analogy with (1.9)

$$\frac{dN^-}{dt} = N^+W^+ - N^-W^-,$$

which can be rewritten

$$\frac{dn}{dt} = -n(W^+ + W^-) + N(W^+ - W^-)$$

At thermal equilibrium $\frac{dn}{dt} = 0$, so that

$$n = N\frac{(W^+ - W^-)}{(W^+ + W^-)} = n_o \qquad (1.10a)$$

and

$$\frac{dn}{dt} = -n(W^+ + W^-) + N\frac{(W^+ - W^-)(W^+ + W^-)}{W^+ + W^-}$$

$$= -\frac{(n - n_o)}{T_1} \qquad (1.11)$$

where this spin-lattice relaxation time is $T_1 = 1/(W^+ + W^-)$. This is a

measure of the time taken for energy to be distributed among the lattice phonons and for thermal equilibrium to be re-established. The combined effects of the microwave field and spin-lattice relaxation on the difference in population can be expressed in one equation by uniting (1.10) and (1.11)

$$\frac{dn}{dt} = -2Pn - \frac{(n - n_o)}{T_1}$$

At thermal equilibrium

$$n = \frac{n_o}{(1 + 2PT_1)} \qquad (1.12)$$

It can be seen then, that provided $2PT_1$ is small and preferably $<<1$, then the population difference in the presence of both spin-lattice relaxation and radio frequency power remains much as if there were no power applied. It will be seen in the next section that $P \propto H_1^2$, for this reason it is usual to operate at low power levels unless saturation is specifically required.

1.4 Energy Absorption by the Sample

If n (equation 1.12) is the population difference in the presence of a radio frequency field and spin-lattice relaxation, then the rate of absorption of energy is given by the expression

$$\frac{dE}{dt} = \frac{n_o}{1 + 2PT_1} \cdot P \cdot h\nu \qquad (1.13)$$

where P and $h\nu$ have the same meanings as before. From time dependent perturbation theory we can obtain the expression for the stimulated

transition probability from the lower to the upper level as

$$P = \frac{2\pi}{\hbar^2} |\langle -|V|+\rangle|^2 \, \delta(\omega_{-+} - \omega) \qquad (1.14)$$

where ω_{-+} = transition frequency, ω = applied microwave frequency and V is the amplitude of the perturbation. This perturbation may be written as the products of the amplitudes, V, and a time dependent part f(t); i.e.

$$V(t) = V.f(t)$$

For the two level system considered here, this takes the form $V(t) = 2g\beta H_1 J_x . \cos \omega t$, the x-component of J being the perturbation operator since H_1 is perpendicular to H_o. We also assume that $H_1 << H_o$, thus perturbation theory applies.

Accordingly from equation (1.12)

$$P = \frac{2\pi g^2 \beta^2 H_1^2}{\hbar^2} |\langle -|J_x|+\rangle|^2 \, \delta(\omega_{-+} - \omega)$$

For $J = \frac{1}{2}$,

$$\langle -| = \langle -\tfrac{1}{2}|, \quad \langle +| = \langle +\tfrac{1}{2}|$$

and

$$P = \frac{2\pi g^2 \beta^2 H_1^2}{\hbar^2} |\langle -\tfrac{1}{2}|J_+ + J_-|+\tfrac{1}{2}\rangle|^2 g(\omega)$$

$$= \frac{\pi g^2 \beta^2 H_1^2}{2\hbar^2} g(\omega) ,$$

where the line shape function $g(\omega)$ has been substituted for the delta function. Owing to the Uncertainty Principle, no energy level is perfectly sharp. There is always a spread in energy of the order

$E \approx \frac{\hbar}{\Delta t}$, where Δt is the lifetime of the electron in the upper state. For this reason, the restriction imposed by the delta function is too rigorous, since absorption lines have a finite frequency spread about the central frequency ω_{-+}. This range of frequencies is defined by the line shape function $g(\omega)$, which is normalised when

$$\int_0^\infty g(\omega)d\omega = 1$$

If we assume a specific shape for the resonance line, for instance a Lorentzian form that results mathematically from the assumption of exponential decays of differential population, we can derive an expression for $\frac{dE}{dt}$.

Let

$$g(\omega) = \frac{T_2^2}{\pi} \cdot \frac{1}{1 + T_2^2(\omega - \omega_{-+})^2}$$

then

$$P = \frac{g^2\beta^2 H_1^2 T_2}{2\hbar^2(1 + T_2^2(\omega - \omega_{-+})^2)} = \frac{\gamma^2 H_1^2 T_2}{2(1 + T_2^2\Delta\omega^2)}$$

where γ replaces $g\beta/\hbar$, and $\Delta\omega = (\omega - \omega_{-+})$.

Hence using equation (1.13)

$$\frac{dE}{dt} = n_o h\nu . \frac{\gamma^2 H_1^2 T_2}{2(1 + T_2^2\Delta\omega^2)} \cdot \frac{1}{1 + \{\gamma^2 H_1^2 T_1 T_2 / 1 + T_2^2\Delta\omega^2\}}$$

$$= \frac{n_o h\nu\gamma^2 H_1^2 T_2}{2(1 + T_2^2\Delta\omega^2 + \gamma^2 H_1^2 T_1 T_2)}$$

Now from (1.10a)

$$n_o = \frac{N(W^+ - W^-)}{(W^+ + W^-)}$$

Since

$$n_o^+ W^+ = n_o^- W^- , \quad \frac{W^-}{W^+} = \frac{n_o^+}{n_o^-} = \frac{1 - g\beta H}{kT}$$

$$\therefore \quad W^+ - W^- = \frac{W^+ g\beta H_o}{kT}$$

We make the approximation $W^+ = W_1$ where $W = \frac{W^+ + W^-}{2}$

$$\therefore \quad n_o = \frac{Ng\beta H_o}{2kT}$$

Also it is noted that the static susceptibility for a two level system χ_o is given by the expression

$$\chi_o = \frac{Ng^2\beta^2}{4kT}$$

Hence the energy equation can be written

$$\frac{dE}{dt} = \frac{\chi_o H_1^2 T_2 \omega_o \omega}{1 + T_2^2 \Delta\omega^2 + \gamma^2 H_1^2 T_1 T_2}$$

The maximum absorption of power occurs at the centre of the resonance, where $\omega = \omega_o$.

$$\therefore \quad \left(\frac{dE}{dt}\right)_{max} = \frac{\chi_o H_1^2 T_2 \omega_o^2}{1 + \gamma^2 H_1^2 T_1 T_2} \qquad (1.15)$$

For a system with a very short spin-lattice relaxation time - i.e. one that is not liable to saturate

$$\left(\frac{dE}{dt}\right)_{max} = \chi_o H_1^2 T_2 \omega_o^2 \qquad (1.16)$$

The ratio (1.15) to (1.16) gives the saturation factor: $\frac{1}{1 + \gamma^2 H_1^2 T_1 T_2}$.

This factor shows that if too much power is applied to a system where T_1, T_2 are not very short, then a reduction in the maximum power absorbed takes place. This reveals itself as a reduction of peak intensity of the observed spectral line.

It is a useful exercise to compare the power absorption as calculated by counting the number of radiation induced transitions per second, with that obtained by considering the absorption of power from the oscillating magnetic field by the paramagnetic sample. In the second case we are concerned with the susceptibility of the whole specimen. For slowly varying magnetic fields, the susceptibility will be normal since the mechanisms responsible for re-orientation will have time to act. But for high frequencies the susceptibility falls since the individual paramagnets have no time to relax. By analogy with phase lag in alternating current theory, we can speak of an out of phase magnetisation in addition to the reduced component in phase with the magnetic field. It is convenient to define a complex susceptibility, $\chi = \chi' - i\chi''$, where χ' is the in phase part and the imaginary part is the out of phase component. An applied field $2H_1 \cos \omega t$ induces a magnetisation

$$M = 2\chi' H_1 \cos \omega t + 2\chi'' H_1 \sin \omega t \ .$$

Since the energy of a magnetic dipole $\underline{\mu}$ in a field H_1 is $\underline{H}.\frac{d\underline{M}}{dt}$ per unit volume per second, over one cycle

$$E = \int_0^{2\pi/\omega} H(dM/dt)dt$$

and the average rate of absorption of energy becomes

$$\left(\frac{dE}{dt}\right) = \frac{\omega}{2\pi}\int_0^{2\pi/\omega} 4H_1^2\omega(\chi'' \cos^2\omega t - \chi' \sin \omega t \cos \omega t)$$

$$= 2\omega\chi''H_1^2 \qquad (1.17)$$

The rate of absorption of energy depends then on only the complex part of the mass susceptibility in addition to the frequency and the field.

Comparing (1.16) with (1.17), it is seen that the peak imaginary susceptibility is given by the expression

$$\chi'' = \tfrac{1}{2}\chi_o\omega_o T_2 .$$

Taking $\omega_o = 10^{10}\text{rad.sec}^{-1}$, $T_2 = 10^{-7}\text{sec}$, then

$$\chi''/\chi_o \doteq 10^3$$

This shows that the resonance method of detecting paramagnetic susceptibility is very sensitive and also improves with frequency.

CHAPTER II

IONS IN CRYSTALLINE LATTICES

2.1 The Crystal Field

The results obtained in Chapter 1 were for an electronic system with total quantum number $J=\frac{1}{2}$. The situation will not necessarily be so simple when the paramagnetic entity is present in an insulating crystal. Spin and orbital angular momentum may or may not couple to give a resultant $\underline{J}$, depending on the magnitude of the crystalline electrostatic field. Three cases are generally distinguished since the method of incorporating the crystal field into the overall Hamiltonian depends on the strength of the crystal field. Since perturbation methods are usually employed, it is necessary to determine whether spin-orbit coupling is applied as a perturbation to the crystal field, or vice versa.

If the reference ion is one of the rare earth group, the effect of a crystalline electric field on the deep lying unpaired 4f electrons is small. The L-S coupling is not disturbed and L and S precess about the resultant total angular momentum, $\underline{J}$. $\underline{J}$ in turn precesses about the direction of the magnetic field when this is applied, and the resolved components, M_J, label the resulting 2J+1 energy levels. In calculating the energies of these levels, the crystal field is considered to be weak and is applied as a perturbation after the effects of spin orbit coupling have been considered.

When electrons are less well shielded from the crystalline environment as in the transition metal ions, the electric field may be strong enough to uncouple $\underline{L}$ and $\underline{S}$. $\underline{J}$ now has no meaning, and the orbit and spin angular momentum vectors precess independently about the electric field. Owing to quantisation of the orbital angular momentum by the internal field, the observed orbital magnetic moment is reduced or even eliminated for all normal magnetic fields. This is the effect known as quenching of the orbital angular momentum. M_L and M_S are the proper quantum numbers, levels having different M_L values being split in the crystal field. Since this splitting is usually quite large, being of the order of $10^3 cm^{-1}$ only the lowest level is appreciably populated with electrons at normal temperatures. For the case of this medium to strong crystal field, it is usual to treat the effect of the crystal field on the free ion terms and then apply spin-orbit coupling as a perturbation. The effect of the interaction remaining between $\underline{L}$ and $\underline{S}$ depends, of course, inversely on the strength of the crystal field.

For strong to very strong crystal fields, not only is spin-orbit coupling broken down, but also the coupling between spins of the individual atoms. In such cases the individual spins tend to pair off, leaving a single unpaired electron. Both the free ion spin magnetic moment and the orbital moment are reduced. The case corresponds to a covalent bonding between the reference ion and its neighbours, which implies a degree of overlap between bonding orbitals. This makes for added difficulties in the treatment of strong field complexes.

Because of its relevance to the present measurements the treatment of paramagnetic ions in crystalline lattices having medium crystal fields will be outlined. If the interaction between the ion in question and its diamagnetic environment only is considered, neglecting for the present the effects of other neighbouring defects, the field is made up of contributions from all the other electrons and nuclei in the crystal. Calculation of the field in this manner is not possible at present, so approximate methods have to be adopted. The most frequently used of these is the crystal field theory developed by Bethe[1] and Van Vleck[2]. Essentially, it assumes that the ions, atoms or molecules surrounding the reference ion can be represented by point charges or point dipoles which lie wholly outside it. Care must be taken in not extending this theory too far when the bonding between neighbours is more covalent than electrostatic, for the exchange of electrons overrides the assumption of "wholly external point charges".

Since the symmetry of the crystal field is determined by the symmetry of the point charges around the reference ion, the splitting of the energy levels of the latter can be evaluated qualitatively by group theoretical methods, although the magnitude and sign of the splitting can not be obtained in this way. Consider the free ion, one electron solutions to the Schrödinger equation.

These can be written in the general form:

$$\Psi = R(r).Y^{m}_{\ell}.\psi_{s}$$

where R(r) is dependent on the radial distance from the nucleus, and ψ_s is

the spatial independent spin function and Y^m_ℓ are spherical harmonics depending on the polar angles θ, ϕ. Under spherical symmetry Ψ is invariant, but in a crystal field which has a symmetry lower than spherical, this may not be the case. We derive first a representation for which the Ψ form a basis under full symmetry and then examine the ways in which this representation is reduced with respect to a lower symmetry group. For full spherical symmetry, the group of interest is the full rotation group in three dimensions which contains an infinite number of rotations about each of an infinite number of axes. Despite this, finite dimensional representations do exist. The simplest case occurs for rotations about the z axis. Since ψ_s is independent of orbital functions it can be ignored, as can R(r) since it has no angular dependence. Restriction of rotation to the z axis makes θ invariant also. For a rotation through angle α about the z axis we have the transformation $\theta \to \theta$, $\phi \to \phi + \alpha$, and the spherical harmonics $Y^m_\ell(\theta,\phi)$ become

$$Y^m_\ell(\theta,\theta + \alpha) = \exp(im\alpha)Y^m_\ell(\theta,\phi)$$

since

$$Y^m_\ell(\theta,\phi) = (-1)^m\left(\frac{(2\ell + 1)}{4\pi} \cdot \frac{|\ell - m|!}{(\ell + m)!} \cdot P_\ell^{|m|}(\cos\theta)\exp(im\phi)\right.$$

The transformation matrix acting on the column vector representing the Y^m_ℓ is therefore

$$\begin{bmatrix} e^{i\ell\alpha} & & & & \\ & e^{i(\ell-1)\alpha} & & & \\ & & e^{i(\ell-2)\alpha} & & \\ & & & \ddots & \\ & & & & e^{-i\ell\alpha} \end{bmatrix}$$

This has the character

$$\chi(\alpha) = \frac{\sin(\ell + \frac{1}{2})\alpha}{\sin(\ell/\alpha)} \qquad \text{for } (\alpha \neq 0).$$

Comparison of the characters of operations within this full rotation group with those taken from character tables of the required crystal symmetry will enable a reduction of the representation to be made. Consider for example the f-electron wave functions which have spherical harmonics of the form

$$Y^m{}_3(\theta,\phi) = (-1)^m \{\frac{7}{4\pi} \cdot \frac{(3-m)!}{(3+m)!}\}^{\frac{1}{2}} P_3^{(m)} \cos\theta \, e^{im\phi}$$

The rotation matrix of these functions for an angle α about the z axis has character

$$\chi(\alpha) = \frac{\sin 7\alpha/2}{\sin \alpha/2} .$$

If the atom or ion is placed in a square planar environment with ligands along the $\pm x$, $\pm y$ axes, or in an octahedral complex with a very large tetragonal distortion, the degeneracy of the f-electron levels is lifted. The ion in a square planar environment has point symmetry D_{4h}, for which the character table (rotations only) is:-

D_{4h}	E	$2C_4$	C_2	$2C_2'$	$2C_2''$
a_{1g}	1	1	1	1	1
a_{2g}	1	1	1	-1	-1
b_{1g}	1	-1	1	1	-1
b_{2g}	1	-1	1	-1	1
e_g	2	0	-2	0	0
a_{1u}	1	1	1	1	1
a_{2u}	1	1	1	-1	-1
b_{1u}	1	-1	1	1	-1
b_{2u}	1	-1	1	-1	1
e_u	2	0	-2	0	0

For these rotations, the characters of the full rotation group are

$\chi(E) = 7$, $\chi(C_4) = -1$, $\chi(C_2) = \chi(C_2') = \chi(C_2'') = -1$.

This representation is reducible to a linear combination of D_{4h} irreducible representations which can be shown to be $a_{2u} + b_{1u} + b_{2u} + 2e_u$. If rotations only were considered, the even (g) representations would fit equally well. However f-orbitals are not symmetrical under reflections in planes containing the C_4 axis, and consequently the uneven subscripts are added. In physical terms, this reduction in symmetry corresponds to a splitting of the f-orbital energy levels by the crystal field:- a single, sevenfold orbitally degenerate level is split into three singlet and two doublet levels.

This result derived for the one electron case is equally applicable to terms appropriate to a multi-electron system. The M_s value for one electron wave functions is replaced by M_s for many electron systems, and there is a direct correspondence in the behaviour under crystal fields between s and S, p and P, d and D and f and F electronic states. For example Co^{2+} has seven 3d electrons and has, according to Hund's rules, a ^4F ground state. In tetrahedral symmetry, T_d, the ^4F-state splits into a singlet and two triplets according to $A_2 + T_1 + T_2$. The terms "Gerade" or "Ungerade" now have no meaning since a tetrahedral environment lacks inversion symmetry.

By symmetry arguments alone, the decomposition of free ion terms in chemical environments can be explained, but to obtain information about the state energies, more quantitative methods must be employed. For instance, which of the three states of Co^{2+} is lowest in a tetrahedral field can be seen by considering the spatial relationship between the f electron orbitals and the ligand ions. The splitting of the F-state will then be analogous, except that we are dealing effectively with two d electrons outside a half filled shell. Although this may invert the order of the levels it will not alter the number of levels or the splitting between them.

The real forms of the f orbitals are obtained by taking the linear combinations of the imaginary parts of the solutions of the one electron Schrödinger equation. These can be divided into three types according to the directions in which the lobes point:- f_{xyz} is alone, having lobes directed towards each corner of a cube or through the faces

of an inscribed octrahedron; $f_{z(5z^2-3r^2)}$, $f_{x(5x^2-3r^2)}$, $f_{y(5y^2-3r^2)}$ have lobes directed along the axes, while $f_{x(y^2-z^2)}$, $f_{y(z^2-x^2)}$, $f_{z(x^2-y^2)}$ have lobes predominantly between the axes. Quantitatively, it can be seen that a tetrahedral distribution of charges, where ligands occupy alternate corners of a cube surrounding the ion, will leave the f_{xyz} orbital highest in energy owing to the repulsion between the electrons of the orbital and the negative ligands. The set of orbitals directed along the axes will be affected least by the crystal field, while the $f_{x(y^2-z^2)}$ type will lie intermediate in energy in the field. The result is that for one f-electron the A_2 singlet lies highest in energy, with the T_1 triplet level as the ground state.

For the "two electron" case of divalent cobalt the order of energy levels is inverted. This can be seen from a more rigorous treatment of the splitting, which leads to numerical values for the energy differences between levels as well as the wave functions for the orbitals involved. Consider the potential set up at the central ion by the surrounding ligands which in tetrahedral symmetry takes the form

$$V_{(xyz)} = \sum_{i=1}^{4} ez_i/r_{ij}$$

where r_{ij} is the distance of the i^{th} ligand with charge z_i from the central ion at point (xyz). Since the ligands are at the points $(\pm a/\sqrt{3}, \mp a/\sqrt{3}, a/\sqrt{3})$ and $(\pm a/\sqrt{3}, \mp a/\sqrt{3}, -a/\sqrt{3})$, where a is the dimension of the unit cube, $V_{(xyz)}$ can be evaluated in terms of spherical harmonics up to order six. The resulting expression can then be used as the perturbation on the electronic term the Hamiltonian. A secular

determinant may be set up and solved, the eigenvalues of which are the energies of the levels split by the crystalline field. Eigenfunctions corresponding to these energies may also be derived.

The example of the Co^{2+} ion serves to illustrate the characteristic behaviour of an ion in a weak to medium crystal field. It is not intended as a comprehensive treatment of the subject, nor should it be assumed that other ions behave similarly. Each case has to be treated individually, and although many similarities arise between different ionic members of the transition groups, the final ground state depends intimately on the ion and the crystal field in which it resides. Specific cases of interest in this work will be treated in greater detail later, where appropriate.

The presence of the crystal field results in one ionic energy level being lower than the others. It is in this level that electronic transitions can be excited under suitable conditions. It is not usual for the ground state to retain a high degree of orbital degeneracy, since this is often removed by the crystal fields of lower symmetry, or by spin-orbit interaction. There results a further splitting of the levels.

As a simple illustrative example consider a reference ion surrounded by six negative ligand ions equidistant along the ±x, ±y and ±z axes. The central ion then resides in a field of octahedral symmetry O_h. If the ion has four d electrons giving rise to a free ion ^5D ground term, a ^5E_g term will be lowest if the crystal field is not too strong. Suppose now that the ligands on the ±z axes are pulled further out, resulting in a tetragonal distortion and D_{4h} symmetry. The orbital

doublet ground state splits into two orbital singlets $^5B_{1g}$ and $^5A_{1g}$, while the triplet upper level, $^5T_{2g}$ in the octahedral field, splits into ^5E_g and $^5B_{2g}$. The same result can be obtained qualitatively and less rigorously by inference from the effect of field distortions on the electron d-orbital energies. The lowest orbital singlet is still five fold degenerate in spin, but will be further split by fields of orthorhombic symmetry or by spin-orbit coupling. If the splitting is not too great, resonance transitions may be observed between the spin levels.

It is useful at this stage, as a guide to discovering the nature of the final ground state of an ion in a crystalline lattice, to introduce two theorems due to Kramers, and to Jahn and Teller respectively.

Kramers' theorem states that in a system containing an odd number of electrons there will always be levels left with at least a two-fold spin degeneracy in the presence of an electric field, no matter what the symmetry. This degeneracy is related to the invariance of the system under time reversal provided magnetic fields are not present. In the absence of a magnetic field, the Hamiltonian contains only even powers of the momenta of electrons, since for example kinetic energy = $P^2/2m$. On time reversal, the energy is unchanged in sign. But with a magnetic field present the linear term $\beta\underline{H}(\underline{L} + 2\underline{S})$ is included, which suffers a change in sign with time reversal. This implies a lifting of the spin degeneracy by a magnetic field.

By applying the time reversal operator T to the eigenfunctions of an electron system it can be shown that Ψ and $T\Psi$, which belong to

the same electron level, since ψ and T commute, are linearly independent only if n is odd. If n is even, the level degeneracy is lifted by an electric field.

The Jahn and Teller theorem indicates that non-linear molecules or complexes with orbitally degenerate ground states will distort spontaneously to remove all or part of this degeneracy. Kramers' doublets are not affected since they are not spatially degenerate. The reason for the distortion is the lowering of the energy of the system. The simple case of a d^9 complex in an octahedral field can be considered. This has a lower filled T_{2g} level and an upper E_g level containing three electrons. These electrons can have two configurations:-

$$d(x^2 - y^2)^2\ d(z^2)^1 \quad \text{or} \quad d(x^2 - y^2)^1\ \ d(z^2)^2,$$

where $d(x^2 - y^2)$, $d(z^2)$ represent the d electron orbitals with lobes pointing along the x and y axes and along the z axis, respectively. In the first configuration the ligands along $\pm z$ will be less strongly repelled than those along the other coordinate axes. A more stable structure will result if the complex distorts by a lengthening of the $\pm x$, $\pm y$ bonds. Similarly, the ionic environment will be more stable in the second configuration if the $\pm z$ bonds lengthened. Which of these possibilities occur is not obvious. A distortion along a fixed direction would result in a static Jahn-Teller effect, whereas if the structure resonated between them, a dynamic effect exists. Whether the distortion is static or dynamic, there results a lowering of the symmetry at the ionic site, and a consequent lifting of orbital degeneracy of the levels.

It may be instructive to note the complexes in which Jahn-Teller distortions are anticipated. Considering again octahedral symmetry, it is clear that no distortion occurs for spherical distribution of electrons. In the 3d group the spherical symmetric ions are $3d^3$, $3d^5$ (weak field), $3d^6$ (strong field), $3d^8$ and $3d^{10}$. If an electron is removed from any of these, a non-spherical charge distribution occurs. The complexes in which distortions can be expected are set out below. Since the T_{2g} orbitals are little influenced by the ligands, the greatest distortions occur when there is an odd number of Eg electrons. This is not necessarily the case when there is extensive covalent bonding between the central ion and its neighbouring ligands.

Strong Jahn-Teller Effect:

High Spin	d^4 $(T_{2g})^3$ $(E_g)^1$	Cr^{2+}, Mn^{3+}
Low Spin	d^7 $(T_{2g})^6$ $(E_g)^1$	Co^{2+}, Ni^{3+}
	d^9 $(T_{2g})^6$ $(E_g)^3$	Cu^{2+}, Ag^{2+}
High Spin	d^6 $(T_{2g})^4$ $(E_g)^2$	Fe^{2+}

Weak Jahn-Teller Effect:

	d^1 $(T_{2g})^1$ $(E_g)^0$	Ti^{3+}, Sc^{2+}
	d^2 $(T_{2g})^2$ $(E_g)^0$	V^{3+}
Low Spin	d^4 $(T_{2g})^4$ $(E_g)^0$	Cr^{2+}, Mn^{3+}
Low Spin	d^5 $(T_{2g})^5$ $(E_g)^0$	Fe^{3+}

2.2 Spin-Orbit Coupling

As we have seen, crystal fields, whether they be purely of one symmetry or a combination of more than one, give a ground state which is orbitally non-degenerate, but still degenerate in spin. The magnetic field will split the spin states, enabling E.P.R. transitions to be induced between them. Before these levels can be fully defined, the effect of spin-orbit coupling must be considered. Mention was made at the beginning of Chapter I, that the resultant angular momentum of an electron can be made up of spin plus orbital angular momenta which are added together through the effect of spin-orbit coupling. This coupling arises, since the moving electron in the electric field of the nucleus experiences an effective magnetic field. The electron spin interacts with this orbitally derived field, giving overall an effective coupling between spin and orbital angular momenta. The operator representing the perturbation by spin-orbit coupling is, for one electron, $\zeta \underline{\ell}.\underline{s}$ where the coupling parameter ζ can be shown to be

$$\zeta = \frac{Z_{eff}e}{2m^2c^2} \cdot \overline{r^{-3}}$$

where r is the radius of the d electron orbital.

For a term, the one electron operator is summed over all the electrons to give the familiar result

$$\sum_i \zeta_i \underline{\ell}_i \cdot \underline{s}_i = \lambda \underline{L}.\underline{S}$$

where $\lambda = \pm\zeta/2S$.

This result is only exactly true when the electric field experienced by

the electrons is spherically symmetric. The approximation is good enough for ions in weak or medium crystal fields, but breaks down in the presence of extensive covalent bonding. The effect of spin-orbit coupling on the electronic ground state can be found by applying $\lambda \underline{L}.\underline{S}$ as a perturbation since we are dealing with crystal fields of only medium strength. The resulting ground state contains an admixture of the higher levels, and consequently there is a partial reinstatement of orbital angular momentum. The latter was, we remember, quenched by the medium crystal field. The amount of orbital angular momentum mixed into the perturbed ground state is of order λ/Δ where Δ is the crystal field splitting. It is clear that because of this admixture, transition metal ions do not behave exactly as spin only paramagnets. On the other hand, rare earth ions have considerable amounts of orbital angular momentum in their ground state since spin-orbit coupling is a major contributor to ground state energy. Therefore the E.P.R. spectra depart rather less from pure spin phenomenon for the transition ions than for the rare earth ions.

2.3 Other Interactions affecting the Ground State

There are a few other contributions to the ground state energy, that can be considered prior to the introduction of an external magnetic field. They are much less important than the crystal field effects and spin-orbit coupling, and may give energy shifts several orders of magnitude smaller. The first such effect occurs when the ion possesses a nuclear spin, $I > 0$, which can interact with the electronic spin to produce hyperfine structure. Nuclear hyperfine structure may be divided

into two parts. Firstly the anisotropic or magnetic dipole term may be written as

$$H'_{SI} = g\beta g_N \beta_N \left[\frac{\underline{S}.\underline{I}}{r^3} - \frac{3(\underline{S}.\underline{r}).(\underline{I}.\underline{r})}{r^5} \right]$$

where g, g_N are the electronic and nuclear g-values and β, β_N the Bohr (electronic) and nuclear magnetons respectively, $\underline{r}$ is the separation between the electron and nucleus, and $\underline{S}$,$\underline{I}$ are the electronic and nuclear spins respectively. This is a purely classical effect. When $\underline{S}$ and $\underline{I}$ are quantised along $\underline{H}_o$ this expression can be written to first order as

$$H'_{SI} = gg_N\beta\beta_N \left\langle \frac{3\cos^2\theta - 1}{r^3} \right\rangle S_z I_z ,$$

θ being the angle between $\underline{r}$ and $\underline{H}_o$. Secondly an isotropic interaction derived from the relativistic Dirac equation and known as the Fermi contact term, takes the form:-

$$H''_{SI} = \frac{8\pi}{3} \cdot gg_N\beta\beta_N |\psi^2(0)| \underline{S}.\underline{I}$$

Since $\psi^2(0)$ represents the unpaired electron spin density at the nucleus, H''_{SI} has non-zero values only when there is a finite probability of an electron being found at the nucleus. We should only expect contact hyperfine interaction then, if the electron were in an s-like orbital. Nuclei with spin $I > \frac{1}{2}$ also possess a quadrupole moment, which interacts electrostatically with the electric field gradient produced by the surrounding valence electrons and other nuclei. The effect is to shift the hyperfine energy levels and to enable otherwise forbidden transitions between hyperfine levels to occur.

The above types of electron-nuclear coupling have counterparts when interactions between electrons are considered. The appropriate dipole-dipole interaction is

$$\mathcal{H}'_{SS} = g^2\beta^2\left[\frac{\underline{S}_1\cdot\underline{S}_2}{r^3} - \frac{3(\underline{S}_1\cdot\underline{r})(\underline{S}_2\cdot\underline{r})}{r^5}\right]$$

whilst the exchange interaction may be written as $\mathcal{H}''_{SS} = J_{12}\underline{S}_1\cdot\underline{S}_2$. The coefficient J_{12} is defined as

$$J_{12} = \iint \psi_1(r_1).\psi_2(r_2).\frac{e^2}{r_{12}}.\psi_1(r_2).\psi_2(r_1)d\tau_1 d\tau_2$$

and represents the exchange integral for a two centre system. These interactions are considered in greater detail later.

2.4 Magnetic Field Effects

When a magnetic ion is placed in an external magnetic field $\underline{H}_o$ the vectors $\underline{S}$, $\underline{L}$ and $\underline{I}$ are scalar coupled to $\underline{H}_o$ as in the Zeeman effect, while $\underline{r}$ is vector coupled to $\underline{H}_o$ giving rise to diamagnetism. The electronic Zeeman term in which originates the electron paramagnetism is given by

$$\mathcal{H}_z = \beta\underline{H}_o.(\underline{L} + g_e\underline{S}),$$

where g_e is the free spin g-value. The corresponding nuclear Zeeman term is

$$\mathcal{H}_N = g_N\beta_N\underline{H}_o.\underline{I}.$$

The diamagnetic term may be written as

$$\frac{e^2}{8mc^2} \sum_i (\underline{H}_o \times \underline{r}_i)^2$$

Since it shifts all levels equally it is usually neglected. Since for E.P.R. $\mathcal{H}_N$ is also small, it is neglected except in cases where it is a convenient thumb-print for the atomic species concerned. Thus the electronic Zeeman term is the dominant interaction between the magnetic field and the electronic ground state. The significance of $\mathcal{H}_z$ is that it describes the splitting of the spin degenerate ground state.

2.5 The Spin Hamiltonian

It is helpful at this stage to summarise the terms in the total Hamiltonian which describe the ion in the crystal field when subjected to an external magnetic field. The total Hamiltonian is written as

$$\mathcal{H} = \mathcal{H}_1 + \mathcal{H}_c + \mathcal{H}_{LS} + \mathcal{H}_z + \mathcal{H}_{SS} + \mathcal{H}_{SI}. \qquad (2.1)$$

$$\mathcal{H}_1 = \left[\sum_i \left(\frac{p_i^2}{2m} - \frac{Ze^2}{r_i}\right) + \sum_{i<j} \frac{e^2}{r_{ij}} \right]$$

contains the electronic kinetic energy, nuclear attraction and coulomb repulsion between electrons. These interactions result in the splitting of a given electron configuration into terms. When the ion is placed in a medium crystal field, $\mathcal{H}_c$ comes into play and the terms are split into energy levels. These levels are in turn modified by $\mathcal{H}_{LS} = \lambda \underline{L}.\underline{S}$ and finally split by $\mathcal{H}_z = \underline{H}(\underline{L}+2\underline{S})$ into spin levels. In some cases it is necessary to consider interactions between electron spins, and for

this reason $\mathcal{H}_S$ is included. These spin levels may be further split if a hyperfine interaction $\mathcal{H}_{SI}$ is present. Contributions from nuclear Zeeman, electric quadrupole and diamagnetic terms are small.

The contributions to the final state energies of the levels between which magnetic resonance transitions are induced may now be listed in descending order of magnitude.

$\mathcal{H}_l \sim 10^5 \text{ cm}^{-1}$
$\mathcal{H}_c \sim 10^4 \text{ cm}^{-1}$
$\mathcal{H}_{LS} \sim 10^2 \text{ cm}^{-1}$
$\mathcal{H}_Z \sim 1 \text{ cm}^{-1}$
$\mathcal{H}_{SS}$ zero to 10^3 cm^{-1} (Includes interionic exchange)
$\mathcal{H}_{SI} \sim 10^{-2} \text{ cm}^{-1}$

Thus only the lowest term associated with $\mathcal{H}_l$ is investigated by paramagnetic resonance. The collective effect of crystal field and spin-orbit coupling on this lowest term is to produce a number of levels between which the resonance transitions are observed. The number of these levels is not necessarily related to the free ion spin value owing to the complex splitting and mixing to which the electron configuration is subject in the crystal field. For this reason it is customary to speak in terms of a "fictitious spin" being associated with the lowest set of energy levels. A spin $\hat{S}$ is assigned when there are $2\hat{S}+1$ levels, whether or not these are pure spin states. It is the number of states produced by a magnetic field which is the important factor.

This fictitious spin is used in an "effective spin Hamiltonian" which describes the paramagnetic resonance properties of the system, without going into details of the complicated interactions that give rise to it. The effective spin Hamiltonian is derived from the general Hamiltonian by applying perturbation theory in second order to the orbital levels only, leaving electronic and nuclear spin operators alone. No representation is chosen for $\underline{S}$ and $\underline{I}$ and the resulting expression in $\underline{S}$ and $\underline{I}$ is the required spin Hamiltonian. The actual energies of the lowest group of levels are the eigenvalues of this derived operator.

Considering a simplified form of the general Hamiltonian (2.1), the perturbation on the crystal field ground state is of the form

$$\mathcal{H}' = \mathcal{H}_{LS} + \mathcal{H}_Z + \mathcal{H}_{SI}.$$

We have omitted $\mathcal{H}_{SS}$ since it will be treated in greater detail later. $\mathcal{H}'$ may be written as[3]

$$\beta\underline{H}.(\underline{L} + g_e\underline{S}) + \lambda\underline{L}.\underline{S}. + A\underline{I}.\underline{S}.$$

A second order perturbation involving the ground state $|0\rangle$, which is considered orbitally non-degenerate, and excited states $|n\rangle$ leads to an expression of the form

$$\mathcal{H}_S = \beta(g_e\delta_{ij} - \lambda\Lambda_{ij})H_iS_i + A\underline{I}.\underline{S} - \beta^2\Lambda_{ij}H_iH_j - \lambda^2\Lambda_{ij}S_iS_j$$

where δ_{ij} is the Dirac delta function and Λ_{ij} is defined as

$$\Lambda_{ij} = \sum_{n\neq 0} \frac{\langle 0|L_i|n\rangle\langle n|L_j|0\rangle}{E(n) - E(0)}$$

The indices i, j refer to cartesian coordinates. $\mathcal{H}_S$ can be written in the more concise form

$$\mathcal{H}_S = \beta \underline{H}.\tilde{g}.\underline{S} + A\underline{I}.\underline{S} - \beta^2 \underline{H}.\tilde{\Lambda}.\underline{H} + \underline{S}.\tilde{D}.\underline{S} ,$$

where $\tilde{g}$, $\tilde{\Lambda}$ and $\tilde{D}$ are second rank tensors.

The first term is the energy of a spin system in a magnetic field described in terms of the g-tensor which may be anisotropic. The angular momentum operator which had previously appeared is taken into account in this second rank tensor. The previous coupling between $\underline{L}$ and $\underline{H}$ has been replaced by an overall anisotropic coupling between $\underline{S}$ and $\underline{H}$. The second term represents the hyperfine interaction. Since the third term, which represents a paramagnetic susceptibility is spin independent, it is usually ignored for the purposes of E.P.R. The fourth and final term in equation (2.1) is the second order effect of the spin orbit coupling which for anisotropic $\tilde{\Lambda}$, represents a zero field splitting of the energy levels. To see how this arises, consider a weak anisotropy resulting from an axis of symmetry. We can then write

$$\Lambda_{zz} = \Lambda_{||}, \quad \Lambda_{xx} = \Lambda_{yy} = \Lambda_{\perp}$$

The other tensor components are zero.

Then

$$\underline{S}.\tilde{D}.\underline{S} = -\lambda^2 \Lambda_{ij} S_i S_j$$

reduces to

$$-\lambda^2 \left[\Lambda_{||} S_z^2 + \Lambda_{\perp} (S_x^2 + S_y^2) \right]$$

This can be rewritten after some manipulation as

$$\tfrac{1}{3}S(S+1)\lambda^2(\Lambda_{||} + 2\Lambda_{\perp}) + D\left[S_z^2 - \tfrac{1}{3}S(S+1)\right]$$

with $D = \lambda^2(\Lambda_{\perp} - \Lambda_{||})$.

The splitting of levels in the absence of a field arises out of the second term since the first term represents a constant shift of all the energy levels. For the case of $S = \frac{3}{2}$ the level $M_s = \frac{3}{2}$ is separated from the level $M_s = \frac{1}{2}$ by $D\left[(\frac{3}{2})^2 - (\frac{1}{2})^2\right] = 2D$.

Fields of orthorhombic symmetry imply $\Lambda_{zz} \neq \Lambda_{xx} \neq \Lambda_{yy}$ and the other elements zero. This results in a term $E(S_x^2 - S_y^2)$ being necessary to describe further splittings of the levels. For this case of orthorhombic symmetry, the spin Hamiltonian can be written in terms of components, making the assumption that the same principal axis system applies to all terms. It takes the form

$$\mathcal{H}_S = \beta(g_z H_z S_z + g_x H_x S_x + g_y H_y S_y) + D\left[S_z^2 - \tfrac{1}{3}S(S+1)\right] + E(S_x^2 - S_y^2) + A_z S_z I_z + A_x S_x I_x + A_y S_y I_y .$$

To obtain the energy levels from this spin Hamiltonian we have to solve the secular equation $\mathcal{H}_S\psi = \varepsilon\psi$ to find the eigenvalues ε. Alternatively, if the terms in D, E and A are very much smaller than the Zeeman term a perturbation procedure may be adopted to find the resultant energies. These methods will be applied to specific examples of interest in this work, in the later chapters.

To summarise, the importance of the spin Hamiltonian lies in the fact that it is possible to give a concise description of experimental results without recourse to a detailed description of the physical mechanisms giving rise to them. Thus g_x, g_y, g_z, D, E, A_x, A_y, A_z are related to the experimental results. It is then up to the theoretician to relate them to the interactions within the system in question.

REFERENCES

1. H.A. Bethe, Ann. Physik., 3, 133 (1929).

2. J.H. van Vleck, J. Chem. Phys., 3, 807 (1935).

3. B. Bleaney and K.W.H. Stevens, Rep. Prog. Phys., 16, 125ff. (1953).

CHAPTER III

MAGNESIUM OXIDE AND $3d^3$ IONS

3.1 The Host Lattice

We discuss first the nature of the host lattice, since its role is not altogether a passive one. The diamagnetic ions Mg^{2+} and O^{2-} both have the neon closed - electron-shell configuration. The bonding between ions in the lattice is highly ionic and consequently magnesium oxide is an insulator with a large band gap. The crystalline form is unreactive with water and air at room temperature, so can be kept without taking special precautions. It provides an ideal medium for studying the E.P.R. of paramagnetic species.

The structure is face centred cubic, the divalent anions and cations being situated respectively at the vertices of two interpenetrating sublattices of face centred cubic form. The unit cube of the oxide is composed of four magnesium-oxygen units situated at the following positions:

Mg^{2+} $(0,0,0)$; $(0,\frac{1}{2},\frac{1}{2})$; $(\frac{1}{2},0,\frac{1}{2})$; $(\frac{1}{2},\frac{1}{2},0)$.

O^{2-} $(\frac{1}{2},0,0)$; $(0,\frac{1}{2},0)$; $(0,0,\frac{1}{2})$; $(\frac{1}{2},\frac{1}{2},\frac{1}{2})$.

The vertices of the unit cell of the bravais lattice can then be defined by the points (0,0,0); (1,0,0); (0,1,0); (1,1,0); (0,0,1); (1,0,1); (0,1,1); (1,0,1). For pure MgO, the length of a [100] type edge is 4.21Å [1]. This is the distance between next nearest neigbour magnesium

ions, while the distance between nearest neighbours along a [110] axis is 2.97Å. Since the ionic radii [2] of Mg^{2+} and O^{2-} are respectively 0.65Å and 1.40Å, the radius of the largest sphere that can be fitted between the atoms in the lattice is 0.09Å. This implies that all impurities entering the perfect crystal, whether as atoms or ions, are of substitutional type since all covalent and all ionic radii for the elements except H^+ exceed this value. In reality, perfect crystals are virtually non-existent and impurities may lodge for example at dislocations or in regions of modified crystal structure. However paramagnetic species at substitutional sites will produce spectra whose intensities will sum coherently over all the similar sites in the crystal. This is unlikely to be the case for spins at randomly oriented macroscopic defects, so in E.P.R. the perfect crystal ideology is followed.

The range of ions detected by E.P.R. in magnesium oxide is large. All ions of the first transition series except scandium have been identified in one valence state or another. There is no evidence to suggest that scandium exists in ionic form in other than the trivalent state, in which case it is diamagnetic. No discussion of the resonance of transition metal ions apart from those with 3d electrons will be entered into here. A recent review paper [3] contains references for work up to 1968 on these species in alkaline earth oxides. The transition metal ions with three 3d electrons are Ti^+, V^{2+}, Cr^{3+} and Mn^{4+}. Any others, e.g. Fe^{5+}, Co^{6+} are not known. The ionic radii of these ions is 0.96, 0.72, 0.64 and 0.52 respectively. It is clear from the existence of their spectra that the last three substitute readily for

Mg^{2+} in the magnesium oxide lattice. Their size is not too different from the 0.65Å radius of Mg^{2+}. But Ti^{+} is too large to enter a magnesium site without seriously deforming the lattice. Furthermore, the univalent state is apparently unstable, so spectra from this ion are unlikely to be observed in this host. A short lived spectrum attributed to Ti^{+} has been observed in irradiated CaO[4], but in this case the size of the substituent differs only slightly from the 0.99Å radius of the calcium ion.

Magnesium oxide crystals may be grown from the melt, but owing to the melting point being near 2800°C, an electric arc is normally required to cause fusion. Small quantities of a desired impurity may be incorporated into the crystal by thoroughly mixing the oxide of the desired transition metal into the starting powder. The magnesium oxide must be of the highest possible purity since this substance almost always contains paramagnetic ions in its commercial state[3]. In addition to the transition metal oxide, other additives may be included to provide alternative charge compensation for the paramagnetic centre should this be necessary. This will be discussed at greater length later. The thoroughly mixed powder is compressed around two or more carbon electrodes in a firebrick crucible and an arc struck. A region of molten oxide is formed in the vicinity of the electrodes whereas the outer layers of powder generally remain solid during the operation. This prevents rapid cooling of the liquid zone, thereby enabling large crystals to form on solidification. These crystals are of varying size, and the degree of doping varies through the melt, being greatest nearer the position of the electrodes. As an example, some MgO doped initially

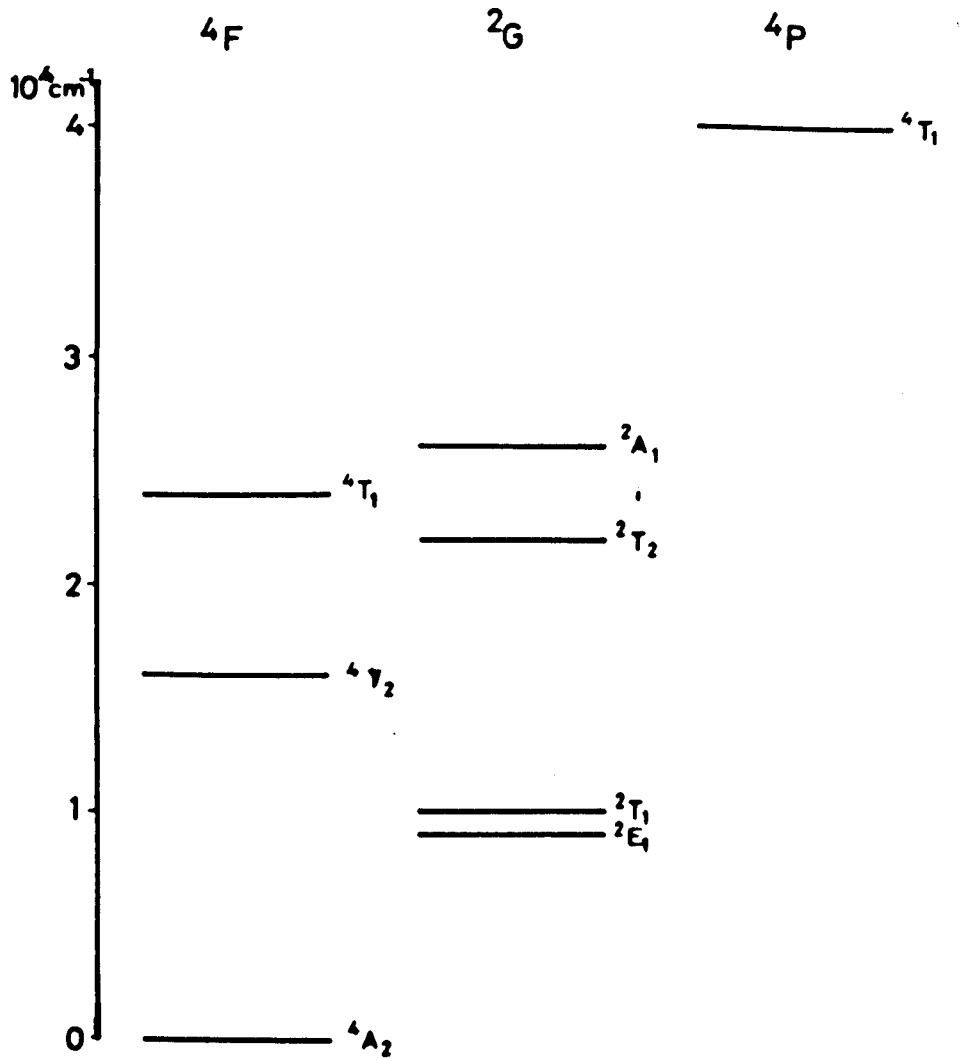

FIGURE 3.1 LOWEST ENERGY LEVELS OF A $3d^3$ ION IN AN OCTAHEDRAL FIELD, $\Delta = 17{,}000\ cm^{-1}$. (AFTER TANABE AND SUGANO, REF. 5)

with V_2O_5 showed predominantly pale green crystals throughout most of the boule. Nearer the electrodes however, the melt appeared black. It was in these black crystals that spectra attributable to next nearest neighbour super-exchange coupled V^{2+} pairs were observed.

3.2 The $3d^3$ Ions

Before discussing the spectra so far observed for $3d^3$ ions in magnesium oxide the origin of the ground level will be briefly explained. This electron configuration, having three d electrons outside an argon closed shell, will according to Hund's Rule give a ^4F ground term with excited levels ^4P, ^2G, ^2H etc. above it. In a crystal field these terms will be split, the ordering of the levels so produced depending on both the strength and symmetry of the crystal field [5]. For MgO, the crystal field is octahedral and for a 3d ion such as V^{2+} the strength of the field is intermediate, and stronger than the spin-orbit coupling, In this O_h symmetry, the ^4F term is split into $^4A_2 + {}^4T_1 + {}^4T_2$, the ^4P term becomes $^4T_1$ and the ^2G term splits into $^2E + {}^2T_1 + {}^2A_1 + {}^2T_2$. The order of levels is shown in figure (3.1). For octahedral symmetry the orbital singlet which arises from the ^4F term always lies lowest. The ^2G term gives rise to the excited ^2E level. The Tanabe and Sugano energy level diagrams [5] give a more complete picture of the ordering of levels, while Runciman and Schroeder [6] calculate values of the energy levels for Cr^{3+} in MgO.

The $^4A_{2g}$ level which is the only one populated under normal conditions is four fold spin degenerate. In an applied magnetic field

the four spin levels $\pm 3/2$, $\pm 1/2$ will diverge linearly with field and E.P.R. transitions may be induced between them. In octahedral symmetry there are three allowed transitions, all of which occur at the same field. Thus only one resonance line is observed. The g-value is expected to have a spin only value since we are dealing with an orbitally non-degenerate state, but there is some reinstatement or orbital angular momentum into the ground state owing to spin-orbit coupling from predominantly the $^4T_2$ level. This lowers the g-value to about 1.98. When the electric field symmetry is lower than octahedral, the levels now termed loosely as $\pm 3/2$ and $\pm 1/2$, will be split even in the absence of a magnetic field. Three transitions for each centre will be possible, the outer two showing a first order dependence on the angle between the axis of the centre and the direction of the applied magnetic field. If the ion has isotopes with nuclear spin, hyperfine structure is expected on each resonance line.

3.3 The $3d^3$ Ions in MgO - A Brief Review

The E.P.R. spectrum of V^{2+} in magnesium oxide was first reported by Low[7], who observed a group of eight hyperfine lines centred at g = 1.9803 and with A = 80.3 gauss. Each of these lines was split into a triplet which Low ascribed to the effects of small deviations from cubic symmetry. This is not the origin of the zero field splitting, since the satellites are isotropic in position, though not in line width. Subsequently Weiringen and Rensen[8] correctly ascribed the splitting to second and third order terms in the hyperfine interaction.

They explained the change in linewidth by introducing small terms in D and E that described the distortions from cubic symmetry. It was necessary to assume that the magnitude of these distortions varied from centre to centre resulting in slightly different energy levels for different ions. The observations that the linewidth of the central $\frac{1}{2} \rightarrow -\frac{1}{2}$ line was isotropic and that the satellites have minimum linewidths along the [100]-directions is consistent with the z axis of the distortion being a [111]-direction. The linewidth varies as $\Delta H = \Delta D(M-\frac{1}{2})(3\cos^2\theta-1) + 3\Delta E \sin^2\theta\cos\phi$, where $\Delta D = \pm 2$ gauss, $\Delta E < 0.7$ gauss. The spin Hamiltonian describing this behaviour may be written in the form

$$\mathcal{H} = g\beta\underline{H}\underline{S} + A\underline{I}.\underline{S} + D(\underline{S}_\zeta^2 - 5/4) + E(\underline{S}_\xi^2 - \underline{S}\eta^2)$$

where ζ, ξ, η are [111], [1$\bar{1}\bar{1}$] and [01$\bar{1}$] axes.
Weiringen and Rensen did not find it necessary to include third order spin terms, e.g. $\underline{H}.\underline{S}^3$ to fit the Hamiltonian to the spectra. They were however introduced recently by Wijn and Schrama[9] to explain the results of ENDOR measurements on V^{2+} in MgO.

More recent work than Weiringen and Rensen's suggests that the small distortions are not caused by impurities other than vanadium in non-localmagnesium sites. Dickey and Drumheller[10] have observed forbidden hyperfine spectra occurring as small doublets between the main allowed lines. These are due to transitions of the type $|\frac{1}{2},m+1\rangle \rightarrow |\frac{1}{2},m\rangle$ and $|\frac{1}{2},m\rangle \rightarrow |-\frac{1}{2},m+1\rangle$ and lie between the $|\frac{1}{2},m\rangle \rightarrow |-\frac{1}{2},m\rangle$ lines, where m labels the hyperfine levels, with $7/2 \geq m \geq -7/2$. The intensity of these forbidden lines is proportional to $(D \sin 2\theta)^2[6\frac{3}{4} - m(m+1)]$.

Their appearance in the E.P.R. spectrum confirms the existence of a zero field splitting and their intensity affords a measure of its magnitude. The size of D was found to be sample dependent, and the principle direction of the distortion was not exclusively along the body diagonal. The experimental evidence suggested that the magnitude of the distortion depended on the vanadium concentration in the crystal.

In MgO the stable state of vanadium is observed to be the trivalent form. Sturge[11] noted that the optical absorption spectrum of V^{2+} is generally too weak to be observed in as received MgO crystals above the background of V^{3+}. However, heating to 1200°C in hydrogen increases the intensity of the divalent ion spectrum relative to that of V^{3+}. The tendency for the oxidation-reduction reaction of vanadium to occur in MgO has also been noted by various other workers[12,13]. Heating in oxygen favours the higher valence state, while heating in vacuum, hydrogen, or subjection to ionising radiation produces V^{2+}. The degree of change from one oxidation state to another depends both on the crystal impurity content and on the duration of the particular treatment. Nevertheless the fact remains that V^{2+} and V^{3+} co-exist in vanadium-doped magnesium oxide. Consequently in heavily doped crystals the V^{3+} ions may effectively distort the symmetry at the V^{2+} sites. On the other hand the distortions may result from charge compensating vacancies remote from the V^{3+} ion.

That charge compensation for aliovalent impurities need not be localised is evidenced by the observation of Cr^{3+} in octahedral symmetry sites. Low[14] reported the spectrum of Cr^{3+} in MgO and indicated that

the chromium plus the six nearest neighbour oxygens form a tightly knit unit with some covalent bonding. This apparently stabilises the charge misfit. The occurrence of vacancies associated with Cr^{3+} in MgO has been suggested by Wertz and Auzins[15]. They find two centres in addition to the cubic one, these having lower symmetry and being associated with neighbouring magnesium vacancies along [100] and [110]-type crystal directions. Since one vacancy will compensate for two Cr^{3+} ions, it is not surprising to find purely cubic symmetry sites in addition to those with local distortions. Spectra observed from the first type of centre, later denoted by T_1, showed axial symmetry about a [100] crystal axis and could be fitted to a Hamiltonian $\mathcal{H} = \beta \underline{H}.\tilde{g}.\underline{S} + D\left[S_z^2 - \frac{5}{4}\right]$ with $g_{\parallel} = g_{\perp} = 1.9782$ and $D = 0.08194\ cm^{-1}$. No E term was required.

Since Cr^{53} has a nuclear spin $I = \frac{3}{2}$, with isotopic abundance 10%, four weak lines are also observed centred on the main transition. These lines are accounted for by including a term $A\underline{I}.\underline{S}$ in the Hamiltonian with $A = 16.2 \times 10^{-4} cm^{-1}$. In addition, a very small effect on the crystal field splitting energy for different isotopes has been measured by Marshall et al.[16]. They find that D for Cr^{52} ($I = 0$) is some 0.1 gauss greater than for Cr^{53} ($I = \frac{3}{2}$). This is attributed to effects of the different isotopic masses on the dynamics of the crystal structure.

The other Cr^{3+} centre in MgO was not fully investigated, but Griffiths and Orton[17] independently observed the spectrum and attributed it to a Cr^{3+} ion in orthorhombic symmetry. The Hamiltonian parameters were given as $D = 0.031 cm^{-1}$, $E = 0.22 cm^{-1}$ with z along an [001] axis. A simple transform of z to the principal axis of distortion would give

$E \leq \frac{1}{3}D$, which complies with the current convention. The much larger splitting than in the tetragonal site was accounted for by the closer proximity of the defect to the paramagnetic centre. In the absence of any other suitable charge compensating impurities the authors came to to the same conclusion as Wertz and Auzins, that the model consisted of a positive ion vacancy in a nearest positive ion position. In addition to the axial spectrum of Cr^{3+} already mentioned, Henderson and Hall[18] have found an associated weaker set of lines which is always present, the intensity depending on the sample. These show an angular dependence of the same sort as the type 1 spectra and can be fitted to a similar Hamiltonian with $D = 798 \times 10^{-4} cm^{-1}$. The spectrum was reproduced when a crystal was grown from a MgO melt containing 0.1% Al_2O_3 in addition to the 0.1% Cr_2O_3. Independent work by Wertz and Auzins, 1967,[19] has revealed the same associated tetragonal (T') centre and also a further rhombic centre (R') with similar symmetry to the centre investigated by Griffiths and Orton. Both pairs of 1967 workers agree that the structure of the T' centre is of a charge neutral configuration where three neighbouring cation sites along a [100] axis have respectively Cr^{3+}, Mg^{2+} vacancy and Al^{3+} ions. This geometry provides charge compensation and the required tetragonal symmetry. The R' centre consists of the same three collinear species, but lying along a [110] direction, to give orthorhombic symmetry.

These doubly associated centres appear to be more stable than the effectively charged T and R centres since heating of Al doped crystals to 400° favours their formation at the expense of the singly

associated defects. This decrease is evidenced by the D and E splitting parameters which are lower for the T' and R' centres than for the T and R species.

The series of known $3d^3$ ions is completed with tetravalent manganese. Spectra from this ion have been observed only in powders until recently. Nakada et al.[20] and Henderson and Hall[18] have reported spectra from cubic Mn^{4+} in MgO powder which had been doped with manganese chloride and lithium chloride prior to firing. The latter authors also found evidence for the existence of Mn^{4+} sites with tetragonal distortion. Since there was a large amount of lithium in the crystal they attributed the departure from octahedral symmetry as being due to a Li^+ ion in a next nearest neighbour Mg^{2+} site. That the tetragonal distortion was due to a next nearest neighbour magnesium ion vacancy seemed unlikely since the zero field splitting $D = 0.028cm^{-1}$, is considerably different from that of the Cr^{3+} T centre in MgO for which $D = 0.082cm^{-1}$.

Davies et al.[21] confirm the existence of resonances from octahedral sites in powders and give values of the spectral parameters as $g = 1.9941$, $A = -70.82 \times 10^{-4}cm^{-1}$. These compare favourably with values given by the previous authors. A further tetragonal spectrum arising from Mn^{4+} in single crystals of MgO was observed. The tetravalent manganese was produced by heat treatment and X irradiation of these crystals which were undoped and had low paramagnetic impurity concentrations. The g and A factors of the spectra were similar to those of Mn^{4+} in already known sites but the D term had a value of $-529 \times 10^{-4}cm^{-1}$. This differs considerably from the values of D for the Li^+ compensated

centre of Henderson and Hall, and from the Cr^{3+} T centre. But in view of the absence of any other impurity in high concentration it seemed probable that the tetragonal field was caused by a next nearest neighbour magnesium ion vacancy. The charge neutral configuration would be expected to confer stability on the centre. A rough comparison of the effects of the second defect on the Mn^{4+} centre and the Cr^{3+} T centre showed that the environments were similar, and that the paramagnetic entities were most probably of the same type.

Before completion of this chapter, mention should be made of the observation of excited state resonances of V^{2+} and Cr^{3+} ions in MgO[22]. An optical method of detection was employed whereby absorption of a microwave quantum by an excited state was revealed by the decrease in intensity of the fluorescence observed from this state. The level of interest here is the ^2E level which arises from the free-ion ^2G electronic term and lies some $17{,}000cm^{-1}$ above the $^4A_2$ ground state. The sample was placed in a K-band microwave cavity lying between the poles of an electromagnet and pumping of electrons into the upper level was performed by shining radiation from a mercury lamp through a hole in the base of the cavity. The fluorescence was detected along the field by leading a light pipe through a hole in the magnet pole piece to a cooled photomultiplier. The spin Hamiltonian describing the resonances was given as $\mathcal{H} = g_1\beta\underline{H}.\underline{S} + g_2\beta\underline{H}.\underline{S}^3 + A_1\underline{S}.\underline{S} + A_2\underline{I}.\underline{S}^3$, where S has an effective value of $\frac{3}{2}$. This arises from the fact that the ^2E level is initially two fold degenerate in both orbit and spin but is split into four levels by the combined effects of spin orbit coupling,

configurational mixing, lattice strains and magnetic field. As may be expected, anisotropy in both g shifts and line widths were observed.

REFERENCES

1. R.W.G. Wyckoff, Crystal Structures, Interscience (1965).

2. R.B. Heslop and P.L. Robinson, Inorganic Chemistry, Elsevier (1963).

3. B. Henderson and J.E. Wertz, Adv. Phys., 17, No. 70,749 (Nov. 1968).

4. A.C. Tomlinson and B. Henderson, J. Phys. Chem. Solids, 30, 1793 (1969).

5. Y. Tanabe and S. Sugano, J. Phys. Soc. Japan, 9, 753 (1954).

6. W.A. Runciman and K.A. Schroeder, Proc. Roy. Soc. Lond., A265, 489 (1962).

7. W. Low, Phys. Rev., 101, 1827L,(1956).

8. J.S. van Wieringen and J.G. Rensen, Proc. 1st Int. Conf. Paramagnetic Resonance, Jerusalem, 1962, Vol. I (1963).

9. H.D. de Wijn and A.H.M. Schrama, J. Chem. Phys., 49, 2971 (1968).

10. D.H. Dickey and J.E. Drumheller, Phys. Rev., 161, No. 2, 279 (Sept. 1967).

11. M. Sturge, Phys. Rev., 130, 639 (1963).

12. J.E. Wertz, J.W. Orton and P. Auzins, J. Appl. Phys. Suppl. 33 No. 1, 322 (1962).

13. J.E. Wertz, P. Auzins, J.H.E. Griffiths and J.W. Orton, Disc. Farad. Soc., 26, 66 (1958).

14. W. Low, Phys. Rev. 105, 801 (1957).

15. J.E. Wertz and P. Auzins, Phys. Rev., 106, 484 (1957).

16. S.A. Marshall, J.A. Hodges and R.A. Serway, Phys. Rev., 136A, 1024 (1964).

17. J.H.E. Griffiths and J.W. Orton, Proc. Phys. Soc., 73, 948 (1959).

18. B. Henderson and T.P.P. Hall, Proc. Phys. Soc. 90, 511 (1967).

19. J.E. Wertz and P. Auzins, J. Phys. Chem. Solids, 28, 1557 (1967).

20. M. Nakada et al., J. Phys. Soc. Japan, 19, 781 (1964).

21. J.J. Davies, S.R.P. Smith and J.E. Wertz, Phys. Rev., 178, 608 (1964).

22. L.L. Chase, Phys. Rev., 168, 341 (1968).

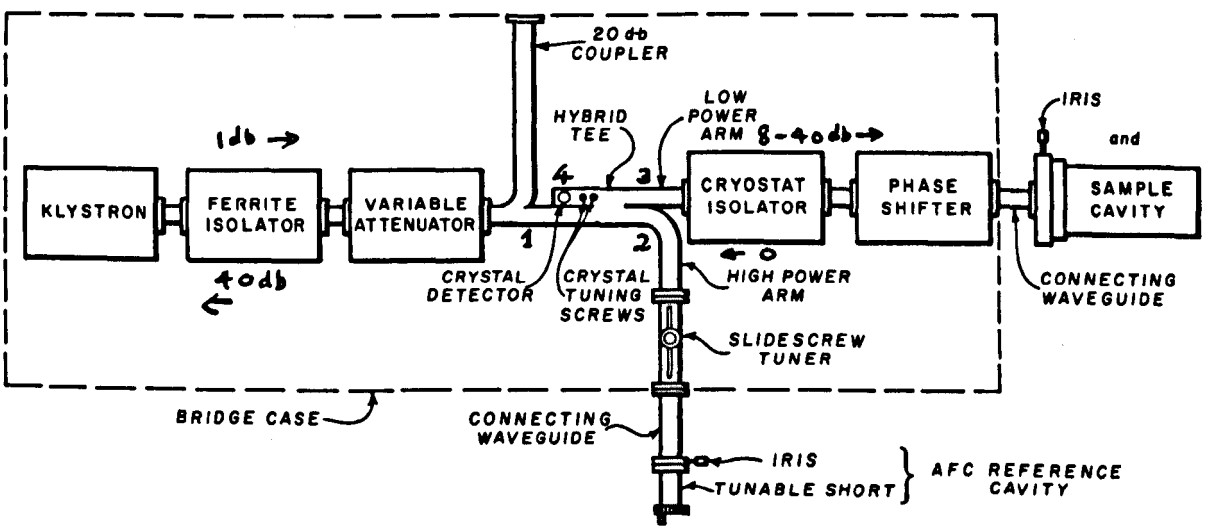

FIGURE 4.1 Varian V-4500 X-band Microwave Bridge.

CHAPTER IV

EXPERIMENTAL ASPECTS

4.1 The Spectrometer

The measurements reported in Chapters V and VI were performed using a Varian V-4502 spectrometer operating at either X- or Q-band. The basic equipment is identical for both frequencies, only the microwave bridge configurations being different. In the X-band microwave bridge, shown in figure (4.1), the power from the klystron passes via the 6db coupler into the resonant cavity: power reflected at the cavity is detected at the crystal in the fourth arm of the coupler. The crystal bias can be set by adjusting the slide screw tuner in arm two. This unit reflects a portion of the power incident on it and is used to alter both the mean level and phase of microwave energy incident on the crystal. The amplitude and phase of power at the cavity is set by the attenuator and phase shifter in arms one and three respectively.

For the purposes of measuring the microwave frequency, a waveguide to coaxial converter was mounted at one end of a second directional coupler. A coaxial cable then takes the microwave frequency to a Hewlett-Packard 540B transfer oscillator, where it is mixed with a variable frequency in the megahertz range. The frequency at which zero beats are observed, is measured with a Hewlett-Packard 524D counter and a plug-in 525C frequency counter unit. Typical frequencies were 9.52GHz from the bridge, which mixed with about 200MHz in the transfer

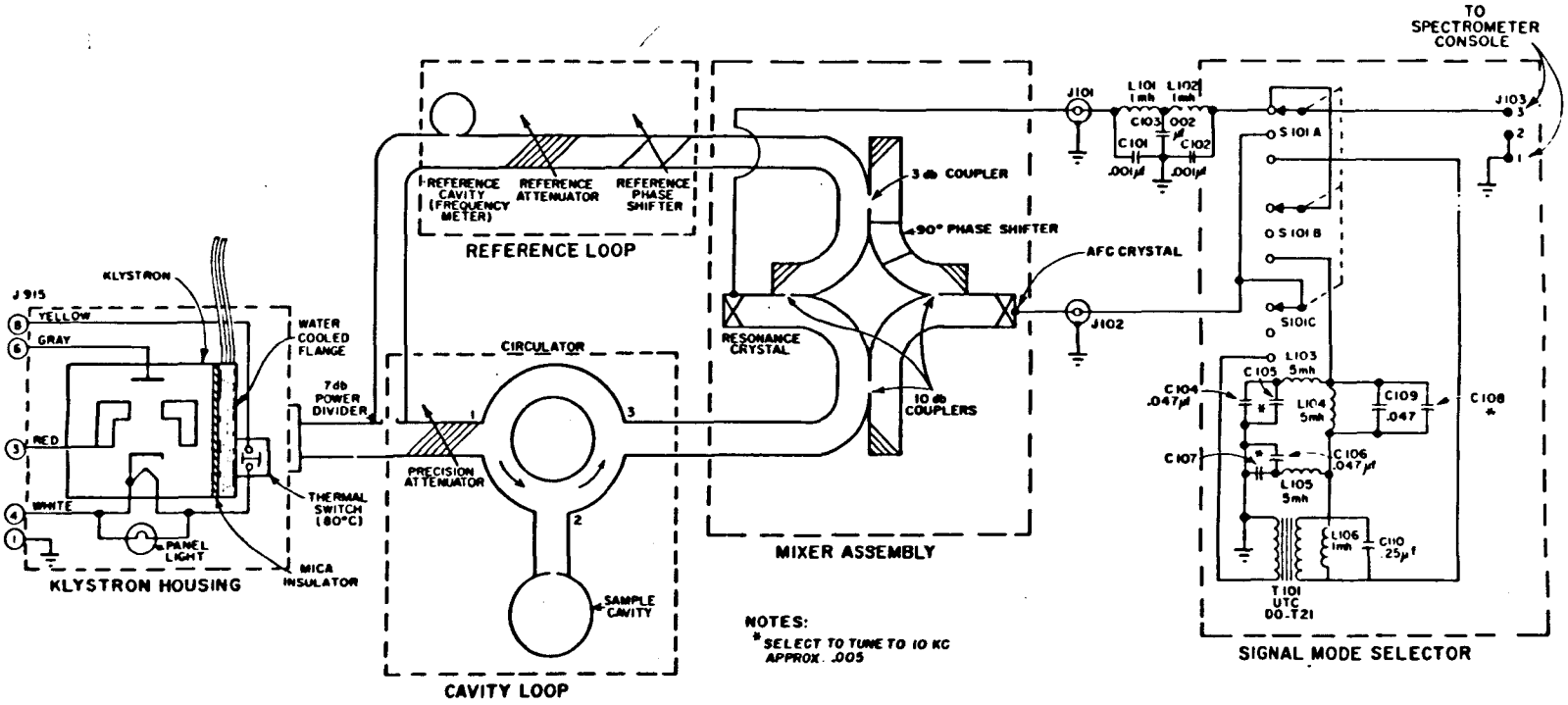

FIGURE 4.2 Varian V-4561 35GHz Microwave Bridge

oscillator. The latter is measured by the counter to better than ±5KHz. The product over difference of two adjacent mixing frequencies producing zero beats gives the microwave frequency. With automatic frequency control the stability of the klystron frequency with respect to the cavity is 1 part in 10^6.

The Q-band bridge differs from the X-band bridge since it employs microwave bucking to set the correct bias on the crystal. Figure (4.2) shows the layout of the waveguide components. The circulator is used in preference to the balanced bridge system used at X-band, since all the klystron power is incident on the cavity. With a magic-tee or waveguide coupler, half the power is automatically lost in the matching arm, and so performs no useful function in the actual resonance. This may not be a problem at X-band where high power microwave sources are readily available, but at Q-band, power outputs tend to be lower. The klystron in this bridge gave about 50mW.

The reflected power from the cavity is separated in the circulator from the incident power, and passes to the mixer. Here it is combined with the power from the bucking arm which can be altered both in amplitude and in phase, which enables selection of either an absorption or a dispersion mode of operation. Since an automatic frequency control system operating at 10KHz is employed, it is necessary to have two crystals in the mixer. When operation in the absorption mode is required, both the 100KHz and 10KHz signals are taken from the resonance crystal, since the phase difference between the microwaves from the reference and cavity arms is zero. In the dispersion mode there is

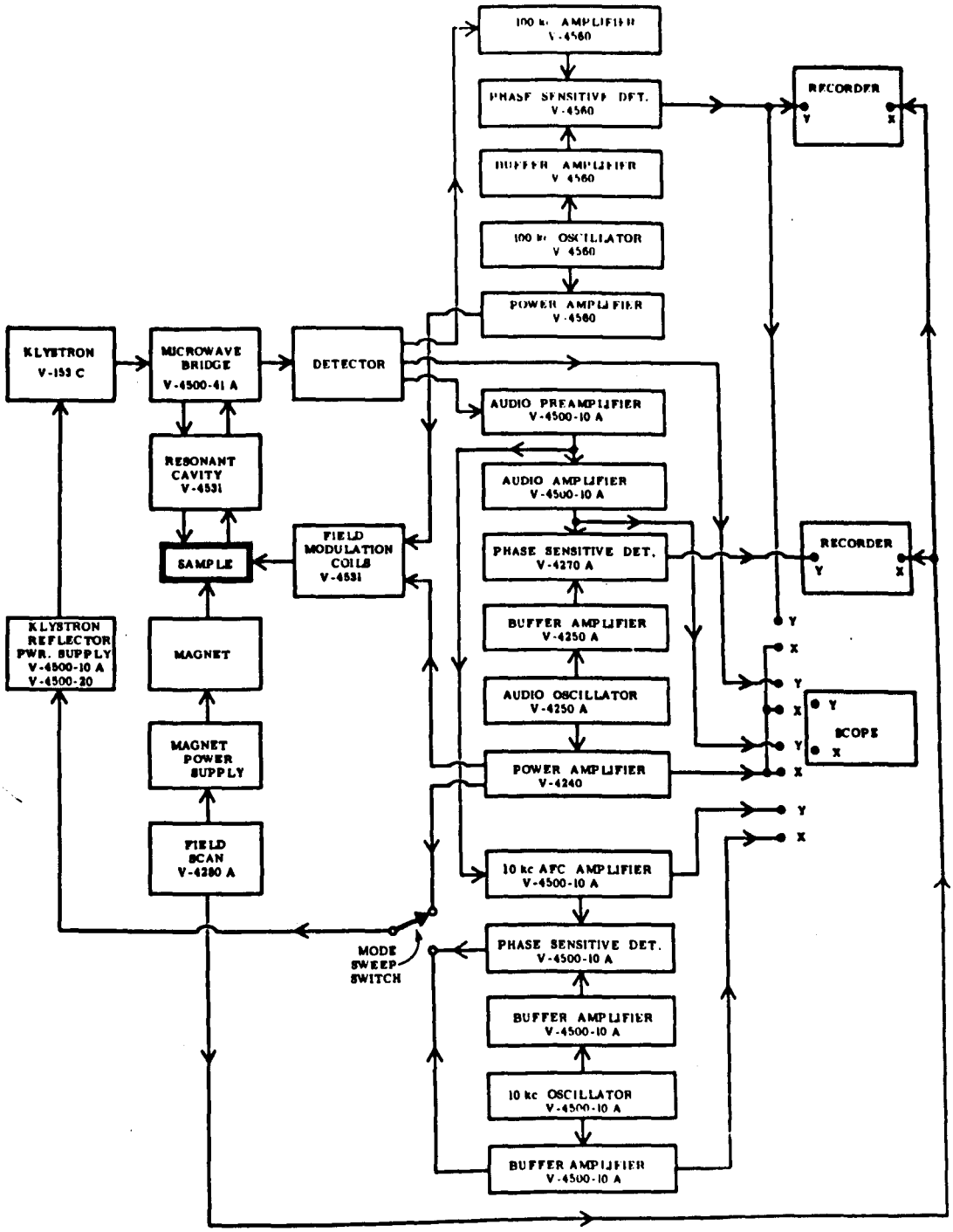

FIGURE 4.3 Block Diagram of the Varian V-4500 E.P.R. Spectrometer.

a 90° phase difference at the resonance crystal, and the 10KHz signal is taken from the A.F.C. crystal. The 90° phase shifter ensures that the resulting phase difference here is zero. The signal mode selector performs the required change over from absorption to dispersion operation. The klystron frequency is monitored by a precision cavity wavemeter in the reference arm. The smallest scale divisions on this are 10MHz apart. In the absence of information to the contrary, the dial is assumed to be correct to this figure. The frequencies generally used lay near 35GHz.

The rest of the spectrometer is as shown in figure (4.3). The A.F.C. system operates in the following way. The reflector of the klystron is voltage modulated at 10KHz, so producing a frequency modulation of the klystron output. This is in turn converted to an amplitude modulation of the microwaves reflected from the cavity. If the klystron is tuned to the centre of the cavity mode, then a zero net output will be obtained. When the klystron drifts, a 10KHz output proportional in amplitude to the slope of the cavity dip, is produced. This signal is fed via the appropriate crystal detector to an audio preamplifier and 10KHz A.F.C. amplifier, prior to being "phase detected". The phase sensitive detector produces a D.C. output proportional to the phase or amplitude difference between the output from the A.F.C. amplifier and a reference voltage of identical frequency. Thus any change in klystron frequency results in a D.C. output which is used as an error voltage to the klystron reflector power supply.

The E.P.R. signals are fed to either the audio or 100KHz circuits depending on the frequency of field modulation. In both cases

lock-in detectors are used. Since the D.C. output level is proportional to the slope of the absorption or dispersion curve, first derivative spectra are obtained. These may be observed directly, on an oscilloscope, or pen-recorded on a strip chart.

4.2 The Resonant Cavities

The cavities for both X- and Q-band spectrometers operate in the cylindrical H_{011} mode. In this mode the microwave field configuration has a maximum magnetic field component along the axis of the cavity, where a sample could conveniently be situated. The X-band cavity was not tunable, but the klystron could be operated over a small range of frequencies. No experimental difficulties are experienced for a wide range of sample sizes and positions. The limitations in sample size and position are more severe at Q-band, and consequently both the klystron and cavity are tunable. Cavity tuning is effected by means of a tuning plunger threaded on to the cavity body. The cavity walls in both cases were formed from a helix of silver wire mounted within an epoxy casting. The advantages of a helix are two-fold. Firstly, high frequency field modulation can penetrate into the cavity with less attenuation owing to the gaps between the windings. Secondly, the currents in the waveguide walls are restricted to circular paths, following the silver windings. This reduces the possibility of the presence of other resonant modes which would lower the cavity Q. To further suppress unwanted modes, the metal end plates were not in electrical contact with the walls. Coupling to both cavities was variable, and matching was achieved by

moving a conducting rod through the iris. The field modulation coils were external to the cavities and were of the Helmholtz configuration, bent to conform to the cavity shape. As the magnet was rotated, the coils were carried round with it, so maintaining a constant modulation amplitude at the sample in all orientations.

4.3 The Magnetic Field

The static magnetic field was provided by a Varian V-3400, 9" electromagnet, operated by a transistorised power supply. Fields up to 10Kg (1 Tesla) could be achieved with a $2\frac{1}{2}$" gap, but this could be reduced to $1\frac{3}{4}$" with coned pole pieces for use at Q-band. Fields up to 15.25Kg were then available. The magnet could be moved on rails from one bridge to the other and could also be rotated about each cavity, so facilitating anisotropy studies. Magnetic field control was performed using a Varian Fieldial Mk I. If the field attempted to change, a Hall effect sensor probe located in the air gap would note the change and give rise to an error signal in the regulator circuits. The field would be corrected to the value set on the field controls.

Calibration accuracy of the instrument was outside the limits given by the manufacturers, which was stated as being ±5 gauss up to 15Kg. In fact, initially, the dial reading was 250g too low at 12.6Kg. The calibration was set correct to ±5g at this field, using the single isotropic line from pitch in KCl. The error was then evident at low field, when X-band resonances were observed. It is clear that a full recalibration of the instrument is required, and to these ends a high

frequency proton resonance oscillator[1] is under construction. The problems of obtaining proton resonances at frequencies up to 60MHz are quite large and, so far no success has been obtained. In view of this, field measurements were taken from the Fieldial, and large tolerances attached to the values of E.P.R. parameters obtained. These errors will be substantially reduced at a later date, since the nature of the centres under investigation has been revealed. The problem is reduced from one of understanding to one of measurement.

Spectra were recorded on a strip chart while the magnetic field was swept by a motor driven potentiometer built into the Fieldial control circuits. Field positions were interpolated from the beginning of the pen recording, the recorder being switched on at the exact start of every field sweep. The field sweep was linear to within the calibration accuracy of the equipment.

4.4 Low Temperature Equipment

All the spectra investigated in this work were readily observable at room temperature. But for investigations of the exchange interaction between pairs of V^{2+} ions (see Chapter VI), lower temperatures were required. Since the magnitude of the exchange energy was not known, a plot of spectral intensity against temperature was required. As a first stage, the range from room to liquid nitrogen temperature (290 to 77°K) was utilised, intermediate temperatures being obtained with a cold gas flow system similar to that used by Vänngard[2]. Since the pair spectra could not be observed at X-band, Q-band

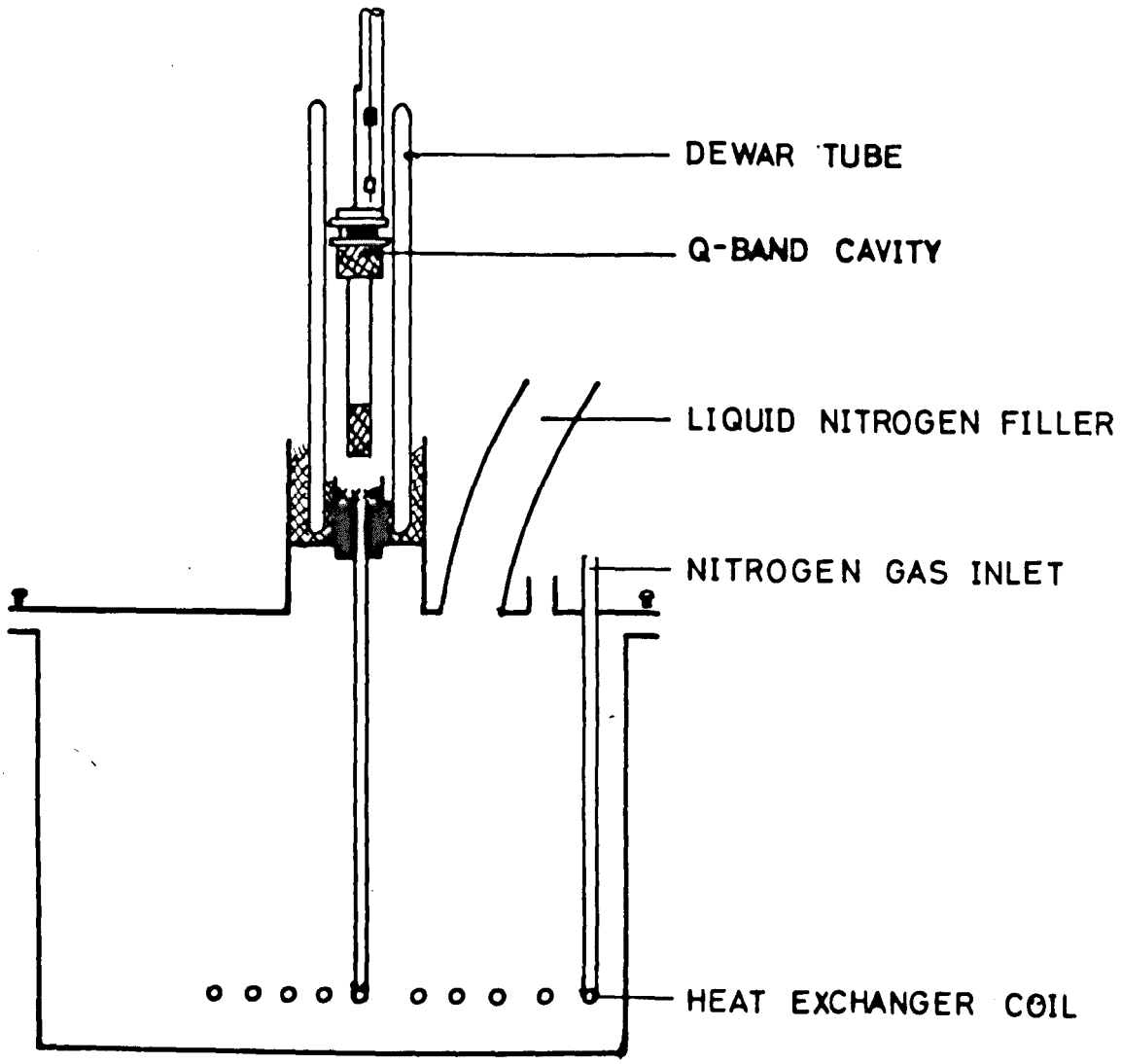

FIGURE 4.4 The Cold Gas Flow System.

frequencies had to be employed. At the lower frequency, one is able to use a double walled insert in the cavity and cool the sample directly with cold nitrogen gas. This is not feasible when the cavity dimensions are small, so it became necessary to cool the whole Q-band assembly.

A drawing of the equipment constructed to achieve this is shown in figure (4.4). The 6" dewar tube surrounding the cavity was supported in a foam rubber seating, by the lid of the liquid nitrogen box. A shortened tuning rod was fitted to the cavity for reasons of space. Also in the lid of the box were a filler tube, a vent and a through connection to the copper heat exchanger coil. The box was constructed out of silver soldered $\frac{1}{16}$" brass plate. When in use, the whole assembly is covered with expanded polystyrene sheets and flakes, to reduce the rate of liquid nitrogen boil-off. Oxygen-free nitrogen gas is supplied to the heat exchanger by a cylinder of compressed gas. The cooled gas is then fed to the bottom of the dewar tube where its passage through several thicknesses of copper gauze ensured thermal homogeneity. The final temperature of the cavity assembly is dependent on both the temperature and flow rate of the gas. Consequently the heat exchanger was deliberately made large to ensure that the gas attained the temperature of liquid nitrogen, no matter what the flow rate. The cavity temperature is then controlled only by the flow rate of nitrogen gas.

In this way continuously variable temperatures in the range 90 - 300^{o}K are possible. At the lower ranges of temperature the system is very wasteful of both gaseous and liquid nitrogen since a high rate

of gas flow is required. For example at 90°K the 2½ litres of liquid nitrogen in the box lasts only about twenty minutes, whereas at 200°K it would last over an hour. Problems of insulation and the inevitable conduction of heat down the waveguide, made temperatures below 90°K an impossible goal. At temperatures above about 200°K, the required gas flow rates were too low for accurate control, and cavity temperatures fluctuated. A much simplified system was then used when temperatures below 150°K were not required. The incoming gas from a cylinder was cooled in a copper coil immersed in liquid nitrogen in a 4½ litre dewar. It was then passed through a polythene tube to the bottom of the dewar tube. The latter was supported in a hole in a wooden block and the gas led through this by a tube.

Owing to the inevitable temperature gradient across the cavity walls and air space within the cavity, the temperature of the sample was always higher than that of the cavity. An initial calibration was performed to relate these two quantities. Two copper-constantan thermocouples were used, one situated at the sample position and the other fitting in a hole in the cavity tuning rod. The reference junctions were placed in a melting ice bath. Thermally generated e.m.fs. were then measured on a Cropico Thermocouple Potentiometer and the corresponding temperatures obtained from calibration tables. Agreement in e.m.f. between the tables and the actual thermocouples used, was checked at liquid nitrogen and solid carbon dioxide/acetone temperatures and found to be within ±3% of these temperatures.

Once the system had settled for twenty minutes after alteration of the gas flow, temperature stability was better than $\pm 2^{\circ}$ over ten minutes, in the most unfavourable temperature region. This length of time was ample to perform the measurements required.

REFERENCES

1. F.N.H. Robinson, J. Sci. Instrum., 42, 653 (1965): "A high field nuclear magnetic resonance probe using transistors".

2. T. Vänngard, University of Gothenburg, Sweden. Private communication.

CHAPTER V

DIVALENT VANADIUM IN MAGNESIUM OXIDE : I - SINGLE ION SPECTRA

5.1 Introduction

Most of the experiments described in this thesis were performed with crystals taken from magnesium oxide boules which had been doped during arc fusion with 1% vanadium pentoxide, V_2O_5. Such crystals are predominantly green, the intensity of colouration, which reflects the vanadium content of the crystal, being much higher (almost black) in crystals taken from the edge of the boule. The colouring is due predominantly to an optical absorption band[1] of V^{3+} centred at 22,200cm^{-1}. Normally vanadium substitutes for Mg^{2+} as V^{3+} in MgO, although a small amount is present as V^{2+}. Since V^{2+} has an orbitally non-degenerate ground state well separated from higher levels, the E.P.R. spectra are easily observed at room temperatures. This is not the case for V^{3+} which has a $^3T_1$ orbital triplet as the ground state. The combined action of lower symmetry crystal fields and spin-orbit coupling will split this term, but the proximity of other orbital levels implies that the lowest will have a short spin-lattice relaxation time. If resonance is to be observed at all, it will only be at very low temperatures. The room temperature spectra observed, then, are from V^{2+}.

Although crystals with both light and heavy doping were examined, most of the work was performed on a black specimen, since here most of the interesting spectra were observed. In addition a green

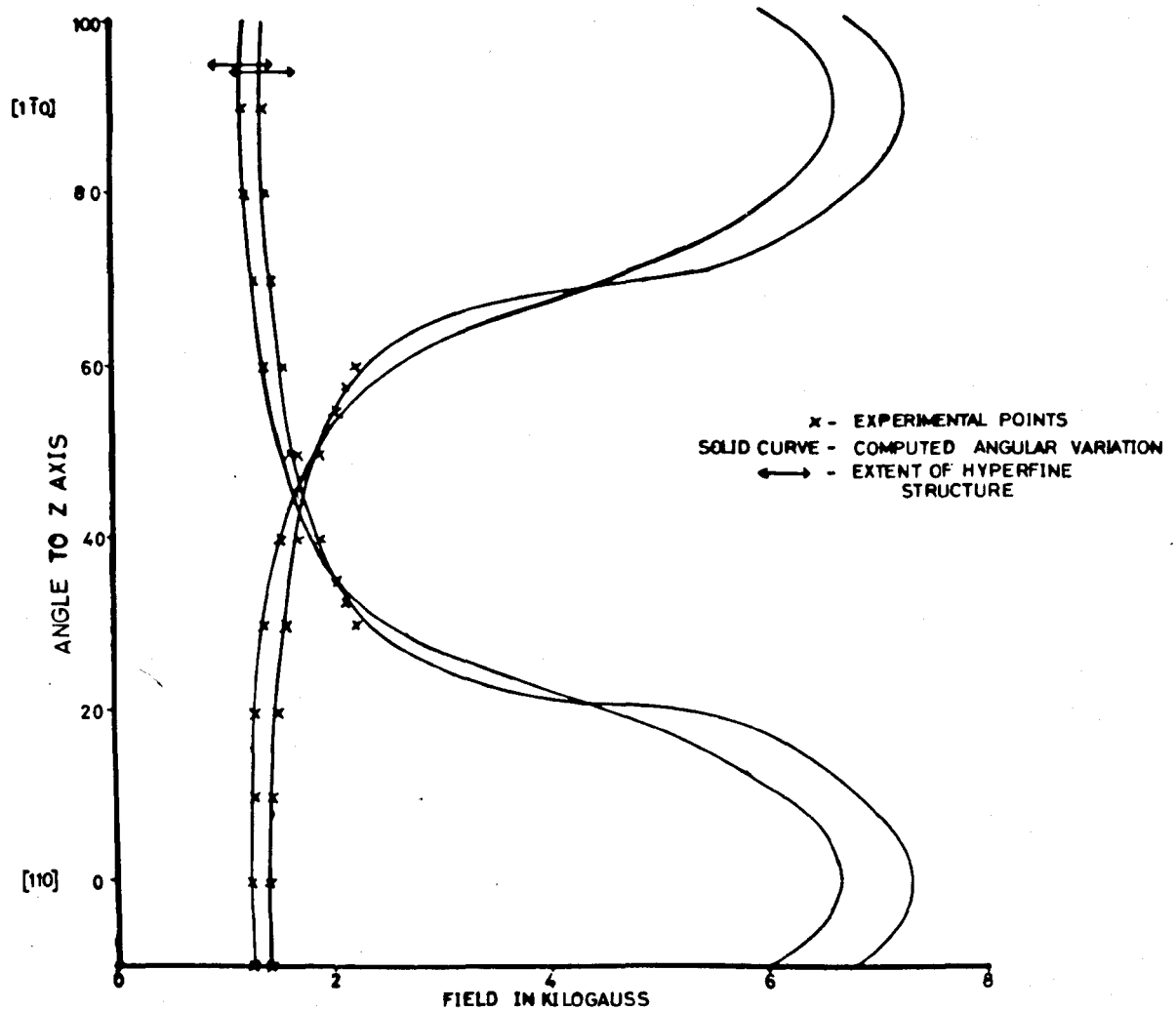

FIGURE 5.1 Angular Variation of the Orthorhombic V^{2+} Spectrum at X-band, in the (100) Plane.

coloured crystal was heated to 1400°C in a stream of hydrogen for some days. This treatment resulted in a colour change from green to pale brown, which was accompanied by a much increased E.P.R. absorption from V^{2+} ions compared with green crystals. The reduction treatment had clearly converted V^{3+} to V^{2+}. The size of the crystals required depended on whether measurements were performed at X- or Q-band. In the former case blocks measuring approximately 5 x 5 x 3mm were suitable. For Q-band measurements crystal cubes measuring no longer than 2mm on edge were used, to minimise degradation in the cavity Q. The cleaving of such blocks from the melt presents no great problem, provided care is taken to select suitable pieces that included large single crystals. The cubic crystal cleaved easily along [100] planes when struck with a sharp edge.

The initial E.P.R. measurements were at X-band frequencies, our objective being to determine the origin of some spectra observed at about half the field value for a g=2 resonance. There appeared to be two distinct sets of vanadium lines, both with turning points about a [110] crystal direction. As the magnet is rotated in the [100] plane from $H_o \parallel [110]$ these lines moved to higher field and crossed another set of lines near a [100] direction. A full orientation dependence is not possible since the lines are too broad for observation at some orientations. The angular variation of the observable lines is shown in figure (5.1). It was thought possible that the spectra were due to "forbidden transitions" between the alternate levels $\pm\frac{3}{2} \leftrightarrow \mp\frac{1}{2}$ of the spin quartet. To investigate their origin further, subsequent

measurements were made at Q-band frequencies, where half-field transitions will be well separated from the g=2 resonances.

The pale green crystals showed little other than the well known cubic field V^{2+} spectrum, which at Q-band is centred on about 12.6kG (1.26 Tesla). The black and dark green crystals, however, showed additional groups of lines. With the magnetic field parallel to a [100] crystal direction groups of weak lines were observed centred at approximately 4, 6, 10, 11.5, 13.5 and 15 kG, plus a profusion of lines lying around g=2, and stretching about 1kG on either side of the cubic spectrum. The lowest field groups did not resemble those at higher field, which all appeared similar. When the magnet is rotated 45^{o} into a [110] crystal direction, the sets of lines at 4, 11.5 and 13.5 kG remained, together with the g=2 profusion. However, the 6, 10, and 15 kG groups disappeared and two new sets of lines become evident at 9 and 16 kG. The high field spectrum could not be observed in its entirety owing to the high field limit of the magnet power supply. Since the lines did resemble the low field group they were attributed to the same centre.

These preliminary observations demonstrate that at least two different centres are present in the crystal, in addition to the octahedrally coordinated V^{2+}. From the subsequent detailed investigations it became clear that the groups of lines at 10, 11.5, 13.5 and 15 kG in the [100]-orientations are due to E.P.R. transitions from pairs of exchange coupled ions. This was evidenced both by the stairstep hyperfine structure and by the hyperfine splitting constant being about half that normally observed for V^{2+} in MgO. This E.P.R. spectrum will be

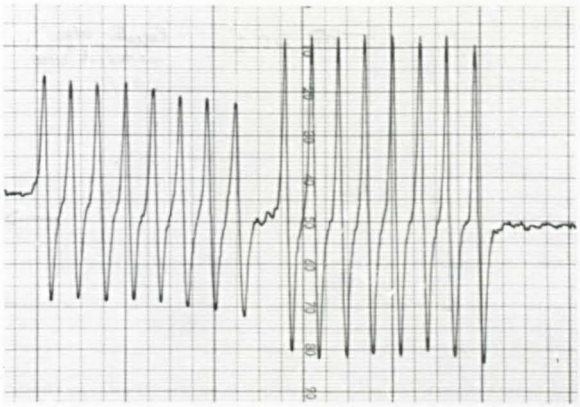

(a) 0° to z-axis

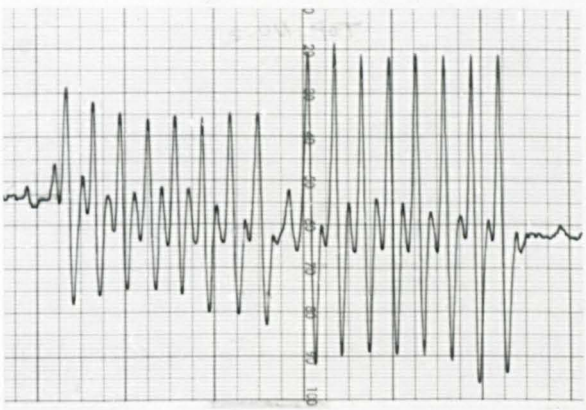

(b) 7° to z-axis

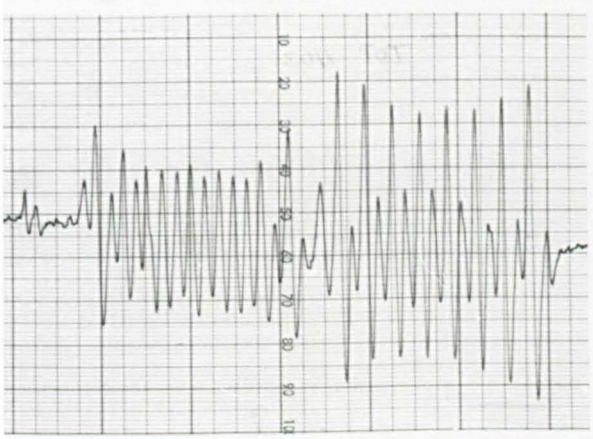

(c) 12° to z-axis

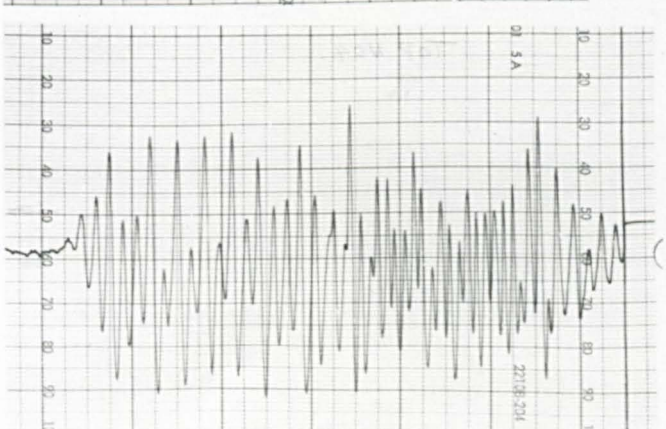

(d) 25° to z-axis

FIGURE 5.2 Angular Variation of Orthorhombic V^{2+} Hyperfine Pattern.

discussed in detail in the next chapter. Most of the remaining lines were thought due to V^{2+} in distorted symmetry sites. These will now be discussed.

5.2 E.P.R. Spectra at Q-band Frequencies of V^{2+} in Distorted Symmetry Sites

5.2.1 Allowed spectra

The appearance of the lower field spectrum in a [110] orientation is shown in figure (5.2a). Since the two sets of eight lines show a hyperfine splitting of about 78 gauss, they imply that the spectra arise from V^{2+} ions. It is not immediately obvious whether the two sets are from the same centre or from two different centres with slightly different zero field splittings. This uncertainty should be removed by fitting a full oriental dependence of the spectra to theory. Although the movement of the lines as a function of the angle between H_o and the crystal axes could be followed to a certain extent, the full angular variation was vitiated by two factors. Firstly, the presence of the strong cubic field lines and the attendant confusion of lines near g=2 made it impossible to follow the spectral shifts through the central region. Secondly, away from the axis there was a major change in the appearance of the hyperfine structure. This was caused by the presence of what are thought to be "forbidden" hyperfine lines between the "allowed" lines. These were larger than the allowed lines when the magnetic field was 12° or more from a [110] direction in the

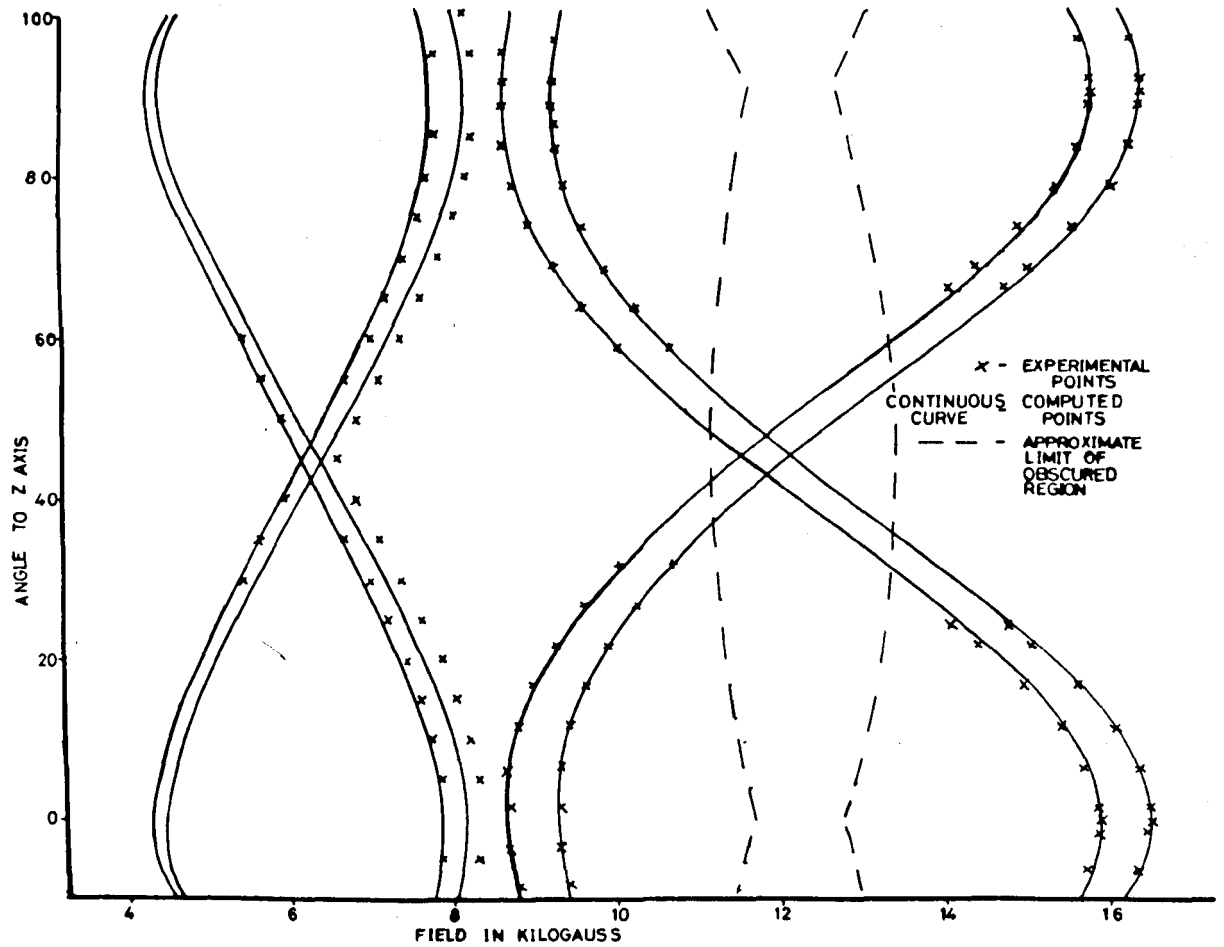

FIGURE 5.3 Angular Variation of the Orthorhombic V^{2+} Spectrum at Q-band.

crystal. This caused considerable difficulty in finding the centre of the spectrum. Their origin will be discussed later in this chapter. The appearance of the low field spectrum at different field orientations in the [100]- plane for rotations about a [100]-axis is shown in figures (5.2b,c,d). The observable angular variation of the centres of each of the groups of eight lines is plotted in figure (5.3). The position of that portion of the spectrum which lay beyond the magnet limit was interpolated from the field value of the first line on the low field side of the high field spectrum. This line always remained within an obtainable field range.

For magnetic field orientations in the (100)-plane the spectrum was repeated every 90° with maximum fine structure splittings occurring along a [110]-crystal direction. With the crystal suspended by an edge, i.e. H_o lying in a {110}-plane, the turning points were every 180°, with subsidiary maxima of splitting about $\pm 55^{\circ}$ from the axis of symmetry of the centre. When the magnetic field was rotated in the plane perpendicular to a [111] direction, turning points were observed every 60°. These observations confirm that the axis of symmetry of the centre coincides with a [110] crystal direction.

For such a case of orthorhombic symmetry one anticipates a total of eighteen sets of eight lines since there are three fine structure transitions possible for each centre, and there are six distinct [110] directions along which distortions may occur. These are the [110], [1$\bar{1}$0], [011], [0$\bar{1}$1], [101], [10$\bar{1}$] directions. However, when the magnetic field lies in a (100) plane and is rotated about a

[100] crystal axis, the [011] and [0$\bar{1}$1] together with the [101] and [10$\bar{1}$] directions are equivalent. Their spectra merely superpose to give doubly intense sets of lines. There are therefore four inequivalent directions of symmetry and a total of twelve expected transitions. Assuming that the four sets of lines already observed are from the same centre, eight more are required to fulfil the predictions. Of these we do not expect to observe the four $\frac{1}{2} \leftrightarrow -\frac{1}{2}$ transitions since they would lie in the region of the strong octahedral field resonances. Second order line shifts of the order D^2/H_o are assumed to be small at Q-band. Four more sets are required. We must conclude, therefore, that these contribute to the large number of overlapping lines found on either side of the g=2 region. This is a reasonable assumption since the four [110] type axes that make 45° to a [100] plane would have a minimum angle of 45° to a magnetic field applied in that plane. Spectra due to centres with distortions along these axes would not be expected to split far from the g=2 region.

The observed spectra are attributed to a centre lying in a [100] plane with [110] principal distortion axes. The outer groups of lines arise when the magnetic field is parallel to a [110] direction, and the inner set when it is perpendicular to this direction. Since the [110] and [1$\bar{1}$0] directions are perpendicular, both a parallel and perpendicular group of lines are observed at both high and low field.

5.2.2 The half-field and third-field spectra

The group of lines observed in the region of 6kG with the field along a [100] crystal direction is attributed to transitions between alternate levels of the spin quartet. These are frequently referred to as the $\Delta M_s = 2$ transitions between $\pm\frac{3}{2} \rightarrow \mp\frac{1}{2}$ levels: this description is convenient rather than explicit when significant mixing between the levels occurs. It is, of course, the impurity of each level that enables these spectra to be observed at all. Transitions where the electronic spin changes by two units are normally forbidden but may occur off axis if some agent is present to mix the levels. Zero field splittings can provide appropriate mechanisms to couple non-adjacent levels.

The angular variation of the lines in this group is shown in figure (5.3). Several interesting points arise. The spectrum shows minimum spread with the field along [100] and a maximum along [110]. There appear to be two sets of lines moving in a similar manner to the $\Delta M_s = \pm 1$ lines, but the exact positions of the turning points cannot be found, since the spectra vanish. There is also a mass of lines near the centre of this spectrum which cannot be resolved into definite sets and which do not appear to depart much from the central region. It is these facts which indicate that these spectra arise from the same centre as the spectra of section (5.2.1). The angular variation is geometrically similar, but as expected, the splitting from the centre of the resonance is about half that observed for the "allowed" transitions. Since two transitions would be expected from each of the four inequivalent distorted sites, eight sets of lines ought to be observable. It is proposed that

the four sets not clearly accounted for contribute to the complex central region.

In view of the fact that transitions at half field are observed it is thought that the 4kG set of lines may be from the $\Delta M_s = 3$ transitions. Since they occur between the $-3/2$ and $+3/2$ levels, the spectra lie at about $1/3$ the field for the allowed lines. The one permitted transition indicates the presence of four groups of eight lines for this centre. The lack of any great angular variation of line positions with field angle made it difficult to interpret the rather peculiar spectrum. The fact that there was little movement of the lines as the magnet was rotated is easily understood, since for fields of about 4kG the separation between $+3/2$ and $-3/2$ spin levels does not vary much. The complicated nature of the spectrum may be explained by the fact that four sets of spectra are partially overlapping in this region.

5.3 Analysis of the Spectra

Now that the single ion spectra observed at Q-band have been described and tentatively ascribed to V^{2+} in a distorted site it is appropriate to carry out a fuller analysis of the results obtained. From the angular variation of the spectra it is clear that the centre involved has its principal axis along a [110] crystal direction. We select this direction as the z axis of the centre. The x and y axis will be at right angles to this and to each other, and for cubic MgO will be inequivalent. This means that the symmetry of the V^{2+} site is orthorhombic, and both D and E terms are required in the spin-Hamiltonian

to describe the angular behaviour of the spectra. The value of D is obtained directly from the spectra.

When the magnetic field and the z-axis of the centre are parallel the spin-Hamiltonian

$$= \beta \underline{H}.\tilde{g}.\underline{S} + D\left[\underline{S}_z^2 - \tfrac{1}{3}S(S+1)\right] + E\left[\underline{S}_x^2 - \underline{S}_y^2\right] + \underline{S}.\tilde{A}.\underline{I}. \qquad (5.1)$$

has solutions:

$$E_M = g_z\beta H_o M + 2D(M-\tfrac{1}{2}) + \frac{E^2}{2g\beta H_o}\left[2S(S+1) - 6M(M-1) - 3\right] + A_z Mm$$

$$+ \text{higher terms in A} \qquad (5.2)$$

The three fine structure transitions occur at resonant fields given by

$$g_z\beta H_1 = g_z\beta H_o + 2D + A_z m + \text{higher terms} \qquad (5.3a)$$

$$g_z\beta H_2 = g_z\beta H_o - \frac{3E^2}{g\beta H_o} + A_z m + \text{higher terms} \qquad (5.3b)$$

$$g_z\beta H_3 = g_z\beta H_o - 2D + A_z m + \text{higher terms} \qquad (5.3c)$$

For the purposes of measuring D, second order and higher hyperfine terms are neglected, since they give corrections of 2 gauss or less at the magnetic fields used for Q-band measurements. Such corrections are within the limit of experimental error. Consequently at this orientation the difference in field between the geometric centres of the high and low field sets of eight lines gives a value for 4D. We find $D = 0.182\text{cm}^{-1}$. If H_o is taken to be half way in field between H_1 and H_3, g_z can be calculated if the frequency is known. g_x and g_y can in

principle be measured in a similar way for H || x,y but in this case only the spectra along one of these directions was visible. Hyperfine separations remained constant at all orientations so we take A as being isotropic. There only remains E to be measured.

As was seen above, the rhombic term does not contribute to the separation between transitions when the magnetic field lies along the principal distortion axis of the centre. However, away from this orientation it does, and has a maximum effect at 90° to the z axis. To obtain an explicit relationship for the field positions at any orientation, it is necessary to relate the magnetic field position to the axes of symmetry of the crystal. This can be done in two different, though equivalent ways. Either we define the magnetic field axes, as fixed in the laboratory frame of reference and choose to rotate the crystal, or we define the crystal axes x,y,z as fixed and rotate the magnetic field. In the former we require to transform spin, zero field splittings and hyperfine terms through the polar angles θ, ϕ to obtain the Hamiltonian relevant to a defect with axes at these angles to the magnetic field. The expressions for the transformed parameters become somewhat cumbersome except along directions parallel or perpendicular to the field. For this reason it is more convenient to fix x, y and z and define the components of the magnetic field as

$$\begin{aligned} H_x &= H_o \sin\theta\cos\phi \\ H_y &= H_o \sin\theta\sin\phi \\ H_z &= H_o \cos\theta \end{aligned} \qquad (5.4)$$

The Hamiltonian can then be written as

$$H_{\theta\psi} = g_z\beta S_z H_o \cos\theta + g_x\beta S_x H_o \sin\theta\cos\psi + g_y\beta S_y \sin\theta\sin\psi H_o$$
$$+ D\left[\underline{S}_z^2 - \tfrac{1}{3}S(S+1)\right] + E(\underline{S}_x^2 - \underline{S}_y^2) + \underline{S}.\bar{A}.\underline{I} \qquad (5.5)$$

A solution to this equation may be found in one of two ways. If D and E are small compared with the microwave quantum, i.e. $D,E \ll h\nu$, perturbation methods may be employed. The energy levels of field positions can be calculated to good accuracy by going to second order of perturbation. If the condition does not apply, then the Zeeman and zero field splitting terms have to be considered together. It is then necessary to set up and solve the energy matrix.

The lengthyperturbation expressions were obtained by Weger and Low[2], and to first order of perturbation can be written

$$H = H_o-(M-\tfrac{1}{2})\{D(3\cos^2\theta-1) + 3E\sin^2\theta\cos2\phi\}, \text{ + hyperfine terms,}$$

assuming an isotropic g-tensor. Along the z-axis of the centre, where $\theta = 0^o$ this reduces to

$$H = H_o - (M-\tfrac{1}{2}).2D + \text{hyperfine terms}$$

which is the same equation as (5.3). When the magnetic field is parallel to an x or y axis, the equation becomes

$$H = H_o - (M-\tfrac{1}{2})\{-D + 3E\cos2\phi\} + \text{hyperfine terms} \qquad (5.6)$$

Since we have already determined D from equation (5.3) E may now be found if ϕ is known. The latter takes values 0^o and 90^o along x and y

axes respectively, so the term in E becomes respectively positive or negative. The problem that now arises is in the choice of axes for the centre. It is not immediately obvious whether a set of spectra obtained with H perpendicular to z should be associated with the x or y axis. We have already defined the z axis as that along which the maximum splitting from H_o occurs, and chose to put D in this direction.
A further convention can now be introduced if we redefine the zero field splitting terms as

$$\underline{S}.\tilde{D}.\underline{S} = D_z S_z^2 + D_y S_y^2 + D_x S_x^2,$$

with $D_x + D_y + D_z = 0$. This expression takes the familiar form if

$$D_z = \tfrac{2}{3}D$$
$$D_x = E - \tfrac{1}{3}D$$
$$D_y = -(E + \tfrac{1}{3}D).$$

The co-ordinate system may be chosen[3,4] such that

$$|D_z| > |D_y| \geq |D_x| \qquad (5.7)$$

In this case

$$\lambda = \frac{E}{D} = \frac{-\frac{1}{2}(D_y - D_x)}{-\frac{3}{2}(D_y + D_x)} = \frac{1}{3}\left[\frac{D_y - D_x}{D_y + D_x}\right]$$

With our choice of D_y and D_x, we find that λ is always positive and less than $\frac{1}{3}$. It is never necessary to express a Hamiltonian with $E > \frac{1}{3}D$, for this would imply that the axes were defined unconventionally.
A simple relabelling of the axes is all that is required to restore

conformity of the zero field splitting parameters with the relationship (5.7). Improper coordinate systems will not lead to incorrect values for resonance fields but will not necessarily be unambiguously related to the crystal structure.

Returning to the problem in hand, the set of transitions obtained with H perpendicular to z must be associated with a y axis if $|D_y|>|D_x|$. It is postulated that the further set that would be observed with H parallel to x are hidden in the mass of lines near g=2. Since the spectra were recorded in the (100) plane of the crystal, we choose the following crystal directions for the axes of the centre

z along $[110]$

y along $[1\bar{1}0]$

x along $[001]$

These are shown in figure (5.4a). The polar angles of the magnetic field at an arbitrary orientation to these axes are shown in figure (5.4b).

It is now possible to calculate E, since ψ can be determined for any orientation of the magnetic field. Unfortunately the large size of D with respect to the microwave quantum (D = 0.18, $h\nu$ = 1.2cm^{-1}) would make perturbation theory rather inaccurate especially in relation to the X-band spectra. Nevertheless, along the axes the errors would not be too great, and an estimate of the size of E can be made.

For H parallel to y, $\theta = 90^{\circ}$, $\phi = 90^{\circ}$

From (5.6) $H = H_o - (M-\frac{1}{2})\{-D-3E\}$ + hyperfine terms.

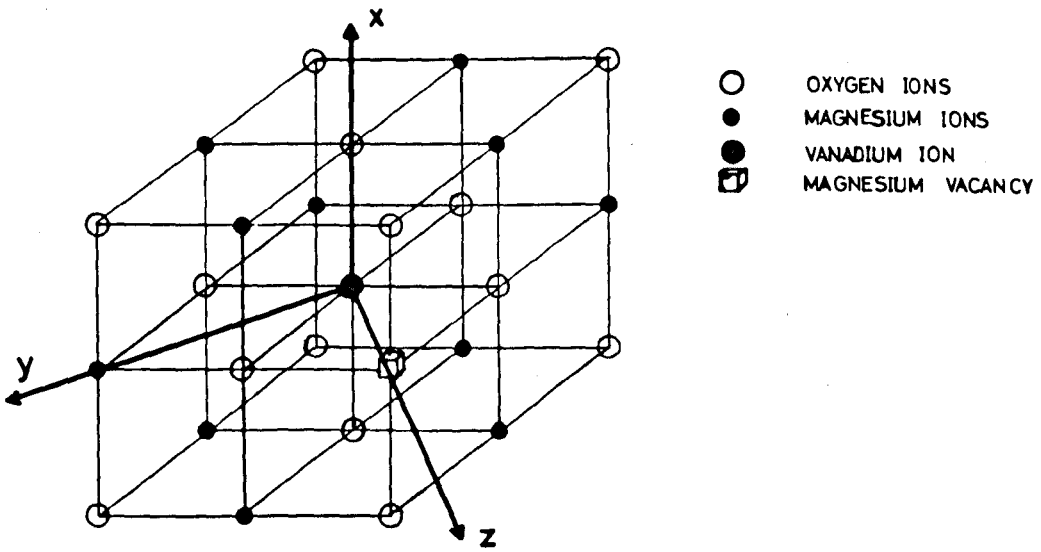

FIGURE 5.4a The Axes of the Orthorhombic Centre.

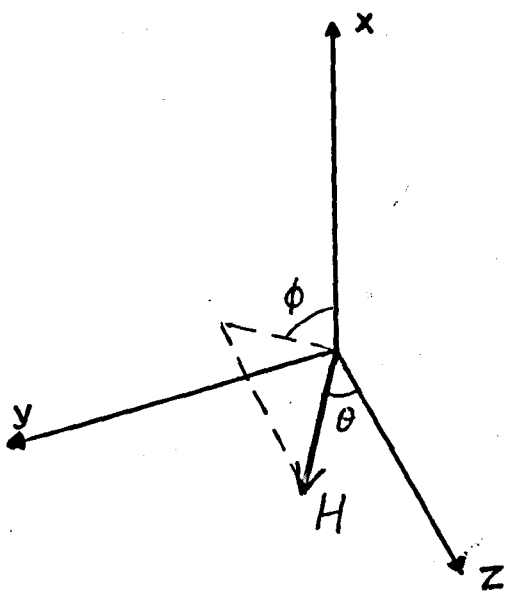

FIGURE 5.4b The Polar Angles of the Magnetic Field.

The separation between the centres of high and low field sets of lines is then

$$\Delta H_y \simeq 2D + 6E \text{ gauss.}$$

This gives E ≃ 450 gauss (= 0.045 tesla) and λ ≃ 0.23, using the value of D obtained above and the measured field separation of the transitions.

For H parallel to x, θ = 90, φ = 0,

so $$\Delta H_x \simeq 2D - 6E \text{ gauss.}$$

If we use the values of D and E just obtained

$$\Delta H_x \simeq 1100 \text{ gauss}$$

This means that the values for the high and low field sets of lines would be approximately 13.1 and 12.0kG respectively, for the field at this orientation. They would not be visible amongst the complicated region of spectrum. The earlier proposal appears correct.

The positions of resonance lines would be predicted with greater inaccuracy by the perturbation formula the further off axis the magnetic field becomes. For this reason, a computer program which set up and solved the energy matrix for chosen parameters of the Hamiltonian was used. The resulting field values enabled a precise analysis of the whole spectrum at both Q and X-bands to be performed.

5.4 Computer Diagonalization of the Energy Matrix

The routine was developed by Dowsing[5] following the work of Swalen and Gladney[6] on the computer analysis of E.P.R. spectra. The g-tensor system of coordinates was used, and the angle of the magnetic field referred to x, y and z in the manner outlined above. The language used was FORTRAN IV, and the computations were performed on an Elliot 41/30 digital computer. A brief description of the program will now be made.

The data required in the program was as follows: the electronic spin, the microwave frequency, g-values, D value and starting values for E, θ, and ϕ. The latter three could be incremented in the course of the program to provide solutions over any desired range of E and polar angles. Also required was the range of field and the step length by which the field was incremented after each iteration (e.g. 200g). The purpose of the iteration will become clear below. The matrix was first set up using the values of $g_{x,y,z}$, D and the starting values of E, θ, ϕ and field H. Computers work on the binary system of numbers, where 0 or 1 can be represented by a particular element of circuit or store being switched off or on. For this reason complex numbers are not recognised. So it became necessary to separate the real and imaginary parts of the energy matrix, a process which involved doubling its size. The eigenvalues and eigenvectors were then separable into real and imaginary sets. The solution of the matrix was performed by a subroutine, adapted[5] from a diagonalisation program developed by Von Neuman[7]. The diagonalisation is the Jacobi method whereby the original matrix A is compared with a unit matrix V of the same dimension. The same operations

were performed on V as on A until A is reduced to diagonal form. The columns of the new V matrix represent the eigenvectors and the diagonal elements of the reduced A matrix, the eigenvalues.

The eigenvalues for this first value of field are stored, and the process of setting up the matrix and solving it repeated for the next field value. After each iteration, the separation between pairs of energy levels was compared with the size of the quantum. The sign of this difference would change if a transition occurred between one field value and the next. In this case the program would enter a sub-iteration to determine the field value for this transition to an accuracy determined by a field tolerance (e.g. 5 gauss) specified by the programmer. A further subroutine would calculate the transition probability. When the computations had been performed for fields up to the maximum specified, details of field, transition probability and wave functions for each transition found, would be printed out.

Then the process would be repeated for different values of polar angles, and finally the rhombic field term would be incremented and the whole iterative procedure performed once more. If required, a digital plotter could be used to provide a diagram of energy levels versus field, for specified values of angles, g-values and zero field splittings.

It is important to note that this version of the program does not take hyperfine terms into account. But for the purposes of discovering the value of E, measurements to the centre of the off-axis spectra

$$g_z = 1.991 \pm 0.008$$

$$g_y = 1.991 \pm 0.008$$

$$(g_x = 1.991)$$

$$|D| = (1819 \pm 8) \times 10^{-4} cm^{-1}$$

$$|E| = (419 \pm 8) \times 10^{-4} cm^{-1}$$

$$\lambda = 0.2306$$

$$|A_z| = (72 \pm 2) \times 10^{-4} cm^{-1}$$

$$|A_y| = (72 \pm 2) \times 10^{-4} cm^{-1}$$

$$(|A_x| = (72 \times 10^{-4} cm^{-1})$$

TABLE 5.1 Measured E.P.R. Parameters for the Orthorhombic Centre

were not of sufficient accuracy to warrant the inclusion of second order hyperfine corrections.

To discover the value of the rhombic field parameter, the procedure was to solve the matrix for fields along the axes. E was altered to provide the best fit with experiment. The θ and ϕ were cycled to provide a prediction of the angular variation of the spectra. By these means, we find the results listed in table (5.1). Figure (5.3) shows a plot of the predicted angular variation of the outer sets of lines from this centre. The remaining eight sets are omitted for the sake of clarity, since they all fall within the central region. The maximum extent of the hyperfine structure is from about 11.7 to 13.2Kg with H_o parallel to [110], and 11.2 to 13.5 with H_o parallel to [100]. It is remembered that the strong cubic field spectrum also lies in this region and adds to the confusion. The experimental points are plotted in the diagram and it is seen that the calculated results are in accord for the allowed spectrum. The discrepancies for the $\Delta M = \pm 2$ transitions are attributed mainly to poor Fieldial calibration.

The calculations were also performed for X-band frequencies. Using the same parameters as above, it is found that the spectra originally observed must be attributed to the allowed transitions of the orthorhombic centre, and not to forbidden spectra. The observed and calculated angular variations are shown in figure (5.1). Since only the "$+\frac{3}{2} \rightarrow +\frac{1}{2}$" and "$-\frac{1}{2} \rightarrow -\frac{3}{2}$" transitions are observed, and then only over a limited range of angles, some explanation must be found for the non-

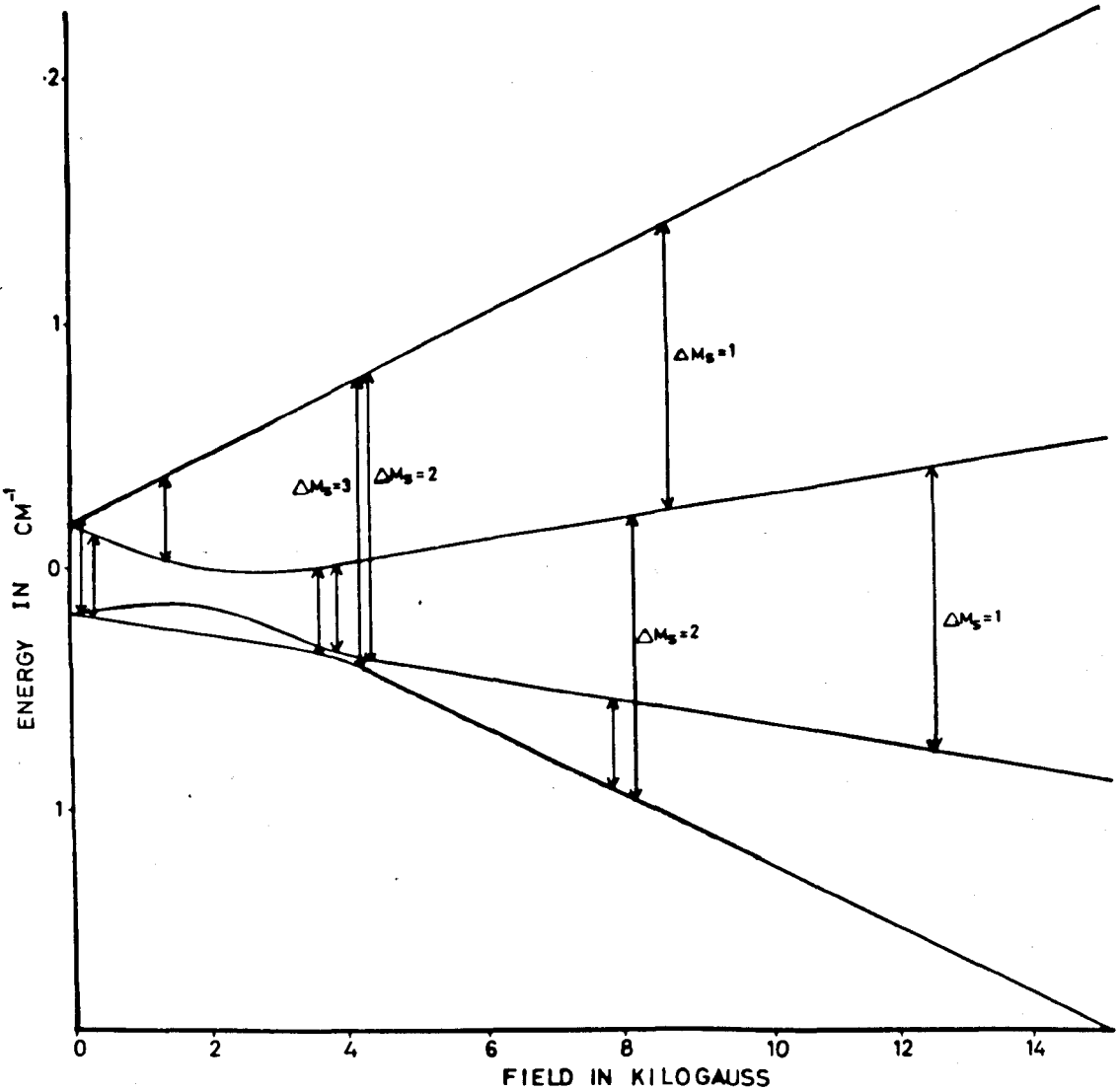

FIGURE 5.5 The Energy Levels and Observed E.P.R. Transitions for the Orthorhombic V^{2+} Centre, with the Magnetic Field along the z-axis.
The longer arrows represent the 35GHz quanta.

appearance of lines. Furthermore, the fine structure splitting in the [110] direction is nowhere near the 8Kg found for Q-band spectra. The answer can be found by examining the energy level diagram shown in figure (5.5). It is evident that for the fields required for X-band spectra there is heavy mixing between levels, and a consequent departure from the linearity obtained at higher fields. Because of this, the low field turning points of the X-band resonance lines will occur at higher fields than might be expected if the energy level linearity is extrapolated to low fields. The disappearance and non-appearance of expected lines can be attributed to the fact that energy levels are frequently nearly parallel at these low fields, so linewidths are large and the spectra unobservable.

5.5 The Hyperfine Structure

In elucidating the symmetry and fine structure of the centre, the hyperfine contributions to the spectra were set aside, since second and third order corrections to the line positions were small. The centre of the hyperfine pattern was taken to be the centre of the resonance. This additional structure will now be examined, with particular reference to the "forbidden" lines which were much in evidence.

The nearly 100% abundant ^{51}V has a nuclear spin of $^{7}/_{2}$ which splits each fine structure transition into eight components. The hyperfine constant A is isotropic for this centre and has the value given in table (5.1). Along the axes of the centre only these eight lines are

apparent, but when the magnetic field makes an angle with an axis, additional lines appear. These have been referred to as "forbidden" lines, but as can be seen from figure (5.2 a-d) they become stronger than the "allowed" lines about 12^{o} off axis. Their origin is attributed to transitions of the type $\Delta M = \pm 1$, $\Delta m = \pm 1, \pm 2$, where M and m are the electronic and nuclear magnetic quantum numbers respectively. Such lines have been observed for V^{2+} in MgO by Dickey and Drumheller[8], but only for the cubic spectra. The transitions were of the type

$$|\tfrac{1}{2},m\rangle \leftrightarrow |-\tfrac{1}{2},m+1\rangle \text{ and } |\tfrac{1}{2},m+1\rangle \leftrightarrow |-\tfrac{1}{2},m\rangle.$$

Bleaney and Rubins[9] have observed the "forbidden" lines for all fine structure components of V^{2+} in $ZnSiF_6.6H_2O$. The lines reported in the present work are assigned to the transitions

$$|\pm\tfrac{3}{2},m\rangle \leftrightarrow |\pm\tfrac{1}{2},m+1\rangle \quad \text{and} \quad |\pm\tfrac{3}{2},m+1\rangle \leftrightarrow |\pm\tfrac{1}{2},m\rangle.$$

The lines become allowed off axis owing to a second order mixing of fine structure and hyperfine structure terms. For $D, A << g\beta H$, Bleaney and Rubins derive the term

$$\frac{3DA\sin 2\theta}{4g\beta H}(I_+ + I_-)\{S_z^2 - \tfrac{1}{3}S(S+1)\}, \qquad (5.7)$$

which can be added to the spin Hamiltonian. For any spin level M, the operators $I_\pm$ connect nuclear levels where m differs by ± 1, and give rise to a breakdown in the usual selection rule, $\Delta m = 0$. The intensity of these transitions relative to the ordinary transitions, where m does not

change, is

$$\left[\frac{3D\sin 2\theta}{4g\beta H}\right]^2\left[1+\frac{S(S+1)}{3M(M+1)}\right]^2\{I(I+1)-m^2+m\} \qquad (5.8)$$

It can be seen to be zero along the axes and greatest when $\theta = 45^{\circ}$. Furthermore, the lines should be more intense at lower fields than at higher.

Further transitions of the type $\Delta m = 2,3$ etc., but with decreasing relative intensities, are also permitted. These arise since non-adjacent hyperfine levels are coupled by terms in $I_{\pm}^2$, $I_{\pm}^3$ arising from a repeated application of (5.8) and from further cross product terms containing nuclear spin raising and lowering operators.

If the term containing the cross-products between D and A is added to (5.1), the resulting perturbation formula for the energy of a state $|M,m\rangle$ can be written

$$E_{M,m} = g\beta H_o M + 2D(M-\tfrac{1}{2}) + AM_m + \frac{A^2}{2g\beta H_o}\{I(I+1)M - S(S+1)m + M_m(M-m)\}$$
$$+ g_N\beta_N H_o m + \{\frac{3D\sin 2\theta}{4g\beta H_o}\}^2\{\frac{2Am}{M}\}\{M^2 - \tfrac{1}{3}S(S+1)\}^2 \qquad (5.9)$$

Since higher terms contribute far less than 1 gauss to the line positions they are omitted. Neglecting for the moment fine structure and all but first order hyperfine terms, the positions of the $\Delta M = -1$, $\Delta m = 0, \pm 1, \pm 2$ lines relative to the centre of the hyperfine pattern are given by the expressions

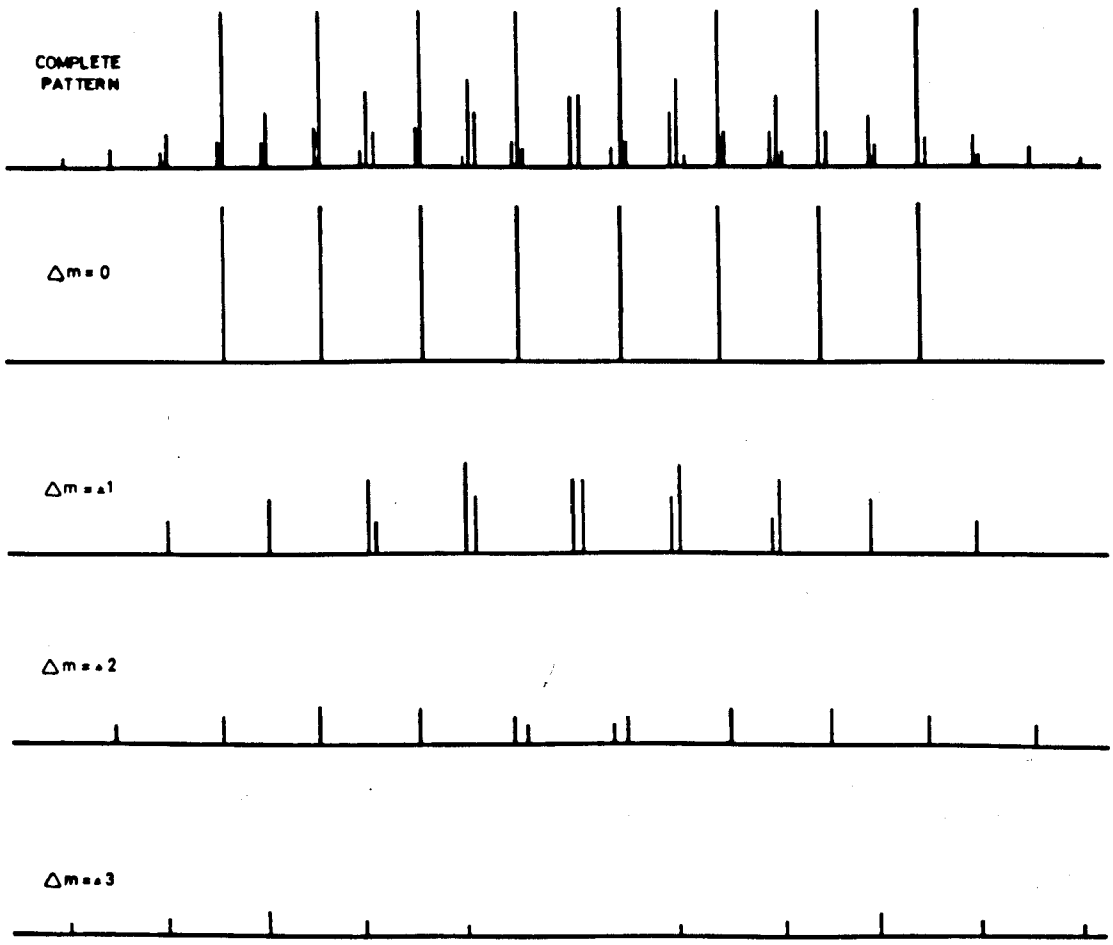

FIGURE 5.6 Analysis of the "Forbidden" Hyperfine Spectrum for M_S = 3/2 to 1/2.

$$\begin{aligned}
&\Delta M = -1, \quad m = 0 \; ; \quad \Delta H = Am \\
&\Delta M = -1, \quad m = +1; \quad \Delta H = A(m - M + 1) \\
&\Delta M = -1, \quad m = -1; \quad \Delta H = A(m + M - 1) \\
&\Delta M = -1, \quad m = +2; \quad \Delta H = A(m - 2M + 2) \\
&\Delta M = -1, \quad m = -2; \quad \Delta H = A(m + 2M - 2)
\end{aligned} \tag{5.10}$$

For $\Delta M = +1$, the expressions are the same, apart from an overall change of sign. If we consider the $^3/_2 \rightarrow \frac{1}{2}$ transition, the line positions will be as shown in figure (5.6). The higher order terms will shift these positions slightly and also provide the indicated splitting between the central doublets.

The spectra shown in figure (5.3) resemble the expected form. But the fairly large linewidth does not permit resolution of the central doublets, nor of the $\Delta m = \pm 2, \pm 3$ transitions from the other lines. Only the outer most of these can be seen in (5.3d).

Since the condition $D << g\beta H_o$ does not hold for this centre, the perturbation expression (5.9) must be used with caution. But providing θ is small, the line positions will be predicted with fair accuracy. This is the case, and the line positions agree with the theoretical values to within the experimental error. For small θ, the $\Delta m = \pm 1$ lines follow approximately the intensity dependence 1 : 1·7 : 3·1 : 4 : 4·3 : 4 : 3·1 : 1·7 : 1, which is calculated from (5.8) by assuming that the five doublets are completely unresolved. Since this appears to be the case, then the effect of second order terms on the five positions must be very small.

The angular variation of the intensities of the $\Delta m = \pm 1$ lines relative to the $\Delta m = 0$ lines agrees well with the theoretical value for small angles from the [110] axes. However, the departure of relative intensity from that predicted increases rapidly beyond about $\theta = 10^{\circ}$. This is for two reasons. Firstly, the formula (5.8) is one derived with the use of perturbation theory, so is inaccurate very far off axis for this centre. Secondly, it is not possible to resolve the $\Delta m = \pm 2$ lines from the $\Delta m = 0$ lines, so the apparent intensities of the latter are larger. In addition, a broadening of those "forbidden" lines, which are formed from the superposition of two lines, occurs off axis as a preliminary to splitting by the higher order hyperfine terms. The intensities of some of the $\Delta m = \pm 1$ lines are, therefore, apparently lower than they should be. A comparison of calculated and measured relative intensities is given in table 5.2.

θ°	I, Calculated	I, Measured
0	0	0
5	0.074	0.072
7	0.14	0.13
10	0.29	0.29
12	0.40	0.33
15	0.61	0.34
20	1.00	0.37

Table 5.2

The usual $\sin^2 2\theta$ angular dependence of "forbidden" spectral intensity appears to apply to this centre, at least for small angles between H and z.

5.6 The Nature of the Centre

We have found V^{2+} in an orthorhombic site in magnesium oxide, where the principal axis of distortion lies along a [110] type crystal direction. A few words, as to the origin of this defect, seem relevant.

By far the most divalent vanadium in this lattice is present in octahedral sites and gives rise to an isotropic spectrum. But about 1% is present in the distorted environment. This approximate figure is arrived at by considering the increase in spectrometer gain required to observe spectra as large as the cubic, and remembering that there are about twenty different transitions between which the intensity is shared. It is supposed that the inequivalence between x, y and z axes is brought about by a point defect along the z-direction. The x-axis is a [100] direction, so is already distinct from y and z. The nature of this point defect is a matter of conjecture, but it seems likely that it is a nearest neighbour cation vacancy. This may seem surprising, since the divalent vanadium does not require charge compensation. But, as mentioned earlier, most of the vanadium in MgO is present in the trivalent state and, as such, needs vacancies or univalent ions to preserve the overall electrical neutrality of the crystal. Since a large amount of vanadium is present, and no monovalent ion deliberately added, there must be a large number

of vacancies in the crystal. Charge compensation need not be local, so it is proposed that a few vacancies are available to distort the divalent vanadium sites. The possibility of distortion by nearest neighbour V^{2+} or V^{3+} ions has been considered. In these cases the spectrum would show additional structure owing to exchange effects between the neighbouring nuclei. None is observed for this centre.

The fact that no spectra due to V^{2+} in tetragonal symmetry are observed may be due to two factors. The first of these is concerned with the stability of the ion-vacancy configuration. The stable oxide of vanadium is V_2O_5. This has orthorhombic crystalline structure, where each vanadium atom lies at the centre of a distorted tetrahedron of oxygen atoms. It is proposed that in the magnesium lattice, the presence of a nearest neighbour vacancy to the vanadium ion stabilises the system more than if the vacancy were at a next nearest cation site. This is due to a slight alteration in the positions of the vanadium and oxygen atoms, and a partial return to the tetrahedral coordination favoured by vanadium. The effects on the crystalline geometry would be slight for the more remote defect.

The second possibility for non-observation of tetragonal lines depends upon the smallness of the expected zero field splitting. The values of $D = -0.053cm^{-1}$ for Mn^{4+} in MgO [10] and $D = 0.082cm^{-1}$ for Cr^{3+} in MgO [11] imply that the value for V^{3+} will be of this order. But the fact that the ion is not a charge misfit suggests that the distortion of the site would not be as great as for the other $3d^3$ ions. The value of

D will probably be smaller than those noted above. If this is the case, then the fine structure components would not be split sufficiently from the g=2 magnetic field to be observable against the profusion of lines in this region.

REFERENCES

1. M.D. Sturge, Phys. Rev. 130, 639 (1963).

2. M. Weger and W. Low, Solid State Physics, Suppl. 2. Paramagnetic Resonance in Solids, Academic Press, p.57 (1960).

3. H.H. Wickman, M.P. Klein and D.A. Shirley, J. Chem. Phys. 42, 2113 (1963).

4. W.E. Blumberg, "Magnetic Resonance in Biological Systems" Eds. A. Ehrenberg, B.G. Malmström and T. Vänngard, Pergamon Press (1967)

5. R.D. Dowsing, Dept. of Computer Science, Univ. College of Swansea, Private Communication.

6. J.D. Swalen and H.M. Gladney, I.B.M. Journal of Research and Development, p.515 (Nov. 1964).

7. Von Neumann, "Mathematical Methods for Large Computers", Ed. Ralston and Wilf, Wiley (1962) Chap. 7.

8. D.H. Dickey and J.E. Drumheller, Phys. Rev. 161, 279 (1967).

9. B. Bleaney and R.S. Rubins, Proc. Phys. Soc. 77, 103 (1961).

10. Chapter 3, Reference 21.

11. Chapter 3, Reference 19.

CHAPTER VI

E.P.R. OF V^{2+} IN MAGNESIUM OXIDE - II PAIR SPECTRA

6.1 Introduction

E.P.R. is a useful technique for studying exchange interactions since under suitable conditions the interactions between near neighbour atoms may be studied directly. The results obtained can then be related to the bulk magnetic properties of the concentrated material, provided that proper account is taken of the differing lattice spacings of the concentrated and diluted systems. More often than not, the isolated ion pair must be created artificially by doping a diamagnetic host to a high degree (~1%) so that appreciable numbers of impurity ions occupy adjacent lattice sites. The system may not then be a realistic one, but we can obtain information about coupled species that may not otherwise be available.

A recent review paper[1] contains numerous references to studies of exchange interactions; no general discussion of other studies is given here, except where directly pertinent to the present results. However the measurements of Smith[2] on V^{2+} in $KMgF_3$ are discussed, since they are of relevance. Smith observed spectra from pairs of V^{2+} ions, super-exchange coupled via an intervening fluorine ion. The exchange interaction was found to be antiferromagnetic and the exchange energy, measured in units of J/k, found to be $6.5^{\circ}K$.

6.2 The Theory of Exchange Coupled Pair Spectra

The spin-Hamiltonian for an isolated ion of spin S_1 situated in a crystal field of orthorhombic symmetry may be written as

$$\mathcal{H}_1 = g\beta \underline{H}\cdot\underline{S}_1 + D_c\left[\underline{S}_{1z}^2 - \tfrac{1}{3}S_1(S_1+1)\right] + E_c\left[\underline{S}_{1x}^2 - \underline{S}_{1y}^2\right] + A\underline{I}_1\cdot\underline{S}_1 \qquad (6.1)$$

where the g and A tensors are assumed to be isotropic and D_c, E_c are crystal field parameters.. Should a second ion be close, the possibility of exchange effects occurs. In this case, we may describe the combined system using the spin Hamiltonian,

$$\mathcal{H} = \mathcal{H}_1 + \mathcal{H}_2 + J\underline{S}_1\cdot\underline{S}_2 + D_e(3\underline{S}_{1z}\underline{S}_{2z} - S_1S_2) + E_e(\underline{S}_{1x}\underline{S}_{2x} - \underline{S}_{1y}\underline{S}_{2y}) \qquad (6.2)$$

Two terms of the type (6.1) have been added, plus additional terms to describe the exchange interaction. J was defined in Chapter II and is the isotropic part of the interaction. We adhere to the convention of writing J positive for antiferromagnetic exchange. Higher order terms[3] such as $-j(\underline{S}_1\cdot\underline{S}_2)^2$, $k(\underline{S}_1\cdot\underline{S}_2)^3$, and possible antisymmetrical couplings[4] such as $d(\underline{S}_1 \times \underline{S}_2)$ are ignored for the present. The terms D_e and E_e describe any low order anisotropy that might occur. They are composed of two parts, where a contribution comes from the dipolar interaction between ions and a part from anisotropic exchange.

For iron group ions equation (6.2) is usually dominated by the isotropic exchange term, written in the form,

$$H_J = J\underline{S}_1 \cdot \underline{S}_2 ,$$

which when expanded gives,

$$H_J = \frac{J}{2}\left[\underline{S}^2 - \underline{S}_1{}^2 - \underline{S}_2{}^2\right]$$

where $\underline{S} = \underline{S}_1 + \underline{S}_2$.

The eigenvalues of this Hamiltonian are,

$$\varepsilon_s = \frac{J}{2}\left[S(S+1) - S_1(S_1+1) - S_2(S_2+1)\right] \qquad (6.3)$$

For pairs of ions with $S_1 = S_2 = 3/2$ the relative energies corresponding to the different states of total spin are:

S	ε_s	$\Delta\varepsilon_s$
0	-15J/4	-
1	-11J/4	J
2	-3J/4	2J
3	9J/4	3J

$\Delta\varepsilon_s$ is the splitting between states S and S-1, and follows a Landé splitting rule. Had we chosen to include the second order exchange term $-j(S_1 \cdot S_2)^2$, the energy interval becomes

$$\Delta\varepsilon'_s = JS - jS\left[S^2 - S_1(S_1+1) - S_2(S_2+1)\right].$$

Each of the states comprises (2S+1) substates, which will be split by the remaining terms of (6.2). Equation (6.2) can be rearranged in the following more useful form, again assuming that J is the dominant term:

$$\mathcal{H} = g\beta\underline{H}.\underline{S} + \frac{J}{2}\left[S(S+1) - S_1(S_1+1) - S_2(S_2+1)\right] + \frac{A}{2}.S(I_1+I_2) + D_s\left[\underline{S}_z^2 - \tfrac{1}{3}S(S+1)\right] + E_s(\underline{S}_x^2 - \underline{S}_y^2) \quad (6.4)$$

D_s and E_s represent the tetragonal and orthorhombic zero field splitting terms compounded from the single ion anisotropic terms and the anisotropic exchange terms, according to

and

$$D_s = 3\alpha_s D_e + \beta_s D_c \quad (6.5a)$$

$$E_s = \alpha_s E_e + \beta_s E_c \quad (6.5b)$$

The matrix elements α_s and β_s are given by

$$\alpha_s = \tfrac{1}{2}\left[\frac{S(S+1) + 4S_1(S_1+1)}{(2S-1)(2S+3)}\right] \quad (6.6a)$$

and

$$\beta_s = \frac{3S(S+1) - 3 - 4S_1(S_1+1)}{(2S+1)(2S+3)} \quad (6.6b)$$

when the coupled ions have the same spin[5]. The hyperfine term in equation (6.4), $\frac{A}{2}S(I_1+I_2)$, shifts each energy level by $\frac{A}{2}(I_1+I_2)$ for transitions of the type $\Delta M_s = \pm 1$. Since I_1+I_2 can take values from $+(m_{I_1}+m_{I_2})$ to $-(m_{I_1}+m_{I_2})$ there is a total of $2(I_1+I_2) + 1$ hyperfine lines expected for each fine structure transition. The intensities of these lines follow a stairstep pattern 1:2:3:4 ..... 4:3:2:1, corresponding to the different possible ways in which I_1 and I_2 can be added

to compound the total nuclear spin. The spacing between each line will be $\frac{A}{2}$ gauss. These two features of the spectra give a clear indication of the presence of exchange coupled pairs.

6.3 The Vanadium Pair Spectra

We expect to observe anisotropic spectra from each of the states S=1, 2 and 3, and also a temperature dependence that is different for each state. For reasons that become evident later, the coupling between spins is assumed antiferromagnetic (J positive). Thus a diamagnetic state is lowest, and the S=3 level highest in energy. If J is not small, then the states are thermally populated to different extents. The spectra from the S=1 state are therefore expected to be the most intense. The observed pair spectra were originally attributed to this total spin, with the spectra from the higher levels too weak to observe. But several factors indicate that this is not the case, and in fact the resonances must be attributed to transitions within the S=2 state.

We shall list the reasons for making this decision.

i) The transitions within the S=1 and S=3 states are broadened by crystal field effects, whereas those of S=2 are not.

ii) Anisotropy plots of H against $\cos 2\theta$ give consistent values of D_s for S=2 from the slopes of low and high field plots but not for S=1. The value of D_s, if the spectra were from the S=1 state would be inexplicably large.

iii) Intensity considerations reveal that both S=1 and S=2 should be

readily observable if (i) is not operative. We discuss the first of these factors now, but defer the other two until sections (6.3.2) and (6.4).

6.3.1 The broadening of lines from the S=1, 3 states

The anisotropy of the spectral lines is expressed in equations (6.5). If the contributions of D_e, E_e, D_c and E_c to these terms is calculated for each spin level, it is found that for the S=2 state, D_c, E_c have no effect. This can be understood by listing the values of α_s and β_s calculated from equations (6.6), for an electron spin of $3/2$.

S	α_s	β_s
1	$17/10$	$6/5$
2	$1/2$	0
3	$3/10$	$2/5$

The zero value of β_s means that only D_e and E_e contribute to the anisotropy in the S=2 state, whereas the single ion crystal field terms have to be included for the other states. If we write the terms of interest as

$$D_c\left[\underline{S}_z^2 - 1/3S(S+1)\right],\ E_c(\underline{S}_x^2 - \underline{S}_y^2)\ ,$$

it is seen that any local variations in D_c and E_c will produce a broadening of the pair lines of states S=1, 3, but the S=2 level will remain unaffected. One such mechanism was introduced in Chapter III, where the broadening of the $\pm^3_2 \leftrightarrow \pm\frac{1}{2}$ transitions of V^{2+} single ions was

discussed. The large linewidth was attributed to small orthorhombic distortions whose magnitude varied from site to site. These departures from octahedral symmetry were variously attributed to nearby impurities of differing kinds or to V^{3+}.

Smith[2] proposed a different mechanism for the broadening of $\pm 3/2 \leftrightarrow \pm 1/2$ transitions of V^{2+} in $KMgF_3$. This would be responsible for the broadening of the S=1, 3 pair spectra in that host, and can also be applied to the present case. The broadening resulted from "vibrating effects" in the lattice that included a dynamic Jahn-Teller effect. In Chapter II we say that such an effect would not generally be expected for the V^{2+} ion since the $3d^3$ electron configuration has spherical symmetry. In other words, the $^4A_2$ ground state, being an orbital singlet, will not be directly affected by lattice phonons. But it is remembered that there is a departure of the g-value from 2.0023 resulting from the combined effect of the spin-orbit coupling and the orbital part of the Zeeman term. The state connected to the ground state by both of these is the orbital triplet $^4T_2$, so admixtures from this are responsible for the g-shift. The resulting impurity of $^4A_2$ term means that lattice vibrations will affect the ground state resonances.

The evidence for this effect was the fact that the widths of the broadened lines were greater at Q-band than at X-band frequencies. This is a result of the time averaging of the crystal field oscillations. For, given a sufficiently low microwave frequency, the broadening effects would be averaged to zero. But at Q-band, relatively few lattice

vibrations occur during the time of absorption of a microwave quantum so the lines are broadened.

The $\pm 3/2 \leftrightarrow \pm 1/2$ transitions of V^{2+} in octahedral symmetry sites in MgO are observed at X-band, although they broaden very greatly when the magnetic field is not along the [100] direction. At Q-band, however, they are never visible, although it is evident that they are present. The main $-\frac{1}{2} \leftrightarrow \frac{1}{2}$ line showed greatest apparent intensity with H || [100], and broadened away from this direction owing to the broadening of the outer fine structure transitions. Since at Q-band the splitting between the central and outer lines is only about 25% of the X-band splitting owing to the term $(A^2/2h\nu)$, their non-resolution at this frequency is readily explained. It is also quite possible that the broadening due to lattice effects also contributes to this effect.

Whatever the mechanism, the broadening of the single ion lines can be accounted for by the use of the term in D_c. This term is also present in the pair spectra Hamiltonian so would explain the broadening and possible non-appearance of all the S=1 and S=3 lines.

6.3.2 Description and analysis of the S=2 spectra

Whether the observed spectra arise from S=1, 2 or 3 states would normally be obvious from the number of observed lines in the spectrum. In the present case, however, most of the central region of the spectrum is obscured, since we are still dealing with the concentrated crystals in which the V^{2+} orthorhombic spectrum was observed. The visible lines could be attributed to any of the three states, since only two outer sets

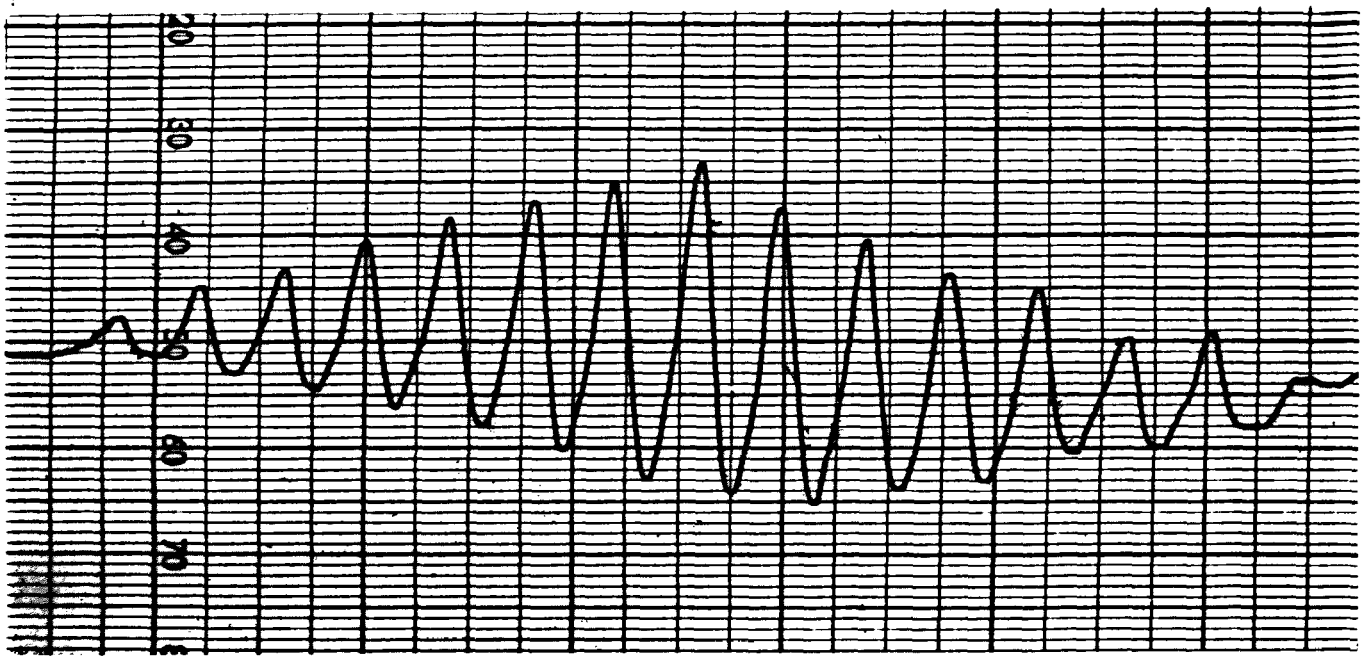

FIGURE 6.1 Pen Recording of V^{2+} Pair Spectra

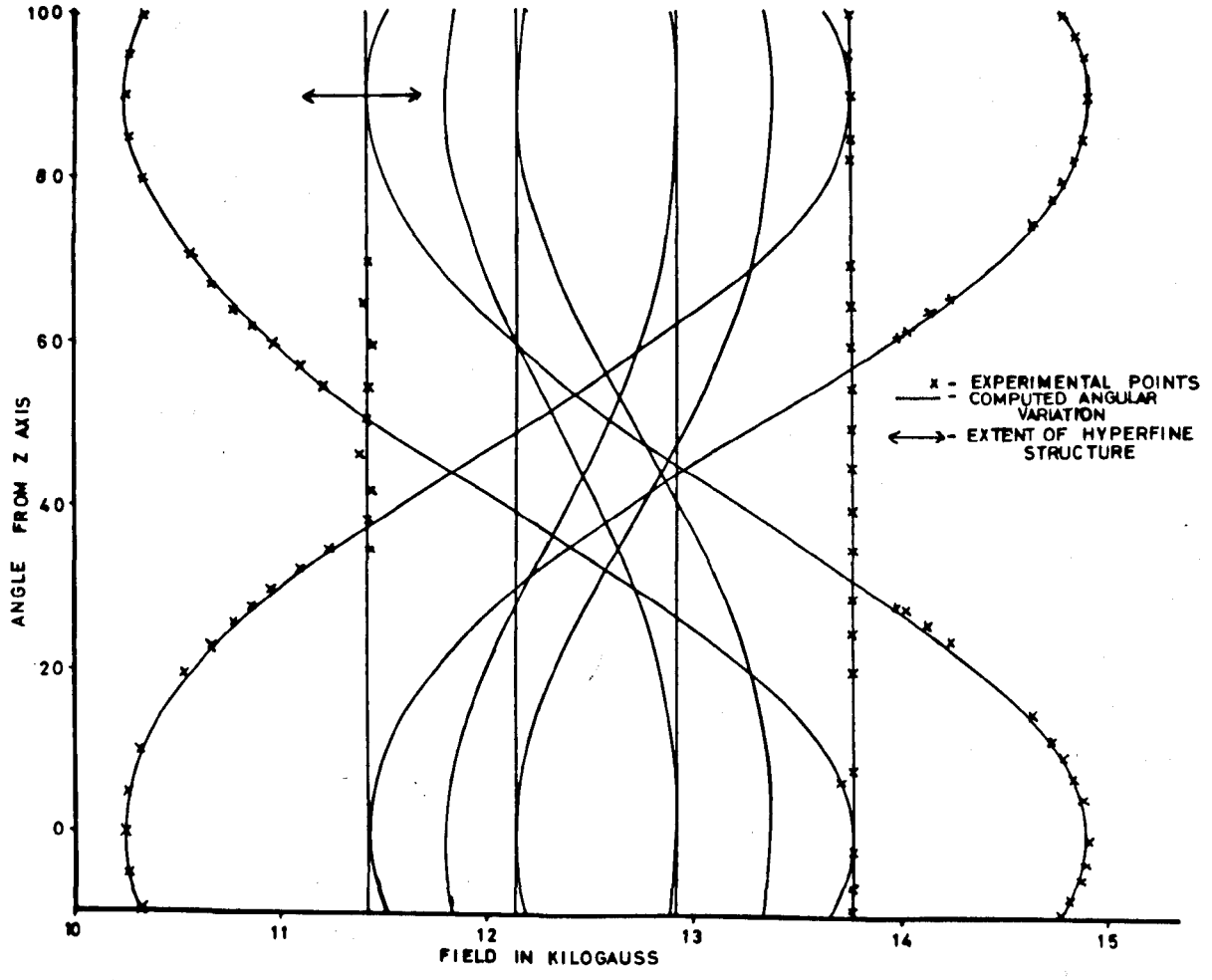

FIGURE 6.2 Angular Variation in the (100) Plane of the V^{2+} Pair Spectra.

of spectra were recorded at both high and low field. These were attributed to transitions where the magnetic field lay respectively parallel and perpendicular to the axis of the system. If the spectra were from S=2, there would be additional sets of lines closer to the central region. For the reasons outlined above, we assume that we observe spectra from the latter state, and shall interpret the results accordingly. The appearance of a typical set of lines is shown in figure (6.1). Here the characteristic stairstep pattern and hyperfine spacing equal to one half that of the single ion spectra is revealed.

The angular variation of the pair spectra with the crystal rotated in the [100] plane is given in figure (6.2). The field measurements were taken on the 8th (central) hyperfine line in all cases. Since this was the most intense line it could generally be clearly distinguished. This shows turning points along [100] directions, where the magnetic field lies parallel or perpendicular to the axis of the system. The spectra at 11.45 and 13.75kG, for the field along [100], are doubly intense, as a result of the superposition of the spectra from centres with [010] and [001] principal axes. The turning points at 10.3kG and 14.9kG occur when the magnetic field is parallel to a [100] axis. Such a pattern is only possible for a [100] principal distortion axis. In other words our pair spectra must be ascribed to next nearest neighbour V^{2+} ions in a [100] direction. There would be an intervening oxygen ion. This analysis was checked by performing the rotation in a [110] plane. Consistent results were obtained, turning points being

180° apart in this case, and no set of lines remaining isotropic as in the first case.

The results may be described using the following spin Hamiltonian:

$$\mathcal{H} = g\beta \underline{H}\underline{S} + \frac{J}{2}\left[S(S+1) - S_1(S_1+1) - S_2(S_2+1)\right] + \frac{A}{2}.S.(I_1+I_2) + D_s\left[\underline{S}_z^2 - \tfrac{1}{3}S(S+1)\right],$$

where $S=2$, $S_1 + S_2 = 3/2$, $I_1 + I_2 = 7/2$.

The measurements were performed at a Q-band frequency of 34.685GHz. From the high and low field turning points from the $M_s = \pm 2 \leftrightarrow \pm 1$ transitions we find $\Delta H = 4.7\text{kG} = 6D_s$.

Therefore $D_s = 776\text{G} = 0.0718\text{cm}^{-1}$

$g_x = g_y = g_z = 1.980$

$A_x = A_y = A_z = 40\text{G} = 0.004\text{cm}^{-1}$

No orthorhombic term is required. The measurement of J will be discussed in section (6.4). The angular variation of the spectrum was computed as in Chapter V. The predicted points are plotted, together with the experimental ones, in figure (6.2). Good agreement is revealed.

Since the intensities of the low field transitions were higher than those of the high field transitions, and the fact that this difference became more marked, the lower the temperature, we can ascribe a negative sign to D_s. This means that at zero field the $M_s = 0$ level lies highest and the $M_s = \pm 2$ levels lowest. The energy level diagram for this state and the measured parameters, is shown in figure (6.3).

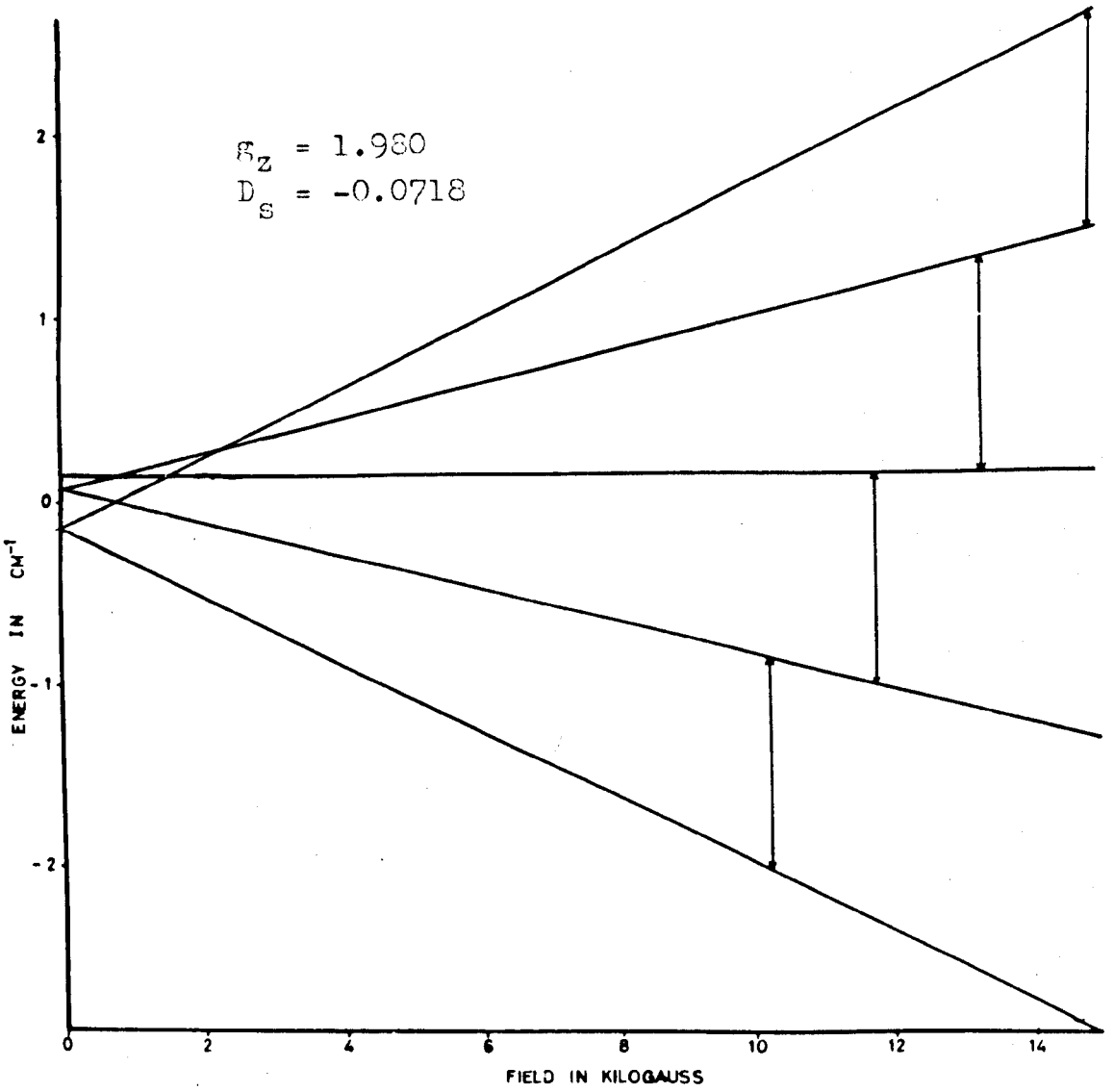

FIGURE 6.3 Energy Levels and Observed Transitions for the S=2 Pair State, with the Magnetic Field along the z-axis.

There is some evidence for the $\Delta M_s = \pm 2$ transitions at low field; these occur at about 6kG, which is in the region of the orthorhombic half field transitions. But when the crystal is rotated in the [110] plane, all the half field transitions split out from the central region, and over the range $\theta = 30^o$ to 70^o some weak lines with a pair-like structure are visible. These do not appear to move very much and are somewhat indistinct, so no measurements were attempted.

To check whether the spectra obtained were in fact from the S=2 state, anisotropy plots[2] of H against cos2θ were made. Starting from the perturbation formula, including only terms in D, up to second order, we write

$$g\beta H = h\nu - (M-\tfrac{1}{2})D(3\cos^2\theta-1) - \frac{1}{8h\nu}\left[D\sin^2\theta\right]^2(2\underline{S}^2-6M^2+6M-3) + \frac{\sin^2\theta}{2h\nu}.D^2\cos^2\theta(4\underline{S}^2-24M^2+24M-9)$$

If the terms in $\cos^2\theta$ and $\sin^2\theta$ are written respectively in terms of $\frac{1}{2}(1 \pm \cos2\theta)$, the equation reduces to the following for the S=2, $M_s = \pm 2 \leftrightarrow \pm 1$ transitions.

$$g\beta H = h\nu \pm \tfrac{3}{4}D_s - \frac{129}{32}\frac{D_s^2}{h\nu} + \cos 2\theta\left[\pm\frac{9}{4}D_s - \frac{3D_s^2}{16h\nu}\right] + \frac{135D_s^2}{32h\nu}\cos^2 2\theta.$$

Differentiating with respect to cos2θ, we obtain

$$g\beta\frac{\partial H}{\partial(\cos2\theta)} = \frac{9}{4}D_s - \frac{3D_s^2}{16h\nu} + \frac{135D_s^2}{16h\nu}\cos2\theta$$

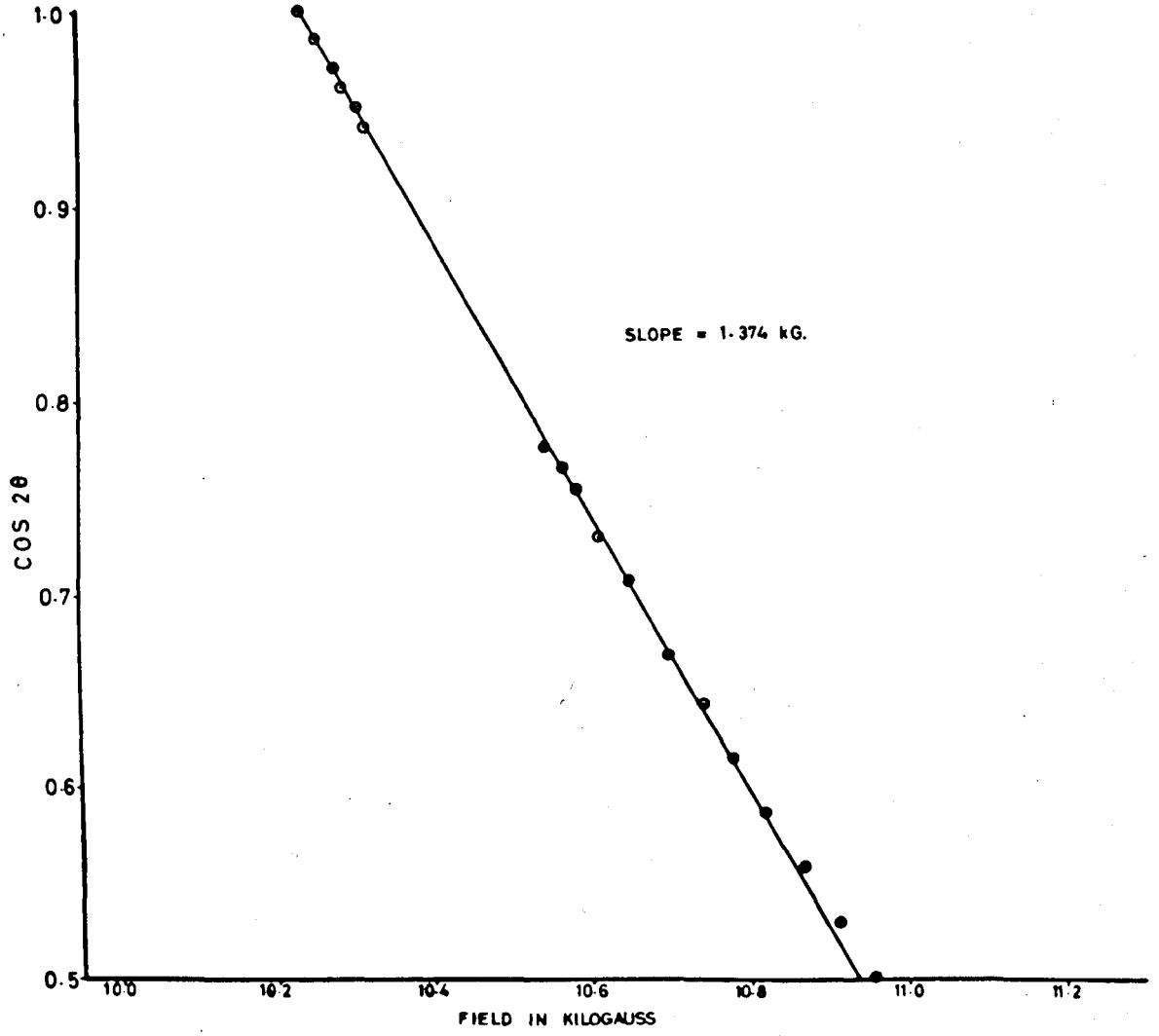

FIGURE 6.4 Low Field Anisotropy Plot.

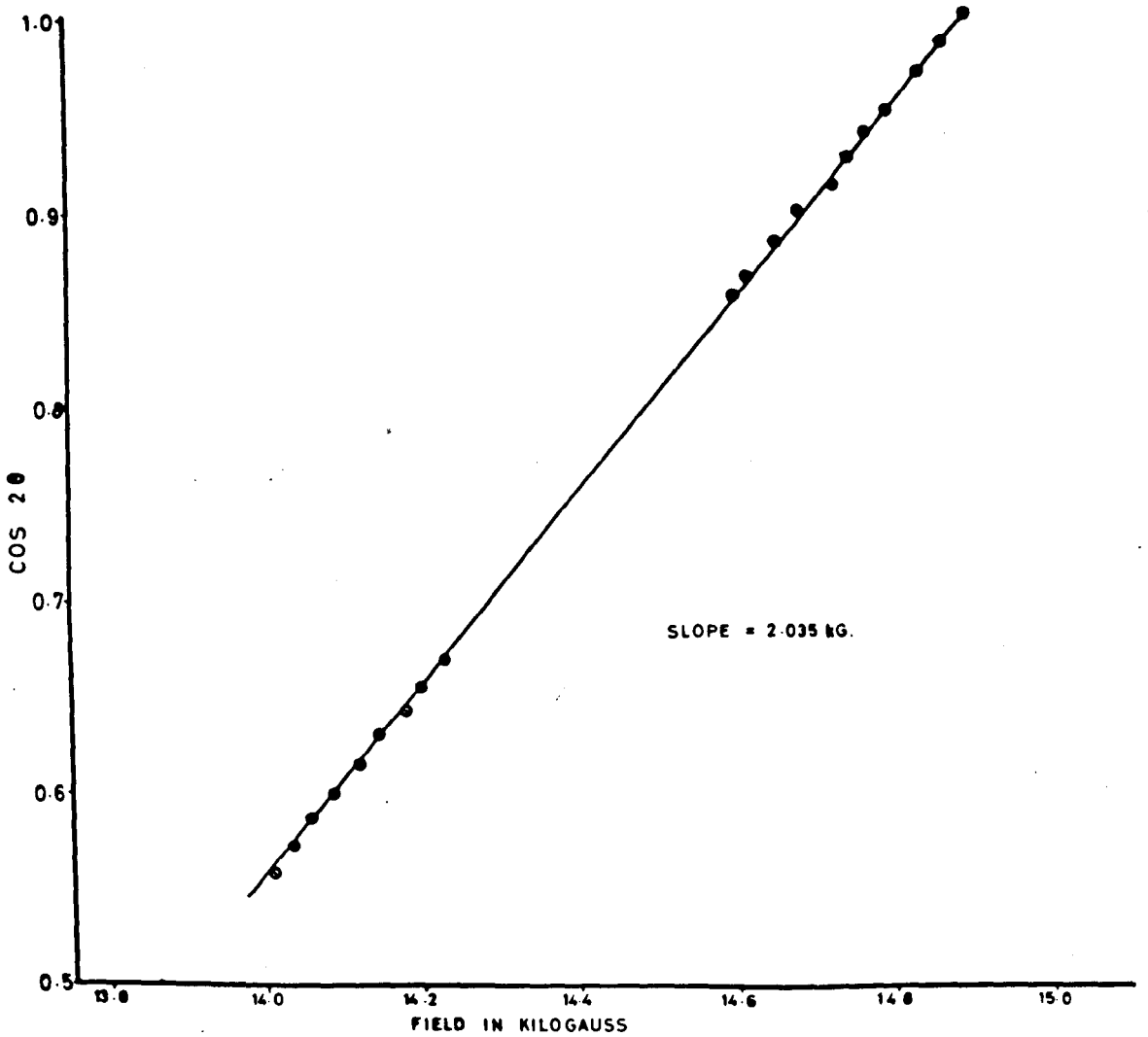

FIGURE 6.5 High Field Anisotropy Plot.

For small θ, this can be approximated to

$$\pm \frac{9D_s}{4} + \frac{33D_s^2}{4h\nu} \qquad (6.7)$$

which gives the slope of the straight line obtained by plotting H against $\cos 2\theta$.

Similarly the slopes of anisotropy plots for $M_s = \pm 1 \leftrightarrow 0$ transitions of the S=1 state are given by

$$\pm \frac{3D}{4} - \frac{D^2}{4h\nu} \quad , \text{ for small } \theta. \qquad (6.8)$$

The plots are reproduced in figures (6.4) and (6.5) are are seen to be linear except at angles where $\theta \gtrsim 25^{\circ}$.

The slopes are $1.374\text{Kg} = -0.1270\text{cm}^{-1}$ (Low field)

and $2.035\text{Kg} = 0.1881\text{cm}^{-1}$ (High field)

Substituting these into (6.7) and (6.8) we find values for D_s. We compare these with the measured values below:

S	D_s(slope)	D_s(meas.)
1	0.275, 0.163	0.215cm^{-1}
2	0.0688, 0.0732	0.0718cm^{-1}

The results for the S=2 state are much more consistent with one another and with the directly obtained experimental value, than is the case for the S=1 state. We submit this as further proof of the correct choice of state. The fact that the two values of D_S obtained for the S=2 case do

not quite agree, may be evidence for a possible anisotropy in the g-value, as Smith[2] found. But without more accurate field measurements, this cannot definitely be established.

6.4 The Measurement of the Exchange Energy

It was stated earlier than the states above S=0 are thermally populated, and that the intensities of the spectra within each state are dependent on temperature. By measuring this variation with temperature, the separation between levels can be determined. This will enable the nature of the exchange interaction to be revealed.

For simplicity, we assume a simple isotropic exchange, which gives rise to levels separated according to a Landé interval rule. The intensity of a transition of the type $\Delta M_s = \pm 1$ within a spin state S can be written

$$I \propto \frac{\exp[-\epsilon_s/kT] - \exp[-(\epsilon_s + h\nu)/kT]}{\Sigma(2S + 1)\exp[-\epsilon_s/kT]} \qquad (6.9)$$

where the denominator is the partition function summed over all the four spin states and the numerator represents the difference in relative populations of the spin levels between which the transition occurs. If we consider the S=2 state, whose energy is 3J above that of the ground state, (6.9) becomes

$$I \propto \frac{[1 - \exp(-h\nu/kT)].\exp(-3J/kT)}{1 + 3\exp(-J/kT) + 5\exp(-3J/kT) + 7\exp(-5J/kT)}$$

This lengthy expression has been programmed, and relative intensities can be very quickly obtained from the computer for any selected value of J and T.

The experimental determination of the temperature dependence of pair spectra intensities is not necessarily a straightforward matter. Factors such as the change in cavity Q and coupling are unpredictable and it would be virtually impossible to allow for them in making intensity measurements. The increase in sensitivity of the resonance technique on lowering the temperature would be another factor requiring correction. For this reason it is necessary to refer pair intensities to the intensity of a standard line that does not show a temperature variation, apart from that attributable to the change in relative populations of adjacent spin levels. This thermal effect acts equally on both reference and pair spectra. The selection of a suitable reference ion has to satisfy certain criteria. The first of these has already been stated. Further requirements are set out below.

1) If possible, the required resonance should come from the same sample as the pair lines. This gets round the difficulty that two different specimens may not be in exactly the same magnetic or microwave fields. With a change in temperature the distribution of these within the cavity may change, thus giving erroneous relative intensities.

2) The reference line should not change its linewidth over the range of temperatures used.

3) The line should be clearly observable and well separated from others,

so that its intensity can be easily measured.

4) The line should, ideally, be of comparable amplitude and width as the pair lines and in a similar region of the spectrum.

Two simple possibilities were tried. The lines selected were one each of the hyperfine components of the single ion V^{2+} and Mn^{2+} resonances. Both of these satisfied conditions (1) to (3), but not (4), as regards the amplitude and field position. The line widths were similar. However, a simple change in spectrometer gain between a pair measurement and a reference measurement got round the problem of different amplitudes. The precision step attenuators fitted to the Varian V-4560 100 kHz field modulation and control unit enabled a return to previously used gain settings. The 2kG difference in field between the pair and reference lines presented no problem either, since the Fieldial regulator permitted easy selection of magnetic field values. The major problem with the V^{2+} single ion hyperfine line was its great intensity. This was such as to alter the D.C. bias at the crystal by as much as 25%, and so modify the sensitivity of the whole system. This effect was magnified at lower temperatures owing to the greater signal strength; it could not be allowed for in the relative intensity measurements. For this reason the weaker hyperfine line belonging to Mn^{2+} was chosen, since the resonance did not affect the leakage at the crystal to any significant extent. Manganese had not been added to the crystal, but was found as an impurity. This is not an uncommon occurrence.

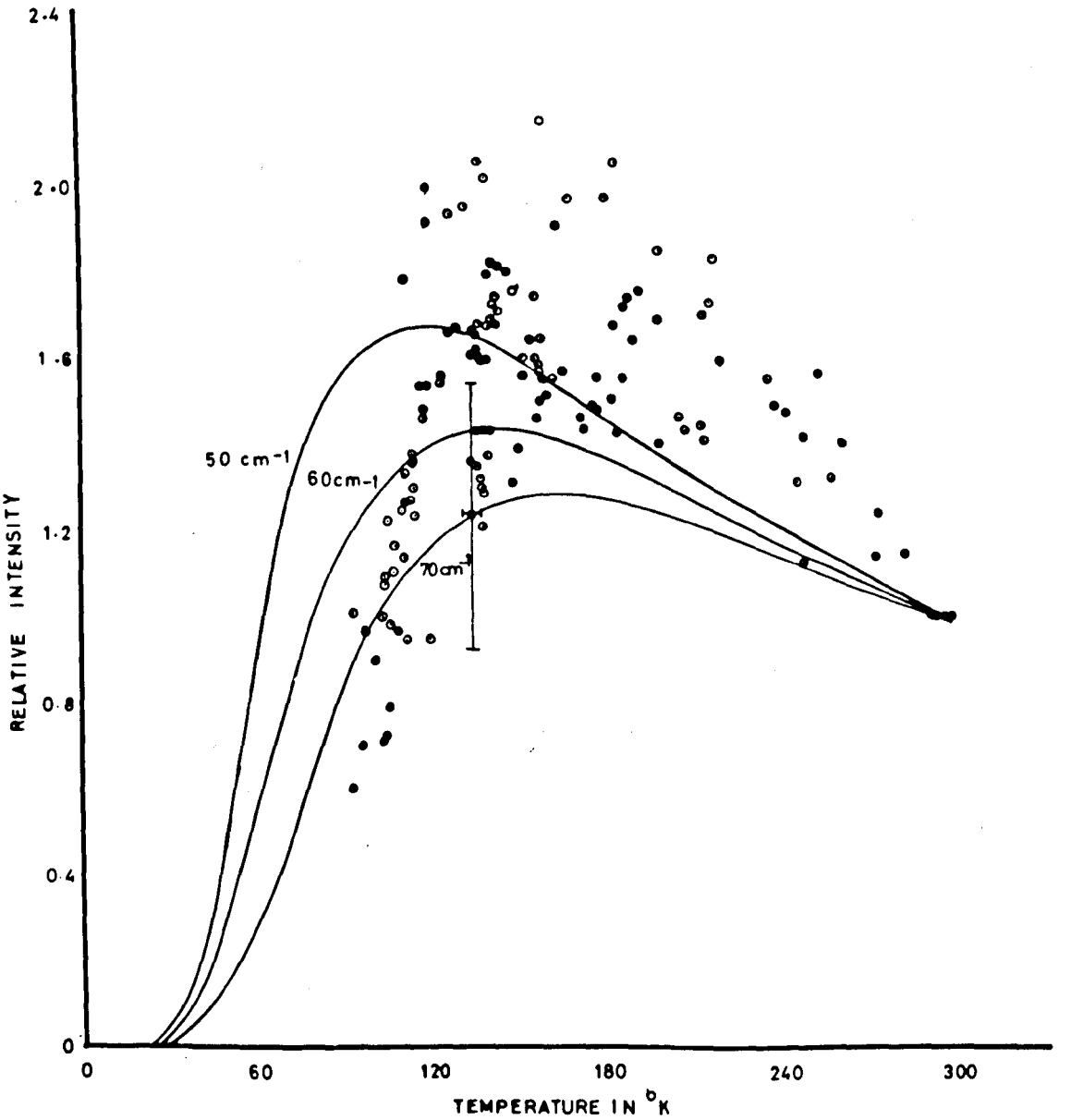

FIGURE 6.6 Experimental and Theoretical Temperature Dependence of Pair Spectra Intensity.

Since no estimate of the size of J was available, it was not known over which range of temperature measurements would need to be made. As a preliminary to plotting a temperature dependence of the pair intensity, the range of temperature from ambient to 77°K was first investigated using the gas flow system (see Chapter IV). The first measurement on any run was always made at room temperature. The eighth pair line was selected for the measurements, since this was easily identified and was the most intense. At lower temperatures no alteration in spectrometer gains for either pairs or reference spectra was required if the initial settings were sufficiently low. Since the linewidth of the pair lines decreased with temperature, the peak to peak height of the second derivative was no guide to the relative intensity of the spectra. So it was necessary to take the mean of the heights, H and widths W of several recordings and take the intensity as $I \propto H.W^2$. We assumed that no lineshape alteration had occurred. The manganese line did not change its linewidth, so approximate integration was unnecessary.

The temperature dependence of pair intensity is recorded in figure (6.6). The large scatter of experimental points gives some indication of the difficulty of obtaining intensities from the first derivative spectrum. The greatest source of error was in the measurement of the pair line width. The individual measurements varied by about ±6% from the mean of several recordings, so produced a larger error when the product of width squared and height was taken. The error in the height was about ±2.5%, and the overall error in calculated intensity

was typically ±25%. This figure is arrived at by considering that the intensities are calculated from the following formula

$$I \propto \frac{P(T)}{P(R)} \times \frac{C(R)}{C(T)} \quad ,$$

where P(T), P(R) are the pair intensities at some temperature, T, and at room temperature respectively. C(R), C(T) have similar meanings for the cubic spectra. The errors in P(T), P(R) taken separately, double when their ratio is considered.

Temperature stability was generally good, provided care was taken to allow the system to settle before taking measurements. However, in the ranges near the low temperature limit of the equipment, measurements had to be taken quickly. Not too much reliance is placed on the experimental points obtained in this region.

The one important feature of the temperature variation that remains clear is the fact that it shows a maximum in the region 130 - 170^{o}K. We can state that for the S=2 state this implies that the exchange temperature J/k must be of order 30% of these temperatures. In an attempt to restrict this range we have plotted the computed curves for various values of J. Although none of these fit the experimental points particularly well, the best fit appears to be for J = 60cm^{-1}.

There may be second order corrections to this, involving the biquadratic term $j(\underline{S}_1 \cdot \underline{S}_2)^2$, but since we are unable to observe spectra from the other states, it is not possible to say anything about the magnitude of j. The correction would in any case be expected to be small

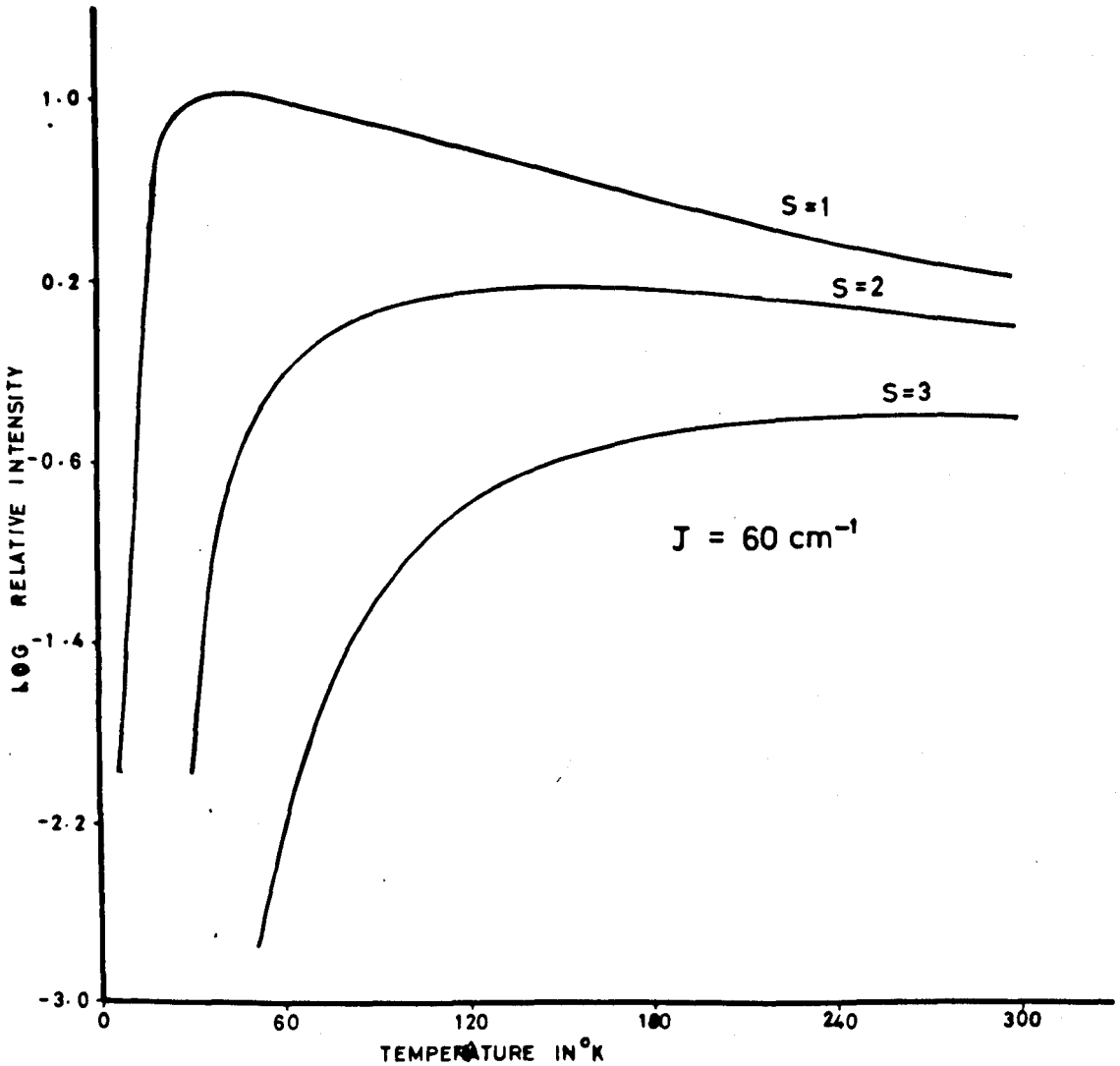

FIGURE 6.7 Computed Temperature Dependence of Intensity of E.P.R. Transitions within the Pair States.

and for a value of $j/J = 0.05$ as found by Harris and Owen, would be about $0.02cm^{-1}$.

Figure (6.7) shows a plot of the intensities of all three spin states as a function of temperature. The logarithmic values of relative intensity underestimate the temperature variation, but were necessary in order to plot the three curves together. A similar plot for $J = 150cm^{-1}$, assuming that the spectra are from an S=1 state, reveals that at room temperature, spectra from the S=2 state would be about one-fifth of the intensity of the S=1 and should be readily observable although weak. None were observed; consequently our assignment appears to be reasonable.

6.5 Discussion of the Anisotropy

In equation (6.5a), we have found $D_s = -0.0718$, $\alpha_s = \frac{1}{2}$, so this gives $D_e = -0.0479cm^{-1}$. This term may be a combination of terms representing the dipolar splitting and other exchange effects:

$$D_e = D_d + D_E \tag{6.10}$$

The magnitude of D_d may be calculated from the expression for the interaction between two magnetic dipoles which is of the form

$$\mathcal{H}_D = -g^2\beta^2 \left[\frac{\underline{S}_1 \cdot \underline{S}_2}{r_{12}^3} - \frac{3(\underline{S}_1 \cdot \underline{r})(\underline{S}_2 \cdot \underline{r})}{r_{12}^5} \right]$$

For a parallel spin alignment this reduces to:

$$- \frac{g^2\beta^2}{r_{12}^3} \left[S_1 S_2 - 3 S_1 S_2 \cos^2\theta \right]$$

r_{12} is their distance of separation. The dipolar splitting term D_d is the coefficient of this expression, i.e.

$$D_d = - \frac{g^2\beta^2}{r_{12}^3}$$

and has value $1.732 cm^{-1}$ for $r = 1\text{Å}$ and $g = 2$.

The problem that immediately arises is what value to choose for r for two vanadium ions separated by an intervening oxygen ion. The normal distance between magnesium ions in the pure crystal of MgO is 4.20Å, but it is not at all certain whether this figure is applicable to the present case. Without information to the contrary, we can only assume that r lies somewhere between 4.20Å and the 4.06Å found for the lattice constant of the cubic vanadium monoxide[5]. This value for r may be quite wrong, however, since vanadium forms other more stable oxides, where the vanadium-oxygen distance varies from as little as 1.76Å (VO_2) to 2.06Å (V_2O_3).

If we take $r = 4.13\text{Å}$, $D_d = -0.0246 cm^{-1}$. Making the unreasonable assumption of $r = 2 \times 1.76\text{Å}$, $D_d = -0.0396 cm^{-1}$. Even the latter is too small to account for the size of D_e purely in the terms of the dipolar interaction, so we return to our reasonable estimate of r. The difference between D_d and D_e amounts to $0.0233 cm^{-1}$; so we seek some other mechanism to account for the additional anisotropy.

The term D_E in equation (6.10) may provide the additional zero field splitting. It can be split into two possible parts, which represent respectively the anisotropic exchange and the antisymmetrical exchange. The origin of these effects lies in the nature of the coupling between spins. If we take a general spin-spin interaction term

$$\underline{S}_1 \, \underline{T} \, \underline{S}_2$$

this can be decomposed into two parts

$$\underline{S}_1 \cdot \underline{T}_s \cdot \underline{S}_2 + \underline{S}_1 \cdot \underline{T}_A \cdot \underline{S}_2$$

where the first is symmetric and the second antisymmetrical under exchange of spins. The symmetrical part is composed of an isotropic part $J\underline{S}_1.\underline{S}_2$ and an anisotropic part $\underline{S}_1.\underline{K}.\underline{S}_2$ while the antisymmetrical contribution to exchange is written as $\underline{d}.(\underline{S}_1 \times \underline{S}_2)$. The overall exchange between spins, is then

$$H_{ss} = J\underline{S}_1 \cdot \underline{S}_2 + \underline{S}_1 \cdot \underline{K} \cdot \underline{S}_2 + \underline{d}.(\underline{S}_1 \times \underline{S}_2) \qquad (6.11)$$

The first term has already been considered, but more needs to be said about the other two couplings which have been implicit in the term D_E up to now.

6.5.1 The antisymmetrical exchange

An antisymmetrical coupling between spins was originally proposed by Dzyaloshinsky[4] on symmetry grounds, to explain the weak ferromagnetism of antiferromagnetic materials such as $MnCO_2$. Moriya[7]

has developed the theoretical basis for this exchange, and has shown that it arises by extending the theory of superexchange coupling to include spin-orbit interactions. The term of the form $\underline{d}.(\underline{S}_1 \times \underline{S}_2)$ produces a canting of spins, since its energy of lowest when the spins are perpendicular. Hence in an antiferromagnet which nevertheless exhibits a weak spontaneous magnetisation, the term considered and the isotropic $J\underline{S}_1.\underline{S}_2$ are in mutual competition. A canting of the sublattice magnetisation occurs and gives rise to a net ferromagnetism.

The size of the term is of the order

$$d \sim (\frac{\Delta g}{g}) J, \quad \text{where } \Delta g = g - 2$$

and represents the effect of the spin-orbit admixture from higher states into the ground state. In our case, for $g = 1.98$, $J = 60cm^{-1}$

$$d \sim 0.6cm^{-1}.$$

This would be far too great to explain the value D_E as it stands, so either we must make a more exact estimate or find a reason to reject antisymmetric exchange between V^{2+} ions. The latter course of action proves a very easy one.

Symmetry arguments indicate that only in cases where the coupled ions are different species or are in non-equivalent crystal sites, is antisymmetric exchange possible. Such is the case for Cu^{2+} in zinc formate dihydrate where the four copper ions in each unit cell occupy two different types of site. Wagner et al.[8] hoped to see E.P.R. spectra

from exchange coupled dissimilar copper ions and included an anti-symmetric term in their spin Hamiltonian. Their failure to observe such spectra was attributed to the smallness of the overall exchange, rather than to the absence of terms in $\underline{d}$.

Also Seehra and Castner[9] have found an unusual linear temperature dependence of the E.P.R. linewidth of Cu in $Cu(HCOO)_2.4H_2O$ which they attribute to phonon modulation of the antisymmetrical exchange term. In addition Duerst and Kokoszka[10] have observed a deviation of the g-tensor of Cu^{2+} - Ni^{2+} pairs relative to that from Cu^{2+} - Zn^{2+} pairs in the dimeric Cu^{2+} complex dichlorobispyridine-N-oxide copper. This appears to be the first direct evidence of antisymmetric exchange. However it is an extremely favourable system since the system lacks a centre of symmetry and the coupled ions are different species.

Since our system has similar ions and is symmetrical about a perpendicular plane midway between them, we choose to ignore the effects of antisymmetry.

6.5.2 Anisotropic exchange

The term $\underline{S}_1.\underline{K}.\underline{S}_2$ in equation (6.11) can be written in the expanded form $J_{zz}\underline{S}_{1z}.\underline{S}_{2z} + J_{xx}\underline{S}_{1x}.\underline{S}_{2x} + J_{yy}\underline{S}_{1y}.\underline{S}_{2y}$ where J_{zz} is chosen as the largest term and represents the diagonal part of the anisotropy. The other terms are off-diagonal in the energy matrix. Between them, these three terms lead to zero field splittings of the energy levels of the state in question, and so can be related to the more usual D and E parameters. In the present case only D is necessary to describe the spectra, so we note that $J_{zz} = D_s$.

The anisotropic term, like the antisymmetric term, arises from higher levels via the spin-orbit coupling. The anisotropy is a feature of the arrangement of atomic orbitals in space. Those orbitals that are directed along the z-axis joining the coupled ions may be involved in exchange, while those perpendicular are not. This asymmetry is coupled to the otherwise orbitally free $^4A_2$ ground state by the spin-orbit coupling, and produces an angular dependent zero field splitting. The magnitude of the anisotropy is of the order

$$J_{zz} \sim (\Delta g)^2 J,$$

where Δg has its previous meaning. Using the previous values of Δg and J,

$$J_{zz} \sim 0.024 cm^{-1}.$$

This is remarkably close in value to the required anisotropy, assuming that no corrections are required. But Smith[2] has performed detailed calculations for V^{2+} in $KMgF_3$ and finds that the order of magnitude anisotropic term must be reduced by a factor $1/48$, making any contribution to the zero field splitting negligible. It is not certain how closely similar is the present case, but if any reduction factor is required, then discrepancies between theory and experiment will arise.

We propose that the anisotropic exchange is in fact small and that the cause of our difficulty is in the use of the classical dipolar expression to derive splittings produced by quantum mechanical effects. The dipolar interaction between ions assumes that these are

localised dipoles, a definite distance r_{ij} apart. Since the V^{2+} ions are super-exchange coupled through the intervening oxygen (section 6.6), there is a considerable interchange of electrons over the system. It is not unreasonable to assume then, that the anisotropy term will be rather larger than that predicted from the classical formula. In view of the strong exchange coupling ($J \simeq 60cm^{-1}$), this magnetic interaction could account entirely for the zero field splitting. We might point out that the problem would be three times worse if we had selected the S=1 state as the source of the spectra.

6.6 The Mechanism of Super-exchange

From the results of the E.P.R. of the V^{2+} pairs we have established that the structure of the centre is $- V^{2+} - O^{2-} - V^{2+} -$. The configuration is linear and lies along a [100] direction in the crystal, the vanadium ions occupying cation sites in the lattice. The oxygen is normally diamagnetic, and direct exchange effects between the paramagnets would be negligible. However, there is always the possibility of electron transfers among the three ions. This may arise in a variety of ways[11], some of which are illustrated below.

i) $- V^{+} - O^{-} - V^{2+}$

ii) $- V^{2+} - O^{-} - V^{+}$

iii) $- V^{+} - O - V^{+}$

iv) $- V^{+} - O^{2-} - V^{3+}$

v) $- V^{3+} - O^{2-} - V^{+} -$

The first two mechanisms are the usual one electron transfer processes, normally referred to as super-exchange. Types (iii) to (v) are double exchange mechanisms. All of these mechanisms may occur to some extent, but we shall only mention the single exchange since this is the most probable.

V^{2+} in the octahedral field of MgO has the t_{2g} orbitals lowest, and each of these is occupied by a single electron. O^{2-} has its 2p orbital full. The transfer of an electron from the oxygen to either neighbouring vanadium ion will give a configuration such as

V^{+}	O^{-}	V^{2+}
↑	↓↑	↓
	↓↑	
↑	↓↑	↓
↑↓	↑	↓
t_{2g}	2p	t_{2g}

where the arrows represent spins up or down. After the exchange there is a parallel arrangement of spins between the oxygen ion and the left hand vanadium ion. The vanadium ion on the right will now tend to align its spin antiparallel to that on the oxygen since this is a lower energy configuration. The overall coupling between vanadium spins is anti-parallel and therefore antiferromagnetic.

In terms of orbital overlap, the exchange operates via the $3d_{yz}$ and $3d_{zx}$ vanadium orbitals and the $2p_x$, $2p_y$ orbitals of the oxygen. The $2p_z$ orbital, although directed towards the vanadium does not interact

strongly with the latter. We should expect a stronger exchange interaction for the present case than for the vanadium ions coupled through an intervening fluorine ion. This is a result of the smaller tendency of oxygen to hold electrons than the more electronegative fluorine. Our result of $J = 60cm^{-1}$ compared with $J = 4.5cm^{-1}$ for V^{2+} pairs in $KMgF_3$ [2] is consistent with this view. For the case of chromium in corundum, the higher oxidation state of the ion presumably makes it more ready to accept electrons from the oxygen than divalent vanadium. So in this case we expect a higher exchange constant, once again. The values of $J = 390cm^{-1}$ for nearest neighbour pairs[12,13] and $84cm^{-1}$ for second neighbours[14] have been measured. It would appear that our value for the intermediate case is a reasonable one.

Huang[15] has performed calculations for the case of right angled exchange between nearest neighbour V^{2+} ions in MgO. The result is $-24cm^{-1}$, which indicates ferromagnetic exchange. The strength of the interaction is encouraging, but since we have observed no orthorhombic spectra, we cannot comment on the exactness of this value.

We can make no comparison between results obtained and the bulk magnetic properties of vanadium oxides, since little is known about them. Antiferromagnetism is suspected in V_2O_3 [16], but none has been reported for the other oxides. Current interest in their semiconductor to metal transitions[17] will no doubt lead to a better understanding of their properties.

6.7 The Temperature Dependence of Pair Linewidth

We shall conclude this chapter with an explanation of the decrease in the width of the pair lines as the temperature is lowered. This effect enables an estimation of J to be made without recourse to integration of spectra and comparison with a standard.

Since the S=2 state is well separated from the other excited levels, we make a simplifying assumption that this state and the ground S=0 state form a two level system. We have found that the separation in energy is 3J. Considering the relaxation of electrons from the S=2 level to the ground state, we restate equation (1.11)

$$\frac{dn}{dt} = -\frac{(n - n_o)}{T_1} \qquad (6.12)$$

where n is the existing difference in populations between the upper and lower levels, n_o is the thermal equilibrium difference and T_1 is the spin-lattice relaxation time. The latter can be defined as

$$T_1 = \frac{1}{W^+ + W^-}$$

where $W^{\pm}$ are the transition probabilities from the upper to lower levels and vice versa. We quote approximately the temperature dependence of these probabilities[18]

$$W^+ \sim \frac{\exp(h\nu_{ph}/kT)}{\exp(h\nu_{ph}/kT) - 1} = \frac{\exp(3J/kT)}{\exp(3J/kT) - 1}$$

$$W^- \sim \frac{1}{\exp(h\nu_{ph}/kT) - 1} = \frac{1}{\exp(3J/kT) - 1}$$

where $h\nu_{ph}$ is a phonon energy equal to the splitting between the levels. From (6.12)

$$T_1 \sim \left[\frac{\exp(3J/kT) - 1}{\exp(3J/kT) + 1}\right]$$

Since ΔH, the linewidth, $\propto \frac{1}{T_1}$ then from consideration of the Uncertainty Principle,

$$\Delta H \propto \left[\frac{\exp(3J/kT) + 1}{\exp(3J/kT) - 1}\right] \qquad (6.13)$$

We distinguish three possibilities:

i) If $3J \ll kT$, we can expand the exponentials and find $\Delta H \propto \frac{2}{(3J/kT)}$ Thus at high temperature the linewidth is proportional to the absolute temperature.

ii) If $3J \gg kT$, we can neglect the units in the numerator and denominator: the linewidth is independent of temperature at low temperature.

iii) If $3J \sim kT$, then we expect a transitional region where the linewidth is non-linearly related to the temperature.

Examination of figure (6.6) indicates that these predictions are upheld for the present pair lines. At the higher temperature a linearity is approached, whereas in the lower temperature region a flattening off is noticeable. In this case the curve is best fitted to an equation of the form[19]

$$\Delta H = \frac{A}{1 - \exp(-3J/kT)}$$

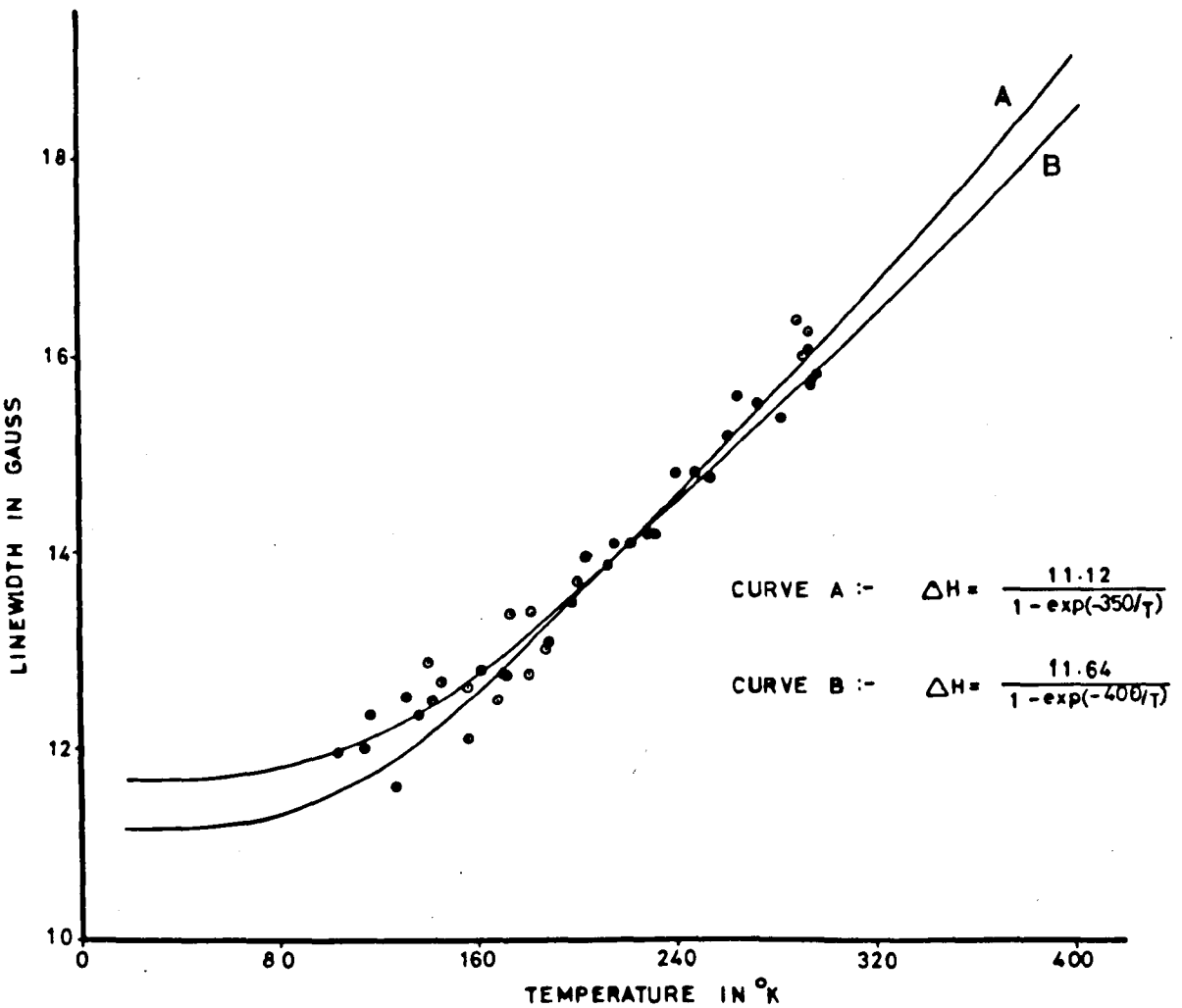

FIGURE 6.8 Temperature Dependence of Pair Spectra Linewidth.

which has the same type of temperature dependence as (6.13). A is a constant. We plot this function for two values of 3J in figure (6.8). With $3J/k = 350^{\circ}K$, the curve fits well the high temperature part of the curve but levels off at too small a linewidth. For $3J/k = 400^{\circ}K$, the fit at lower temperatures is much improved although the curve deviates from the experimental points in the higher regions. The best fit would probably be found at an intermediate value near $3J/k = 375^{\circ}K$ or $J = 90cm^{-1}$.

This value for the exchange constant is in encouraging order of magnitude agreement with the previous value of $60cm^{-1}$. A better agreement would no doubt be obtained (assuming our previous value is not seriously in error) by elaborating the theory. We must in particular consider the effects of the presence of the states S=1,3 since electrons from the upper level will relax partly via the S=2. The latter will also relax partly via the S=1 level, and the overall relaxation time may be different from that of our simple model. A more accurate determination of the transition to a temperature independent linewidth is also required, since the exactness of the theoretical fit - i.e. the accuracy of the choice of J - is tested most in this region. Unfortunately it has not been possible to extend the measurements to the appropriate temperature range. However, it seems clear that, in principle, when we have an exchange interaction $J \sim kT$, the measurement of linewidth variation in this temperature region provides another method of determining J.

The precise mechanism of relaxation is not clear, but it is thought to involve phonons of energy $h\nu_{ph}$, equivalent to the level splittings. The fact that the width of the single ion V^{2+} lines (6.5G) is much less at room temperature than that of the pairs indicates that the latter are relaxing more rapidly. Gill[20] discusses possible mechanisms for the pair relaxation of Cr^{3+} ions in ruby. Although his findings may be relevant here, since we have made no measurements of relaxation times we are not able to consider them.

REFERENCES

1. G.F. Kokoszka and G. Gordon, "Metal-Metal Exchange Interactions" in Transition Metal Chemistry Vol. 4

2. S.R.P. Smith, Ph.D. Thesis, Oxford, 1966. Paper to be published by S.R.P. Smith and J. Owen.

3. E.A. Harris, Ph.D. Thesis, Oxford, 1963; E.A. Harris and J. Owen, Phys. Rev. Letters, 7, 9 (1963).

4. I. Dzyaloshinsky, Phys. and Chem. Solids, 4, 241 (1958).

5. J. Owen, J. Appl. Phys. Suppl. 32, 213S (1961).

6. Chapter 3, Reference 1.

7. T. Moriya, "Weak Ferromagnetism" in Magnetism I, Eds. I.G. Redo and H. Suhl, Academic Press, New York (1963).

8. G.R. Wagner, R.T. Schumacher and S.A. Friedberg, Phys. Rev. 150, 226 (1966).

9. M.S. Seehra and T.G. Castner, Phys. Konders. Maters. 7, 185 (1968).

10. R.W. Duerst and G.F. Kokoszka, Private Communication to Dr. B. Henderson.

11. P.W. Anderson, Reference 7, Chapter 2.

12. H. Statz, L. Rimai, M.J. Weber, G.A. de Mars and G.F. Koster, J. Appl. Phys. Suppl. 32, 218S (1961).

13. Yu.L. Shelekin, M.P. Votinov and B.P. Berkovskii, Soviet Physics Solid State 8, 469 (1966).

14. P. Kisliuk, N.C. Chang, P.L. Scott and M.H.L. Pryce, Phys. Rev. 184, 367 (1969).

15. N.L. Huang, Phys. Rev. 159, 378 (1967).

16. E.D. Jones, Phys. Rev. 137, A978 (1965).

17. D. Adler, J. Feinleib, H. Brookes and W. Paul, Phys. Rev. 155, 851 (1967).

18. J.H. Van Vleck, Phys. Rev. 57, 426 (1940).

19. A.A. Manenkov and A.M. Prokhorov, J.E.T.P. (U.S.S.R.) 42, 1371 (1962).

20. J.C. Gill, Proc. Phys. Soc. (London), 79, 58 (1962).

CHAPTER VII

PART I: TRIVALENT CHROMIUM IN MAGNESIUM OXIDE - ORTHORHOMBIC SPECTRA

7.1 Introduction

The E.P.R. spectrum of Cr^{3+} in magnesium oxide has been investigated by several groups of workers[1] and has been briefly discussed in Chapter III. We have investigated the orthorhombic spectrum at Q-band since work at this frequency has not previously been reported. The angular variation of the positions of the observed lines has been followed and is explained below.

The orthorhombic symmetry has been attributed to a nearest neighbour positive ion vacancy along a [110] direction and is analogous to the orthorhombic vanadium site discussed in Chapter V. Some modifications of this model due to doubly associated defects have been observed by Wertz and Auzins[2]. Owing to the large distortion from octahedral symmetry, a large zero field splitting is expected. Such has been observed by Griffiths and Orton[3] who quote the values $|D| = 0.031 \pm 0.003 cm^{-1}$ and $|E| = 0.22 \pm 0.01 cm^{-1}$. These values imply a zero field splitting of $|3E + D| \simeq 0.69 cm^{-1}$. The later work of Wertz and Auzins[2] gives a value of $\simeq 0.8 cm^{-1}$. There seems to be no explanation of these differences. However, it is clear that we are dealing with a situation in which the energy of the microwave quantum is of the same order as the separation between the energy levels at zero magnetic field. This produces two related effects. The most evident is that observation

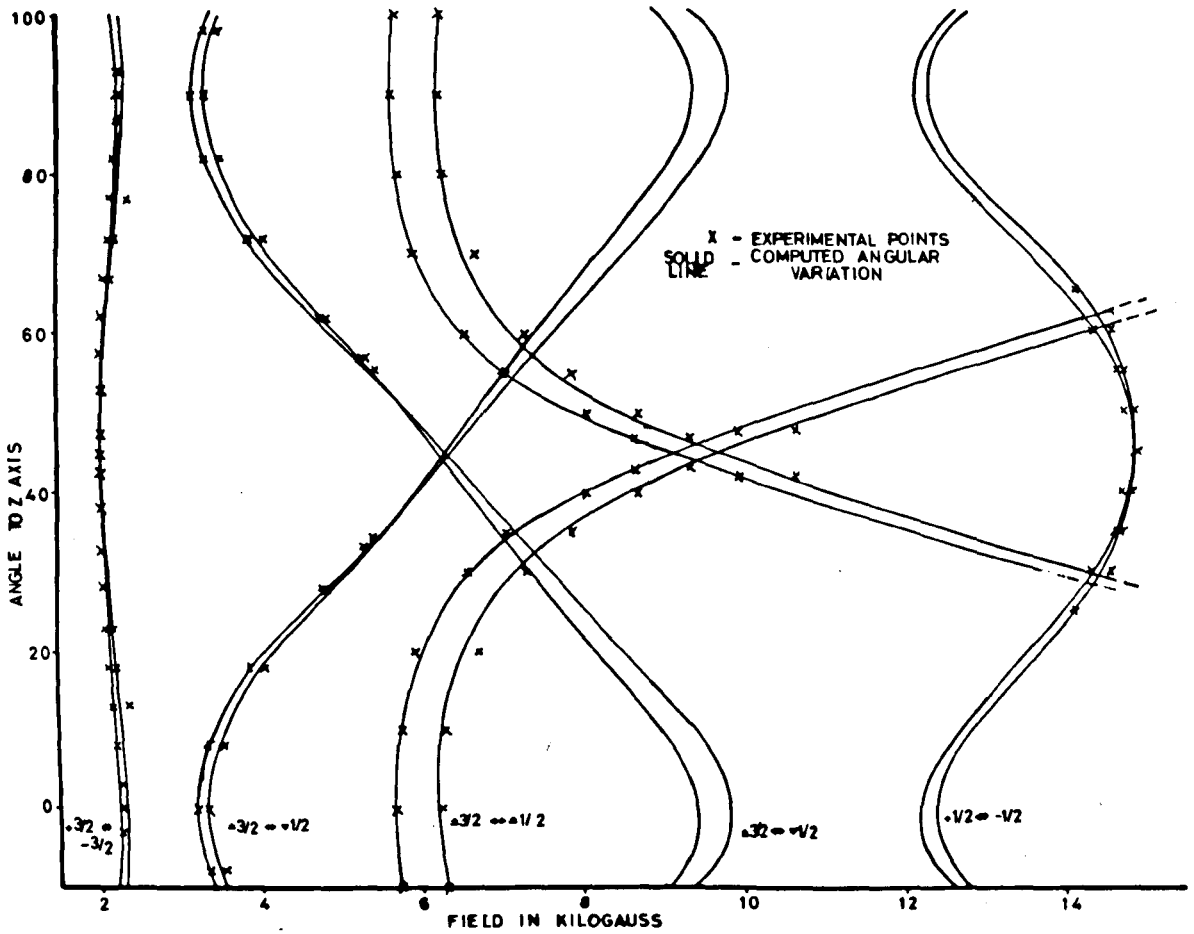

FIGURE 7.1 Experimental and Theoretical Angular Variation in the (100) Plane of Orthorhombic Cr^{3+} Spectra.

of transitions between certain pairs of levels will not be possible at all orientations since the level splittings become too large. Secondly, some transitions are highly anisotropic, moving very rapidly as the field orientation is altered. These effects are more evident at X-band than at Q-band since the microwave quantum of the former is considerably less than $0.7cm^{-1}$.

7.2 The Q-Band Spectrum

Since at Q-band the microwave quantum ($h\nu = 1.2cm^{-1}$) is greater than $|3E + D| = 0.69$, we expect to see all the allowed transitions. In particular, the $+\frac{1}{2} \leftrightarrow -\frac{1}{2}$ and $\pm\frac{3}{2} \leftrightarrow \mp\frac{1}{2}$ transitions, which have not previously been examined, should be observed.

The specimens used in this investigation contained approximately 0.1% Cr^{3+} in substitutional cation ions. The E.P.R. spectrum was complex, despite the absence of a strong hyperfine structure, and many lines were observed in addition to those of current interest. The resonances from Cr^{3+} in orthorhombic symmetry were rather weak in this crystal as compared with the E.P.R. from tetragonal and cubic sites. In view of the omnipresent V^{2+} and Mn^{2+} spectra, the lines due to Cr^{3+} in orthorhombic sites could not be observed at all orientations. The broadening off-axis and large anisotropy also added to the difficulties in obtaining very precise field positions as a function of orientation.

The positions of all expected transitions and also certain "forbidden" transitions are plotted in figure (7.1). The magnetic field

lies in a (100) plane of the crystal and the rotation axis is the [001] direction. For clarity we show only those groups of lines from the two centres with principal axes of distortion lying in this plane, namely those parallel to [110] and [1$\bar{1}$0]. Resonances from the centres having principal axes along the four [110] directions lying at 45° to the (100) plane were also present.

The observed lines can be divided into three groups according to the magnitude of change of the electronic M_s value. For $\Delta M_s = \pm 1$, there is a total of three possible transitions from each of the two centres under consideration, namely the $\pm\frac{3}{2} \leftrightarrow \pm\frac{1}{2}$ and the $+\frac{1}{2} \leftrightarrow -\frac{1}{2}$ transitions. These spin assignments are of course only approximate off-axis since then a heavy mixing between levels becomes evident. The positions of the transitions are indicated in figure (7.1). Turning points occur 90° apart, along [110] directions. The line at 5.7kG arises when H ∥ [110], and that at 6.2kG with H ⊥ [1$\bar{1}$0]. As the magnetic field is rotated, these move to very high field and broaden, becoming eventually unobservable. The $+\frac{1}{2} \leftrightarrow -\frac{1}{2}$ transitions are also anisotropic and are most appropriately observed at their higher field positions where they are clear of the interfering cubic and tetragonal spectra. Again the pair of lines arises from the mutually perpendicular centres.

The "half-field" transitions with $\Delta M_s = \pm 2$ also show the expected large anisotropy. There are observable low field turning points at about 3.3kG, but again line broadening denies the possibility of

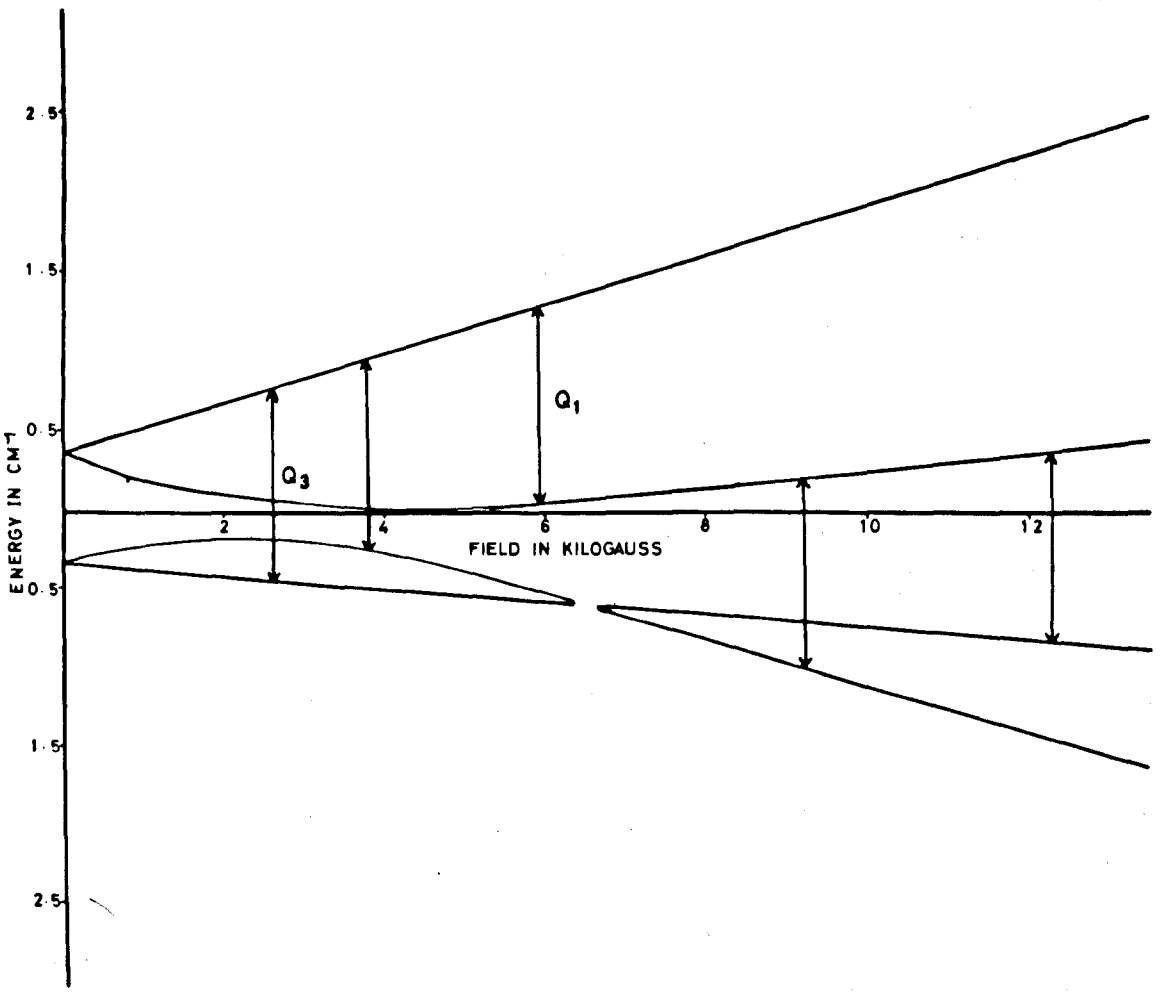

FIGURE 7.2 Energy Levels and Observed E.P.R. Transitions for the Orthorhombic Cr^{3+} Centre, with the Magnetic Field along the z-axis.

observation at the higher fields. Finally, we observe a group of lines at low field. We assign these to transitions of type $\Delta M_s = \pm 3$, occurring between the outer levels of the spin quartet. There is one line possible for each centre.

The field positions are predicted with good accuracy by the computed results. We find that agreement is obtained using the values $|D| = 0.352 \pm 0.010 cm^{-1}$, $|E| = 0.100 \pm 0.010 cm^{-1}$ and $g_x = g_y = g_z = 1.980$. These are in accord with previously quoted parameters except that we have chosen to depart from the original orientation of axes. We adhere to the convention of defining the z-axis as that along which the maximum splitting occurs. This involves inter-changing the x and z axes used by Griffiths and Orton. Thus the chosen axes for the present case are

z along [110]

x along [001]

y along [1$\bar{1}$0]

In this coordinate system the previous values of D and E become $|D| = 0.346 cm^{-1}$ and $|E| = 0.0943 cm^{-1}$.

This centre, then, is analogous to the V^{2+} orthorhombic centre discussed in Chapter V, except that now we have a rather more extreme case. The value of $\lambda = \frac{|E|}{|D|} = 0.287$, approaching the limiting value for any given set of axes. For $\lambda = \frac{1}{3}$ the spectra along z and y would appear the same, and the pairs of lines now observed would become degenerate.

The greater degree of orthorhombic distortion in this case than in the situation discussed for V^{2+}, is attributed to the effects of electric charge. The trivalent ion would tend to interact more strongly with the effectively negative magnesium ion vacancy than would V^{2+}.

The energy levels for the chromium ion in orthorhombic symmetry, for $H \parallel z$ are shown in figure (7.2). The whole scheme is similar but inverted for $H \parallel y$. We have indicated the observed transitions, and note that Q_1 and Q_3 are the higher frequency analogues of K_1 and K_3 observed by Griffiths and Orton. As the field is rotated from $H \parallel z$ to $H \parallel y$, the pattern of levels changes, with the general separation between the upper two decreasing and that between the lower two increasing until the inverted scheme is produced. Thus line Q_1 goes to very high field and is replaced by a transition between the lower pair of levels (cf. K_2, reference 3). The anisotropy of the remaining lines can be understood in similar ways. Line Q_3 does not move very much since the separation between the outer levels remains virtually constant.

PART 2: SUMMARY

We have observed spectra in doped magnesium oxide that arise from V^{2+} and Cr^{3+} ions in orthorhombic symmetry. The cause of the distortion is attributed to a positive ion vacancy in a nearest neighbour position. The former spectrum has not previously been reported and is unusual in the fact that the divalent ion is not a charge misfit and so would not be expected to occur. The concentration of such a centre is,

however, low and the spectrum is only observable in the more strongly doped crystals. We have determined the anisotropy of the resonance lines and have been able to deduce the Hamiltonian parameters with the help of a digital computer. Forbidden hyperfine lines which are allowed owing to the mixing between the zero field and hyperfine interactions, have also been observed for this centre.

The orthorhombic Cr^{3+} spectrum has previously been observed in part. The present measurements at 35GHz have enabled new transitions to be observed and a full analysis of the system to be performed.

In the concentrated vanadium doped crystals one also observes a spectrum from super-exchange coupled next nearest neighbour V^{2+} ions. This spectrum exhibits the stairstep hyperfine structure typical of coupled pairs of ions, with the hyperfine splitting halved in comparison to the single ion spectrum. The spectrum arises from the S=2 state of the manifold of states produced when the two ions with $S = \frac{3}{2}$ are coupled together. Spectra from the S=1,3 states are broadened by crystal field effects.

The angular variation of the spectrum confirms that the ions are situated in a [100] crystal direction and are separated by an oxygen ion through which super-exchange proceeds. The zero field splitting of this tetragonal system has been attributed mainly to magnetic dipolar effects and parly to anisotropic exchange interaction. The isotropic exchange parameter, J, has been measured by plotting the temperature variation of intensity of the pair spectrum. J has also been estimated from the

temperature dependence of linewidth. The decrease in the linewidth is thought due to the decrease in the number of available phonons whose energy is equal to the separation between the S=2 state and the ground state.

REFERENCES

1. Chapter 3, references 15, 17, 18, 19.

2. J.E. Wertz and P.V. Auzins, J. Phys. and Chem. Solids 28, 1557 (1967).

3. J.H.E. Griffiths and J.W. Orton, Proc. Phys. Soc. 73, 948 (1959).